Catalytic applications of layered double hydroxides and the synthesis of inorganic/organic hybrid materials based on MoO_3 and WO_3

Richard Mackey

A thesis submitted in part fulfilment for the requirements for the degree of Doctor of Philosophy at the University of Liverpool

The work described in this thesis was carried out in the Department of Chemistry at the University of Liverpool between November 2006 and February 2010 under the supervision of Dr. Andrew Fogg. All work contained in this thesis is my own work unless stated to the contrary and has not been submitted for any other degree at this or any other university.

Richard Mackey

October 2010

Abstract

Catalytic applications of layered double hydroxides and the synthesis of inorganic/organic hybrid materials based on MoO_3 and WO_3

In this thesis, the work focuses on two areas: the bulk of the work is based upon using layered double hydroxides (LDHs) as catalysts. The final chapter is concerned with the chemistry of MoO_3 and WO_3 and the formation of inorganic/organic hybrid materials using hydrothermal techniques. Introductions to intercalation chemistry and applications of LDHs in the field of catalysis are given in **Chapter 1**.

In **Chapter 2**, the use of the gibbsite family of LDHs $[LiAl_2(OH)_6]X.yH_2O$ (here, X = OH^- and NO_3^-) and $[MAl_4(OH)_{12}]NO_3.yH_2O$ (M = Zn, Co, Ni, Cu) are used to catalyse the gas phase conversion of acetone into methylisobutyl ketone (MIBK). The effectiveness of LDHs as catalysts in this reaction are compared and contrasted with other systems known to be effective in this reaction.

Chapter 3 is concerned with using a LDH $[LiAl_2(OH)_6](WO_4)_{0.5}.H_2O$ with tungstate as the interlayer anion. This material is used to catalyse the bromination of the organic dye, phenol red, which upon bromination becomes bromophenol blue. The catalyst is bio-mimetic in that similar catalysts were inspired by a family of enzymes, the haloperoxidases. From the study of the reaction in detail, various ways of comparing the performance of the catalyst can be deduced, allowing full comparisons between this and other systems.

In **Chapter 4**, the use of another intercalated anion in LDH, molybdate, forming the material $[LiAl_2(OH)_6](MoO_4)_{0.5}.H_2O$ and its usefulness in organic oxidation reactions is explored. Here a test molecule, β-citronellol, is used as a probe. The effectiveness of the material is explored in the oxidiation reaction which is monitored via the use of gas chromatography. Again from a detailed study it is possible to compare this catalyst with others from the literature.

Chapter 5 explores the use of MoO_3 and WO_3 as materials used in the formation of inorganic/organic hybrids. Their synthesis is explored, along with work involving the intercalation of Li^+ ions in vacancies in the hybrid materials. The electrical conductivity of these Li^+ intercalated materials is then explored. All materials are characterised as fully as possible, with crystal structures being found for the hybrid materials, before the addition of Li^+

Experimental procedures and characterisation techniques can be found in **Chapter 6**, with the **Conclusions** to the thesis being found in **Chapter 7**. Additional data can be found in the **Appendices in the attached CD**.

Acknowledgements

Firstly, I would like to thank Andrew, for all of his support, help and patience over the last four years. The other members of the research group, in particular Laura and Jen also deserve special thanks for the long helpful chats where ideas were bounced around and plans hatched.

I am also indebted to Prof. Ivan Kozhevnikov and Dr. Robert Hetterley for their collaboration with the MIBK work carried out in chapter 2, and also Dr. Yaroslav Khimyak and Dr. James Jones for their help with solid state NMR. Thank you also to Dr. John Bacsa for the invaluable help with X-ray crystallography and to Moya Mcarron for all the help on various Friday afternoons with the GC. Thank you also to George Miller for the last minute elemental analyses and Jean for the CHN.

Many thanks must also go to the Wishing Well, where many a lost night has been spent drinking Elephant Beer with Russell and listening to the eclectic jam nights hosted by Laurence and Danny, with a little help from Martin and Sager on the drums.

A special thanks must also go to Mum and Dad, and also to Nic, without whom none of this would have been possible, who have stood by me through all trials and tribulations, and lastly to Darren, for keeping me sane (?) by introducing me to Sponebob Squarepants, Gary, and all the other inhabitants of Bikini Bottom, along with making my defeats on Mariokart all the more embarrassing by you not having a driving licence!

Thank you all

Contents

Chapter 1: Introduction

1.1 Intercalation

Intercalation is the process of inserting a guest species into a host lattice. The species may be ionic, atomic or molecular. Intercalation reactions are generally reversible with the structure of the host being preserved. They also usually need to overcome a relatively small energy barrier with reactions usually occurring close to room temperature, however, if the temperature is to high, the host lattice may become unstable and reorganise. Obviously both of these factors need to be taken into account when considering the necessary conditions for intercalation to occur. The process of intercalation is extremely useful in the modification of the electronic[1], magnetic[2-3] and catalytic[4] properties of materials.

Host materials are generally compounds, with the few exceptions including allotropes of carbon. Host lattices can be classified according to their dimensionality[5] as follows: three-dimensional frameworks, two-dimensional layered materials, one-dimensional chain structures and also zero-dimensional units.

1.2 Zero Dimensional Materials

Fullerenes are typical examples of zero dimensional materials which can also be hosts for intercalation, with alkali metals[6-9] (Figure 1.1) and even halogens such as iodine[10], forming $C_{60}I_4$ (Figure 1.2) with alkali metal intercalated fullerenes exhibiting superconductivity[11].

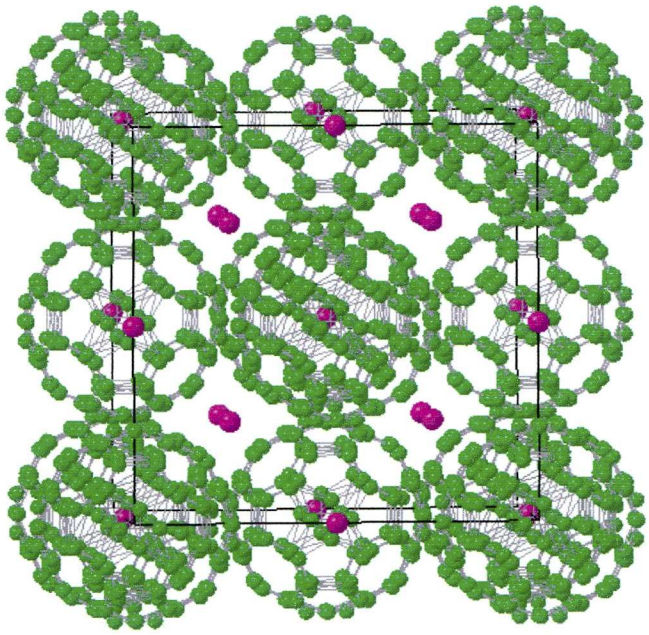

Figure 1.1 K_3C_{60} structure showing K^+ (pink) ions occupying all octahedral and tetrahedral interstitial sites of the host lattice. Carbon atoms are shown in green

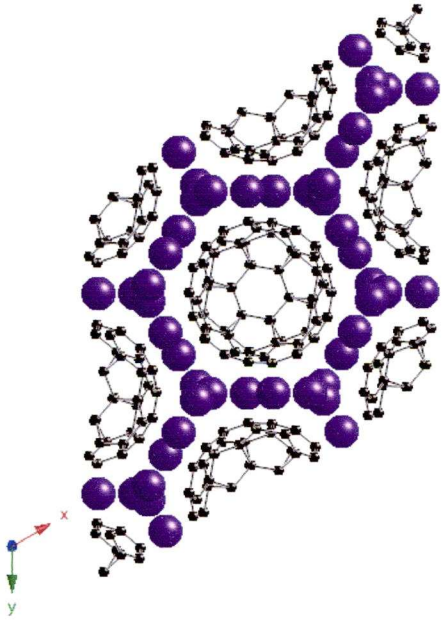

Figure 1.2 $C_{60}I_4$ structure, with the iodine in purple and the carbon atoms in black

1.3 One-dimensional structures

An example of a one-dimensional compound is $NbSe_3$[12] which is an electrical conductor via charge density waves[13-14]. Other examples include carbon nanotubes[15] and 'ladder materials' such as $(VO_2)P_2O_7$[16-17] which are promising quantum magnets (see Figure 1.3). Copper-oxovanadium phosphates[18] (see Figure 1.4) are an example of inorganic-organic hybrid materials exhibiting one-dimensionality. Recent research into one dimensional structures involves nanostructures[15], such the one dimensional conducting[19] molybdenum chalcogenide molecular wires (see Figure 1.5), which have the general formula $M_2Mo_6X_6$ (M=Li, Na; X=Se, Te) and can be thought of as compounds which contain hexagonal close packed chains with the formula Mo_6X_6 [20-21].

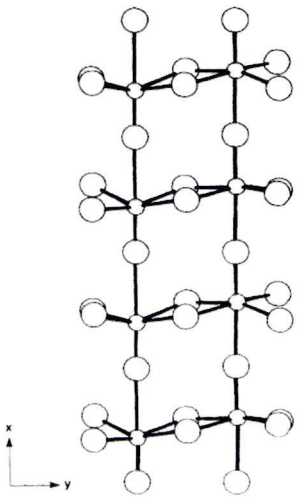

Figure 1.3 A 'ladder' of V^{4+} ions at right angles to the layers in the compound $(VO_2)P_2O_7$. Small circles represent V atoms; larger circles represent O atoms[17]

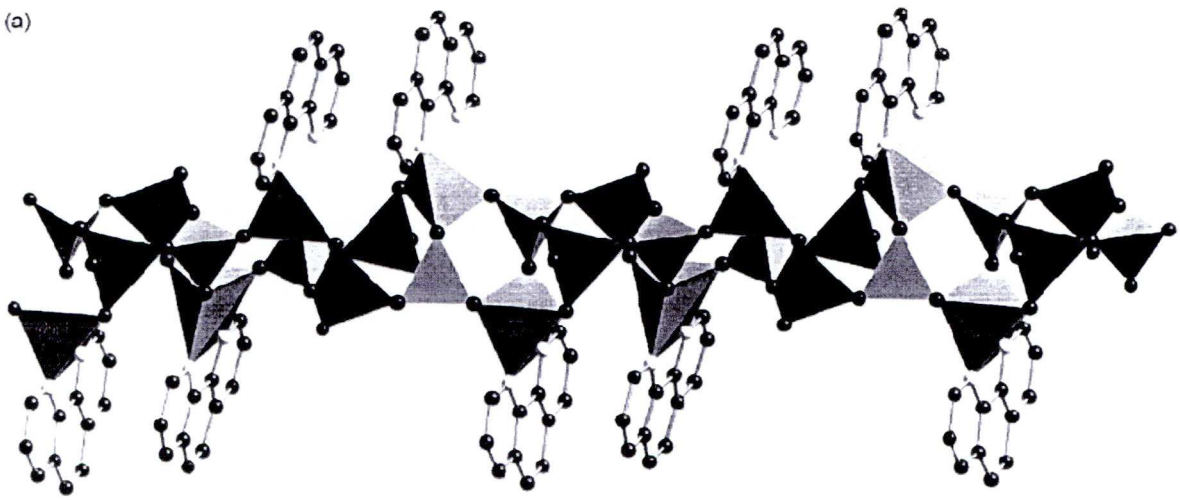

Figure 1.4 [Cu(phen)$(VO_2)(PO_4)$], an oxovanadium phosphate[18]

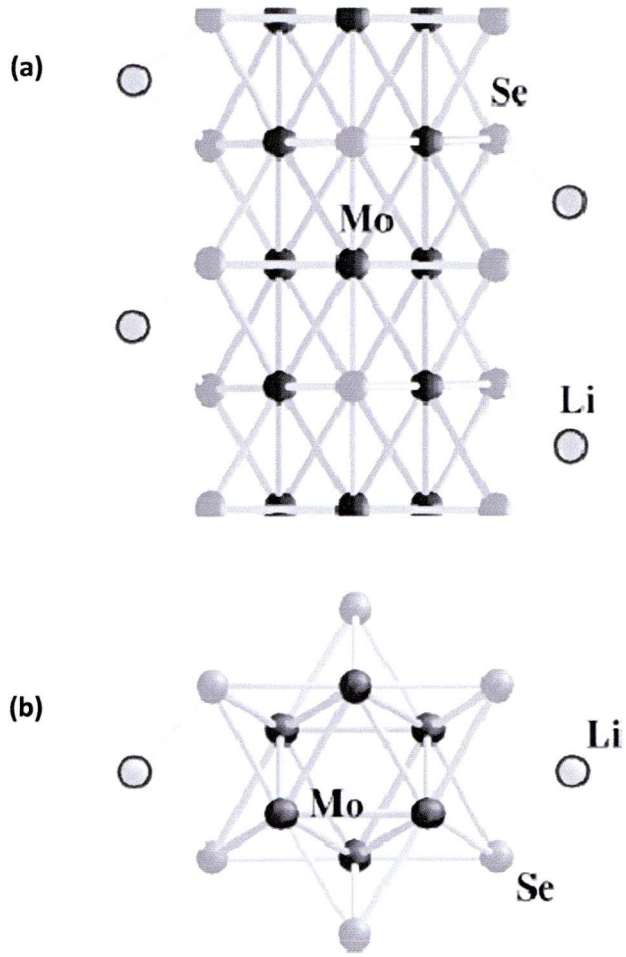

Figure 1.5 $Li_2Mo_6Se_6$ nanowire[22] (a) viewed from side and (b) viewed from above. The structure consists of hexagonal close packed chains of formula Mo_6Se_6 with Li atoms placed between chains

1.4 Layered Materials

Many examples of layered materials exist in nature, with graphite being a familiar example. Its layered structure previously being exploited by its use as 'lead' in pencils. Crystals of graphite contain layers consisting of carbon atoms arranged in hexagons, with Van der Waals forces holding the layers together, which in the most common form of graphite are stacked in a ABAB arrangement[23] (see Figure 1.6).

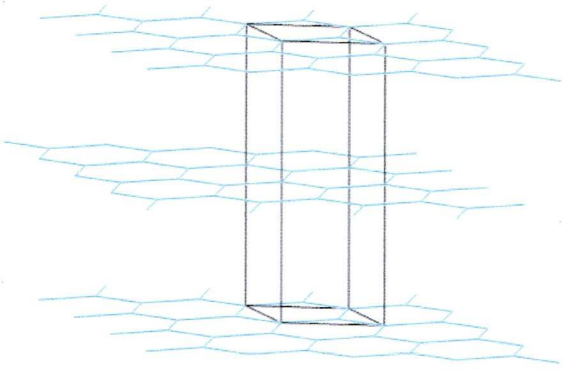

Figure 1.6 Graphite in its standard form showing the ABAB stacking sequence

The graphite structure can also undergo intercalation reactions, with perhaps the most studied reaction occurring with potassium[24]. The compound, KC_8 is prepared by reacting graphite with potassium vapour (for example at 423K[25]). The K^+ ions then sit between the layers[26]. KC_8 is a superconductor below 139mK[24].

Other common examples of layered materials include clays, composed of both tetrahedral silicate $[SiO_4]$ and octahedral aluminate $[Al(O,OH)_6]$ sheets[27]. The silicate layers form by $[SiO_4]$ units linked through three corners forming an infinite layer. The aluminate layers consist of octahedral edge sharing aluminium ions, which are sandwiched between two silicate layers with inward pointing $[SiO_4]$ tetrahedra, with the tetrahedral layers and octahedral layers linked via apical oxygen atoms on the tetrahedral sheets[28]. Smectite clays are formed when silicon or aluminium metal ions are substituted, with ions such as Fe^{3+} with the resulting negative charge residing on the oxygens situated on the layer surface. Charge balancing cations then reside in the interlayer space. An example of a smectite clay is shown in Figure 1.7.

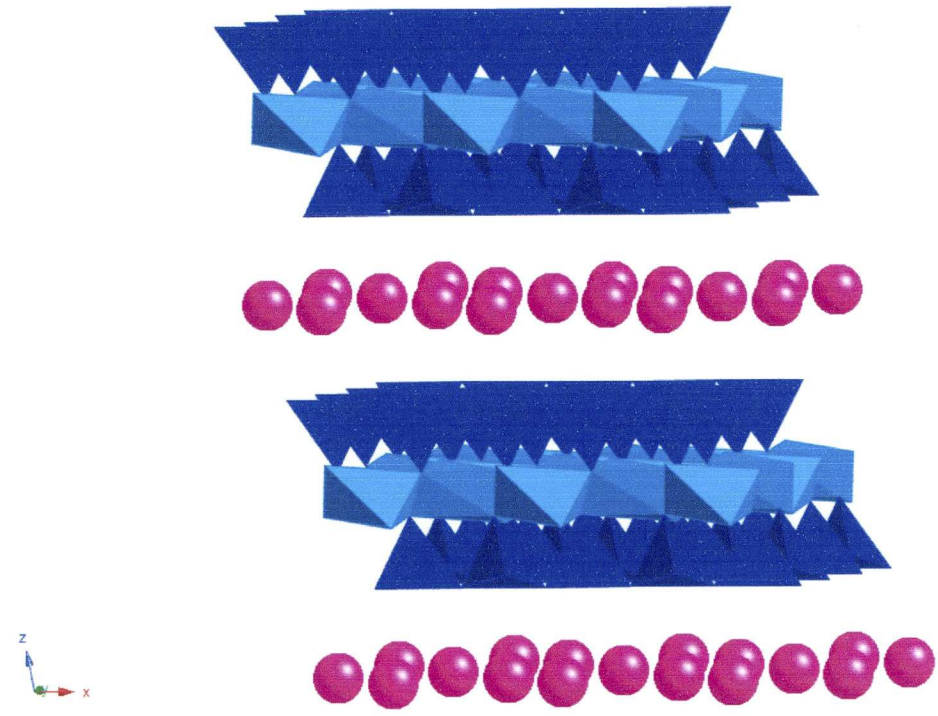

Figure 1.7 Example of a smectite clay structure, montmorillonite, formed when Si^{4+} or Al^{3+} cations are substituted (for example Al^{3+} with Mg^{2+}, or Si^{4+} with Fe^{3+}). Here the layers consist of silicon tetrahedra (dark blue) and aluminium octahedra (light blue) with cesium ions (purple) between the layers to charge balance.

The cations residing between the layers are easily exchanged, for example with H^+, making clays useful as catalysts[29], for example in cracking[30], alkylation[31-33], benzylation[34] and methanol conversion[35]. Clays have also been found to be useful sorbents for pesticides such as paraquat[36], glyphosate[37], organotin contaminants in water[38] and also heavy metals such as cadmium[39-40].

Titanium disulfide is also a useful layered material, with a CdI_2 structure, based upon the close packing of iodide with half of the octahedral holes being occupied by cations. The cations occupy all octahedral holes in every other anion layer[23]. The structure has a high electrical conductivity along the Ti layers[27], which can be improved upon by the intercalation of alkali metal cations (see Figure 1.8), e.g. with Li^+, forming Li_xTiS_2[41], which are promising cathode materials[42] by simply stirring in *n*-butyllithium[43], according to Figure 1.8. Slightly more unusual layered structures include that of MoO_3, with its layers of distorted MO_6 edge sharing octahedra[44] (see Figure 1.9), which also exhibits intercalation chemistry[45].

$$x C_4H_9Li + TiS_2 \longrightarrow \frac{x}{2} C_8H_{18} + Li_xTiS_2$$

Figure 1.8 Synthesis of Li^+ intercalated TiS_2 with the addition of *n*-BuLi

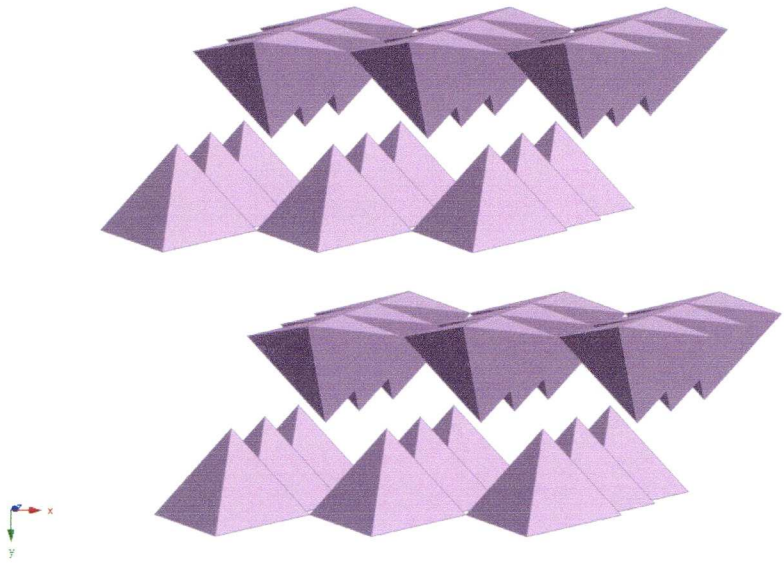

Figure 1.9 Structure of MoO_3

1.5 Three dimensional Frameworks

Three dimensional frameworks consist of channels within a rigid structure with common examples being zeolites, such as ZSM-5[46] (Figure 1.10) and metal-organic frameworks[47-48], the most famous of which being MOF-5[49] (Figure 1.11). These materials have been applied in the field of catalysis[50-51], with zeolites also being commonly used as molecular sieves and shape selective catalysts[52-53], which allows the selection of a particular zeolite to be used for specific catalytic applications[54]. Classic examples include the selective alkylation[55] of aromatic rings, where the selectivity arises due to restricted transition states[56] in the zeolite pores (see Figure 1.12). MOFs are also used in catalysis[57], with chiral MOFs having the advantage of being relatively easy to synthesise by the use of chiral bridging ligands[51]. It is much more challenging to synthesise chiral zeolites, with only around 20 chiral silicate zeolites being known[58], with typical syntheses employing chiral templating agents to achieve the desired products[59]. MOFs have also found applications in gas storage[49, 60-62] and separation[63-64].

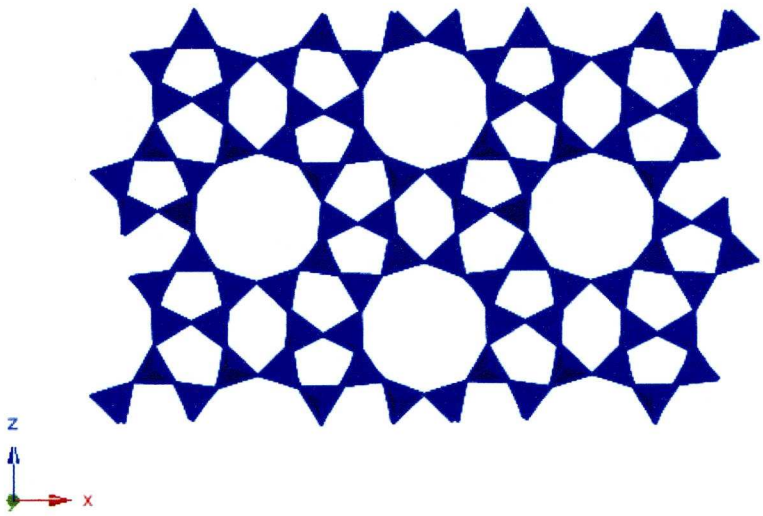

Figure 1.10 Zeolite ZSM-5

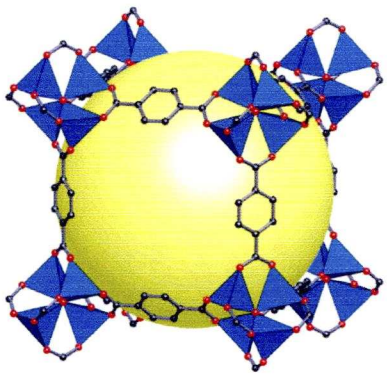

Figure 1.11[60] MOF-5, the most studied MOF

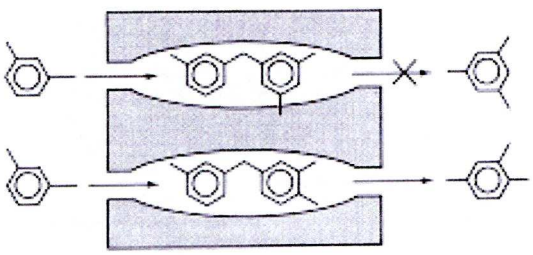

Figure 1.12 Selective alkylation of aromatic rings via a zeolite. The selectivity arises due to restricted transition states

1.6 Intercalation Compounds of WO_3

WO_3 adapts the ReO_3 structure with corner sharing WO_6 octahedra (as shown in Figure 1.13). The structure is three dimensional and, having interstitial sites, intercalation can occur in the channels such as in the formation of tungsten bronzes where alkali cations such as Na^+ and K^+ form the intercalation compounds Na_xWO_3[68], which exhibit superconductivity[69] and are made by heating metal halides along with the WO_3[70]. The structures can either be cubic[71] (which is analogous to the perovskite structure, where the alkali cation is situated at the centre of the unit cell), tetragonal[72] or hexagonal[65](shown in Figure 1.14). A likely mechanism for the superconductivity of the tungsten bronzes is the overlap of the t_{2g} orbitals on tungsten indirectly via oxygen π orbitals (direct interaction between W orbitals is not possible as the W atoms are separated by too great a distance). This overlap would form a partially filled π^* band throughout the WO_3 structure. At values of $x < 0.3$ in the M_xWO_3 compounds (M=Na, K, Rb, Cs), the bronzes become semiconductors rather than metallic. At these lower values of x, structural distortions also exist which would inhibit the formation of the conduction band. Intercalation compounds of WO_3, can form compounds known as planar intergrowths[27] where a particular solid will contain more than one structure with clear interfaces between the two solids, for example if a tungsten bronze is formed when WO_3 is reacted with metallic Bi to form Bi_xWO_3 where $x \geq 0.02$[73] where the hexagonal tunnels are arranged in a singular fashion (see Figure 1.15). As the concentration of Bi is decreased, the hexagonal tunnel separation increases.

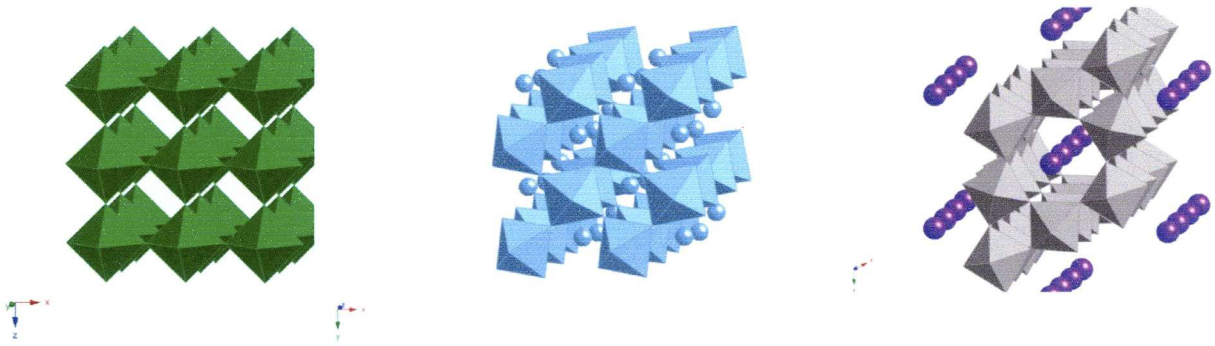

(a) (b) (c)

Figure 1.13 (a) Structure of WO_3 showing WO_6 corner sharing octahedra, in a ReO_3 type structure; (b) Structure of $CaTiO_3$, a perovskite, where the calcium is shown as the spheres; (c) a typical tungsten bronze where an alkali metal cation (here potassium in purple), is found in the middle of the unit cell

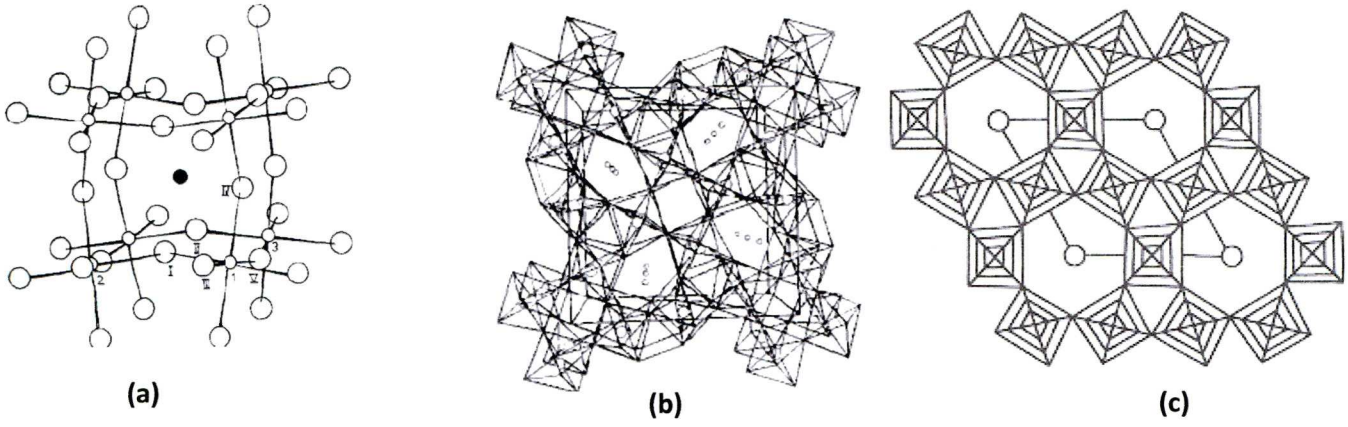

(a) (b) (c)

Figure 1.14 Tungsten bronzes in (a) cubic[71]; (b) tetragonal[72] and (c) hexagonal[27] structures

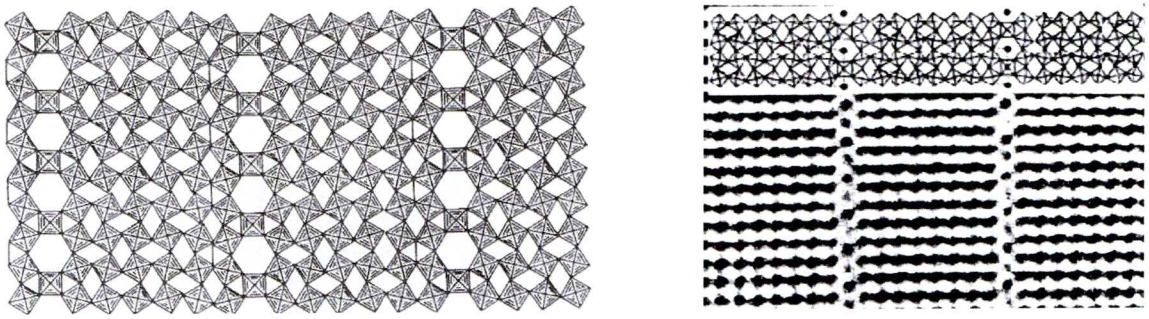

(a) (b)

Figure 1.15 (a) idealised structure of intergrowth tungsten bronze containing single rows of tunnels[27] (Bi atoms omitted for clarity); (b) superimposed on an electron micrograph[73] this time with Bi atoms

Insertion compounds of WO_3 and MoO_3 have been known for some time in the form of bronzes, which were discovered by Wohler in 1824 by the reduction of a mixture of Na_2WO_4 and WO_3 with H_2 at red heat[44]. The resulting compounds were a series of nonstochiometric materials of the general formula M_xWO_3, where M is an alkali metal cation, $x<1$ and W is in an average oxidation state between +5 and +6. The structure of the tungsten bronzes can be compared to that of a perovskite lattice, where the structure consists of WO_6 corner sharing octahedra with the alkali metal cation in the interstitial sites[65] (Figure 1.24). Perovskites form when a divalent cation (e.g. Ca, Sr, Ba) which is significantly larger than a tetravalent cation (typically Ti^{IV}) form a mixed oxide with the general formula ABX_3, where A is the larger cation and coordinated to 8 Ti cations at the corners of the unit cell and to 12 oxygens at the midpoints of the cell edges[27]. The perovskite structure is important in solid state chemistry, not least because many high temperature superconductors are based upon it[66].

The structure of WO_3 adopts that of ReO_3, where $[WO_6]$ octahedra corner share (Figure 1.13 (a)). The structure has a 3 dimensional array of channels, which can incorporate alkali cations. When the amount of alkali cation lies in the range ≤ 0.3 x ≤ 0.9 in the formula M_xWO_3, the structure becomes similar to that of perovskite (Figure 1.13 (b), where the alkali metal resides in the middle of the unit cell (Figure 1.13 (c)).

1.7 Aluminium Hydroxide

Aluminium hydroxide is a layered material which exhibits intercalation. There are four polytypes of naturally occurring $Al(OH)_3$; gibbsite[74] (Figure 1.16 (a), bayerite[75] (Figure 1.16 (b)), nordstrandite[76] and doyleite[77]. All polytypes exhibit the same layer structure, however different stacking sequences are found. The materials consist of double layers of hexagonally packed O atoms, with Al atoms occupying two thirds of the octahedral holes in the layers in a ordered manner (see Figure 1.16). Small distortions in the AlO_6 octahedra cause gibbsite and bayerite to adopt monoclinic symmetry and nordstrandite and doyleite to adopt triclinic symmetry. The gibbsite polymorph has a pseudo-*aba* stacking sequence with bayerite having a pseudo-*aa* sequence. High pressure phases of gibbsite have also been studied[78] (Figure 1.17) which can be recovered at ambient pressure. The high pressure phase, as expected, exhibits a contraction and distortion of the unit cell.

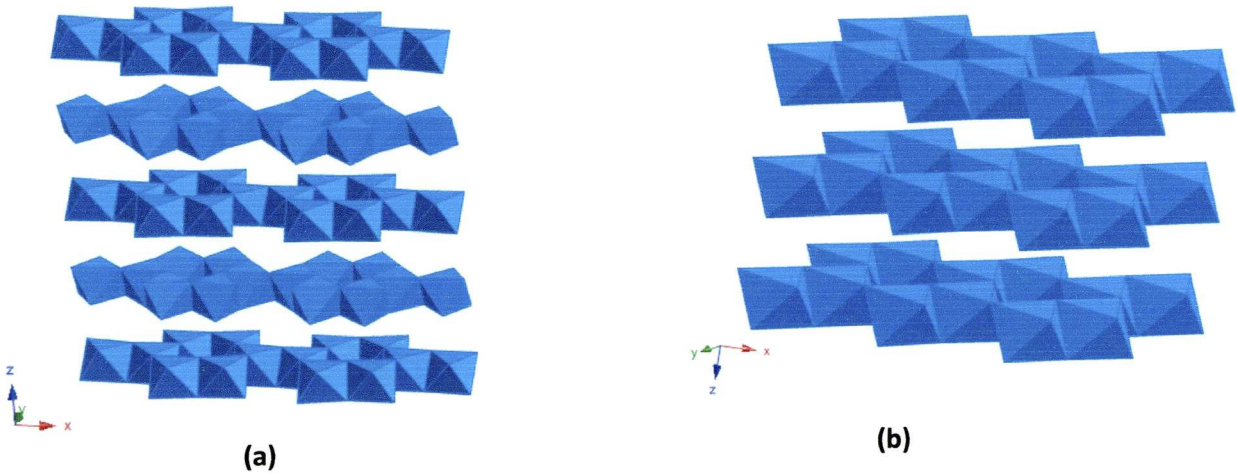

(a) (b)

Figure 1.16 Stacking sequences of (a) gibbsite and (b)bayerite

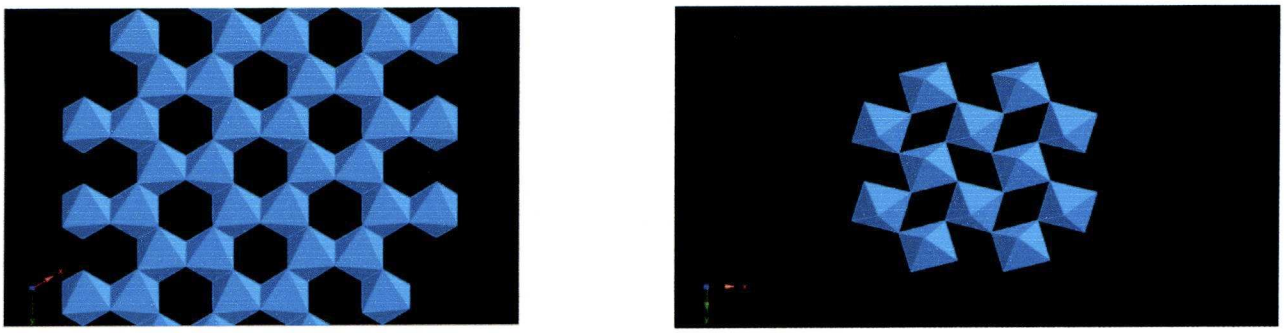

(a) (b)

Figure 1.17 (a) Gibbsite, γ-$Al(OH)_3$ and (b) A high pressure polymorph of gibbsite σ-$Al(OH)_3$

1.8 Layered Double Hydroxides

1.8.1 Structural Chemistry of Layered Double Hydroxides

Layered double hydroxides (LDHs) were first observed in the mid 19th century, with the naturally occurring hydrotalcite mineral. However, it wasn't until 1915 that the chemical composition was determined to be $[Mg_6Al_2(OH)_{16}]CO_3.4H_2O$, with the full structure not being understood until the 1960's, when it was found to have a rhombohedral symmetry[79]. LDHs have the general formula $[M^{z+}_{1-x}M^{3+}_x(OH)_2]^{q+}(X^{n-})_{q/n}.yH_2O$, where x is the ratio $M^{3+}/(M^{2+}+M^{3+})$. Usually z=2, with M^{2+} being Ca^{2+}, Mg^{2+}, Mn^{2+}, Fe^{2+}, Co^{2+}, Ni^{2+}, Cu^{2+} or Zn^{2+}. M^{3+} can be any trivalent transition metal cation apart from Ti^{3+}, due to the instability of Ti in this oxidation state. Other trivalent cations can also be used such as $Al^{3+}$and Ga^{3+}. There are also examples of z=1, where $M=Li^+$ and $M^{3+}=Al^{3+}$, hence the layer charge is q=x for divalent cations, and q=2x-1 for monovalent cations with pure phases existing for $0.2 \leq x \leq 0.33$[80-82]. This thesis focuses solely on LDHs containing Al^{3+} as the trivalent metal cation along with Li^+, Zn^{2+}, Ni^{2+}, Co^{2+}, or Cu^{2+} as the divalent metal.

The structure of LDHs is best understood by considering brucite $[Mg(OH)_2]$, as shown in Figure 1.18. Here, trivalent cations replace the Mg^{2+} ions giving the layers a net positive charge. To compensate for this, charge balancing anions then occupy the space between the layers, as well as water molecules, which are in a constant state of flux, with the water molecules being bound to the layers and to the interlayer anions by hydrogen bonding[83]. It is also possible to exchange the interlayer host anions by reaction with large excesses of guest anions[80].

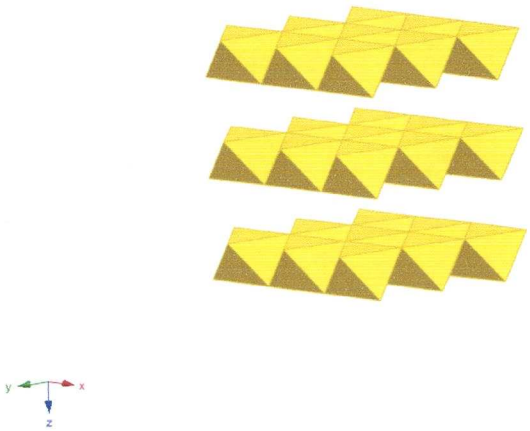

Figure 1.18 Structure of brucite, $Mg(OH)_2$ where octahedral MgO_6 units edge share to form infinite layers

Considering the structural features of LDHs it becomes clear why there are limits to the x values of for $0.2 \leq x \leq 0.33$ in the formulae of pure LDHs. If an LDH has intermediate values of x, the M^{3+} cations in the layers will be separated by relatively large distances by virtue of their electrostatic repulsions, but at high values, they will be forced into adjacent positions, which will inevitably lead to the formation of $M(OH)_3$ phases, whereas in low values of x, $M(OH)_2$ phases will form for similar reasons[84]. For Mg/Al-LDHs, multinuclear NMR studies[85] have shown that for Mg:Al ratios of 2:1, the metal cations are completely ordered whereas at lower levels of Al^{3+} the Al^{3+} is distributed so as to minimise Al^{3+}-Al^{3+} interactions.

LDHs can either have rhombohedral symmetry, with an *abca* stacking sequence, where there are three layers in each unit cell, which stack with a 120° rotation, or hexagonal symmetry, with an *aba* layer stacking sequence, two layers in each cell, and a 180° rotation between the layers, as shown in Figure 1.19.

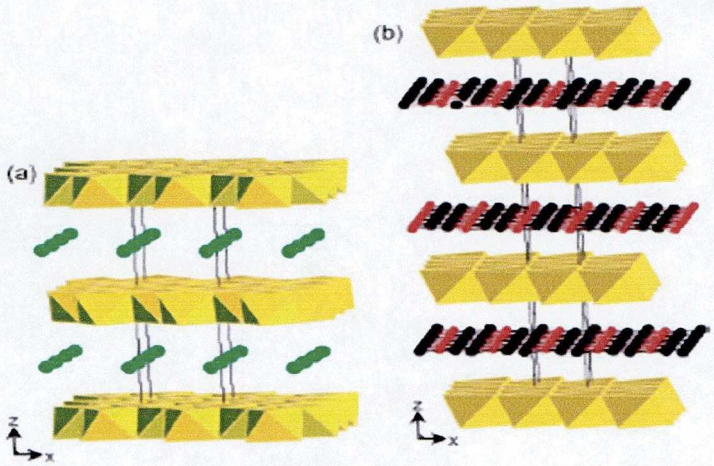

Figure 1.19[86] Hexagonal and rhombohedral forms of LDHs

1.8.2 Novel Layered Double Hydroxides

Along with brucite LDHs, there also exists a family of LDHs based on $Al(OH)_3$. The first reported synthesis of this family was via the hydrolysis of aluminium tri-(sec-butoxide) in the presence of Li_2CO_3[87], forming $[LiAl_2(OH)_6](CO_3)_{0.5}.H_2O$. Further research has illuminated a more general preparative route which permits the synthesis of the new family of LDHs with a variety of anions such as SO_4^{2-}, NO_3^-, Br^-, Cl^-, I^-, CH_3COO^- by direct reaction of their Li salts with a polymorph of $Al(OH)_3$[82]. Here, the metal cations occupy the octahedral holes in the $Al(OH)_3$ starting material. For the Li/Al-LDHs the cations occupy every hole. It is also possible to fill the octahedral holes with divalent cations[88] such as Zn^{2+}, Cu^{2+}, Co^{2+} and Ni^{2+} by reactions of the gibbsite polymorph, activated γ-$Al(OH)_3$ with concentrated solutions of the metal nitrates. The incorporation of M^{2+} cations in this way requires much more forcing conditions, with higher concentrations of the metal salts and higher temperatures proving necessary for a reaction to occur. Here the cations occupy only half of the holes.

1.8.3 Synthesis of Layered Double Hydroxides

1.8.3.1 The Co-Precipitation Method

The standard technique for synthesising LDHs is via a co-precipitation route[89] which allows control over M^{2+}/M^{3+} ratios along with control over particle morphology. Typically[90], the pH of around 100ml of deionised water is adjusted to 10±0.2 using 1M NaOH. Before the simultaneous addition of 120ml of 0.3M $Al(NO_3)_3$ and 120ml of 0.7M $Mg(NO_3)_2$ at a rate of 60ml/hour. The pH of this slurry is maintained at 10±0.2 using the 1M NaOH. After the complete addition of the metal nitrates, the solution is stirred for 24 hours at room temperature before filtering and washing the white precipitate. This method would be used to synthesise a Mg/Al-NO_3-LDH. Obviously by changing the

ratios of $Mg(NO_3)_2$:$Al(NO_3)_3$, the ratios of Mg:Al could be controlled in the final LDH. Other metal cations and organic/inorganic anions can be used. Overall this is an incredibly versatile method for the synthesis of LDHs, however, in order to obtain highly crystalline samples, a degree of ageing is usually required, for example treatment of the resulting gel at 180-200°C under pressure[91].

1.8.3.2 The Urea Method

A variation upon the co-precipitation technique is the use of urea to assist in precipitation. This method is reliant upon the precipitation of metal ions from 'homogeneous solutions'. Urea is able to precipitate several metal cations as hydroxides or insoluble salts when a suitable anion is present. Urea is a weak base and highly soluble in water, and its hydrolysis rate is easily controlled by temperature. The hydrolysis rate increases approximately 200 times when the temperature of water is increased from 60-100°C. The hydrolysis of urea produces ammonium carbonate which makes the solution around pH 9. This is high enough to precipitate many metal hydroxides.

1.8.3.3 The Salt-Oxide Method

This method[92] comprises of the slow addition of a 1M soluble salt (for example $CrCl_3$) solution to a suspension of a metal oxide (e.g. ZnO) with stirring at constant temperature. The reaction can be monitored by measurement of the pH. Upon the addition of the acidic $CrCl_3$, the pH drops, but is buffered by the ZnO. The reaction being complete when this ceases to happen. This method of monitoring the reaction has been shown to be valid by simultaneous pH monitoring and X-ray diffraction studies.

1.8.3.4 Hydrothermal Methods

A novel route to Al^{3+} containing LDHs has recently been noted, where the octahedral holes in different polytypes of $Al(OH)_3$ were filled with metal cations such as Li^+ [82, 93] and later Zn^{2+}, Co^{2+}, Cu^{2+} and Ni^{2+} [88]. Here the synthesis is hydrothermal, with lower temperatures and concentrations of metal salts being required for the $LiAl_2$-LDHs than for the MAl_4-LDHs. Furthermore, to synthesise the MAl_4-LDHs it is first necessary to activate the gibbsite. This is done by grinding the powder in a ball mill for several days in a small amount of water. This has the effect of creating more defect sites in the gibbsite allowing the reaction to proceed, as can be seen from the SEM images in Figure 1.20.

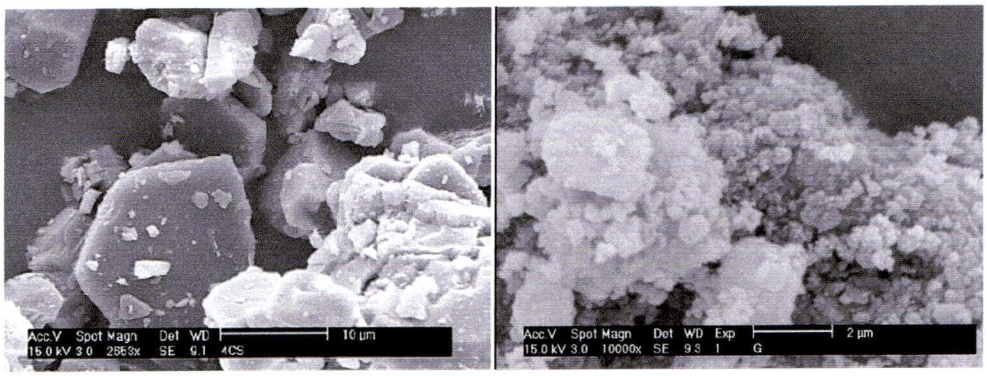

Figure 1.20 SEM images of gibbsite; (left) before grinding, (right) after grinding[88]

1.9 Layered Double Hydroxides and Catalysis

Research into the use of layered double hydroxides as catalysts started in the 1980s, where work into the intercalation of catalytically active metal complexes such as $Rh(PPh_3)_n^+$ was already taking place on clays[94]. The first successful reactions were halide exchange reactions between alkyl bromides and halide containing LDHs of the formula $[Zn_2Cr(OH)_6]X.nH_2O$ where X=halide[95]. The mechanism appears to be a direct exchange reaction, whereby the halide in the LDH and the halide on the alkyl group are swapped, however, the LDH here is non-catalytic as it is clearly changed during the reaction. This problem was tackled by Suzuki *et al*[96] by using another organic component in the reaction (see Figure 1.21) where an organic halide (here benzyl chloride) was added to constantly replenish the LDH in a continuous cycle. The LDH used in this reaction was $[Mg_3Al(OH)_8]Cl.2H_2O$. A similar reaction by Ono *et al*[97] used $[NiCl_4]^{2-}$ in the interlayer region to convert butyl bromide into butyl chloride, with the interlayer $[NiCl_4]^{2-}$ being converted into $[NiBr_4]^{2-}$ in the process.

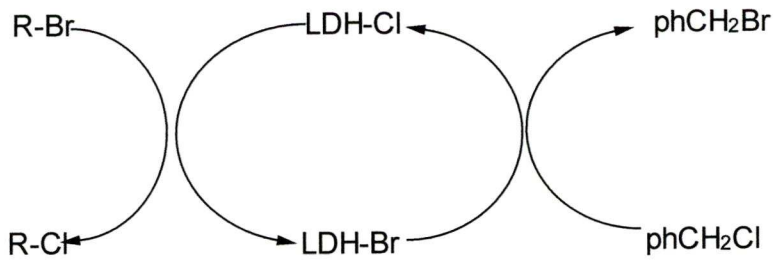

Figure 1.21 Halide exchange reaction scheme where benzyl chloride was used to constantly replenish the LDH, thereby making the LDH catalytic

With their anion exchange capabilities, LDHs can be synthesised where catalytically active anions reside in the interlayer space. A second feature of LDHs useful in catalysis is their basic nature. In the

hydrated phase, the main source of basicity is the presence of hydroxyl ions, whereas in the dehydrated phase, strongly basic O^{2-}-M^{2+} pairs exist[98] give rise to the possibility of both Lewis acid and Lewis base catalysis[99]. It is possible to compare the number of basic sites present in LDHs by adsorbing a suitable indicator onto the solid[100] and judging the strength of the acidic/basic sites by the resulting colour change, however, this method already being somewhat inaccurate is also limited to LDHs which are white or very lightly coloured. It is also possibly to probe basicity of an LDH by studying chemical reactions which it is able to catalyse. The Knoevanagel condensation reaction is sufficiently well studied to explore this. In a study by Tichit *et al*[99] the rate of reaction between substituted benaldehydes and an excess of acetone allowed LDHs to be compared to organic bases such as pyridine and piperidine, which then allowed an estimation of the basicity of the LDH. Simple titration using dilute solutions of benzoic acid in toluene can also be employed, however, this method is inaccurate due to the likelihood of the LDHs stacking in the hydrophobic toluene[101]. A more accurate method was found to be the comparison of colour changes differing LDHs had on pH sensitive dyes via the use of UV-Visible spectrometry[101]. Another method is measuring the changes in concentration to dilute phenol solutions[102-103] (again via UV-Visible spectrometry). A possible problem with this method is the sensitivity of the resulting equilibrium on temperature.

1.9.1 Layered Double Hydroxides as Catalyst Precursors

As well as comparing the number of basic sites present in differing LDHs, it is also possible to compare the relative number of basic sites compared to the number of acid sites. A probe reaction for this is the intramolecular cyclisation of acetonylacetone, which under basic conditions cyclises to form 3-methyl-2-cyclopentenone and under acid conditions yields 2,5-dimethylfuran (see Reaction Scheme 1.1). The relative amounts of each product can be used to show the proportions of acidic and basic sites in a LDH, which is highly dependant upon temperature[104], as upon heating, the LDH structure disintegrates, eventually forming mixed metal oxide compounds. It is possible to track the changing acidity/basicity of LDHs as a function of increasing temperature by measuring the heat of adsorption of CO_2 on the LDH at various temperatures[99], here the CO_2 reacts with the hydroxyl groups on the LDH (when calcination temperatures are low enough to still allow the presence of OH^- in the LDH structure) and also the Lewis acid sites. Analysis of the infra-red spectra of the CO_2 adsorbed, calcined LDHs shows the O^{2-} sites are relatively inert towards CO_2 adsorption.

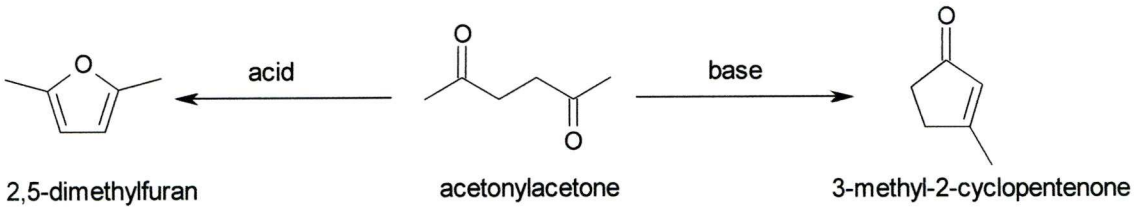

Reaction Scheme 1.1 Intramolecular cyclisation of acentonylacetone

LDHs which have undergone full calcination form thermally stable spinel (AB_2O_4) phases[105] however, calcination at lower temperatures (typically 500-700°C) an inverse spinel is formed[106] which in the case of Ni containing inverse spinels exhibit high catalytic activity in the conversion of methane and CO_2 into syngas due to the location of the catalytically active octahedral Ni^{2+} ions on the surface of the material. In the conversion of methane and CO_2 into syngas, coking is commonly attributed to the use of Ni, whereas if the spinel $NiAl_2O_4$ is used, the coking is reduced[107]. Friedel-Crafts alkylations have also been reported[108] to be catalysed by calcined Zn/Al-LDHs with aromatic alkylations also being reported with using methanol and calcined Mg/Al[109] and calcined Mg/Al-LDHs substituted with Fe^{3+} and Cr^{3+} [110]. The N-methylation of aniline again using methanol was also found to be catalysed by calcined Mg/Al-LDHs[111]. Mixed oxides, derived from LDHs such as $Co_{2.5}Mg_{0.5}$/Al-LDH and $Co_{2.5}Mg_{0.5}/X_{0.5}/Al_{0.5}$-LDH (where X=Fe, Mg, Zr and La) have also been used in NO trapping[112], a process crucial in the catalytic cleaning of exhaust gases in cars.

The memory effect where LDHs can reconstruct after being partially decomposed can also be exploited in the production of LDH based catalysts. The reconstructed LDHs are strongly basic, as the interlayer anions are mainly OH^-. This property makes them useful in base catalysed cross condensation reactions such as the Knoevanagel, Claisen-Schmidt and Michael addition reactions[113-116]. This allows the chemical process to be substantially greener, as traditionally, NaOH and KOH are used, which generate large amounts of salt waste upon neutralisation, along with being corrosive and non-recyclable. The catalysts produced by the memory effect can be further improved upon if they are subsequently doped with alkali metal cations (Na, Li, K), creating substantially basic catalysts[117].

1.9.2 Using the metals contained in Layered Double Hydroxides as Catalysts

Layered double hydroxides have many application in heterogeneous catalysis, where the metal cations in the LDH structure are the active species. Cu/Cr and Mg/Al LDHs were found to be catalytic in the ethoxylation of butanol using ethylene oxide to produce commercially valuable glycol ethers[118]. Dumitriu and co-workers[119] described the oxidation of thioethers into sulphoxides and

finally sulphones using hydrogen peroxide as the oxidant (see Figure 1.18). The reaction uses a Mg/Ni/Al LDH and is important in the manufacture of chemically and biologically important molecules. Other oxidation reactions involve phenol hydroxylation, using a Cu/Al-CO_3-LDH[120] and H_2O_2. It was found that in this case the Cu^{II} was crucial for the reaction to work. The proposed mechanism, elucidated by measurements and comparisons of redox couples to other systems[121] being that the H_2O_2 upon being adsorbed upon the LDH surface causes a redox reaction to take place whereby Cu^{II} is oxidised to Cu^{III}, with the H_2O_2 then forming $OH^{\cdot}$ and OH^- with the radical then going on to react to produce diphenols (see Reaction Scheme 1.2).

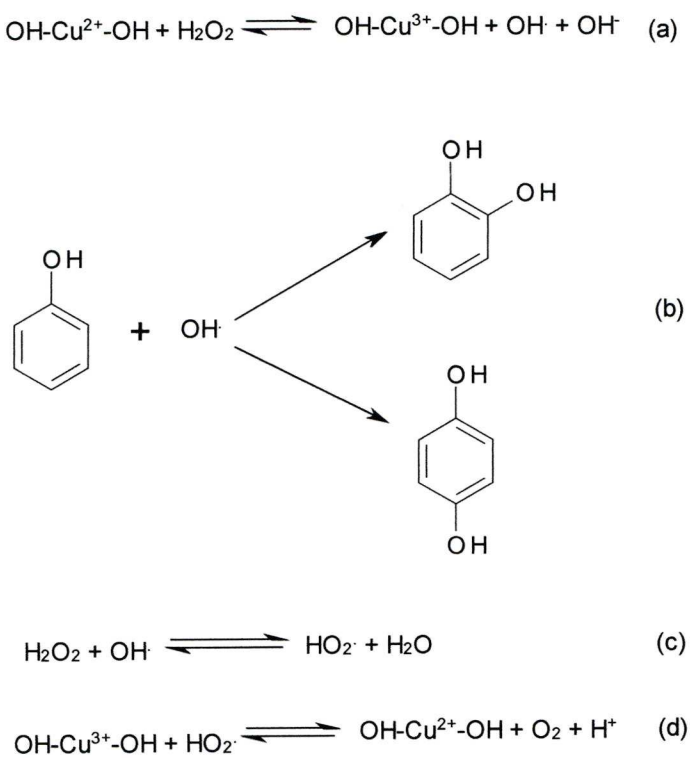

Reaction Scheme 1.2 Cu based LDH being used in the hydroxylation of phenol. (a) Redox reaction between Cu^{2+} and H_2O_2 forming OH^- and $OH^{\cdot}$, (b)$OH^{\cdot}$ going on ton react with phenol in the 2 or 4 positions, (c) possible side reaction where $OH^{\cdot}$ reacts with a further molecule of H_2O_2 forming the radical $HO_2^{\cdot}$ which then reacts in (d) with Cu^{3+}, reducing it back to Cu^{2+}

Another heterogeneous reaction, this time employing Mg/Al and Mg/Ga based LDHs is the hydrolysis of nitriles to their corresponding amides[122] as described in Figure 1.19. The epoxidation of olefins can also be catalysed using a Mg/Al based LDH in the presence of benzonitrile, using hydrogen peroxide as the oxidant[123]. This synthetically useful reaction produces important intermediates in organic synthesis (see Figure 1.20). LDHs can also catalyse the double bond migration in the conversion of eugenol into iso-eugenol[124] using M^{II}/M^{III} LDHs (where M^{II} was Mg, Ni,

Co, Cu, Zn and M^{III} was Al, Fe, Cr, La, V) an important step in the synthesis of pharmaceutically active compounds[125] (see Reaction Scheme 1.3).

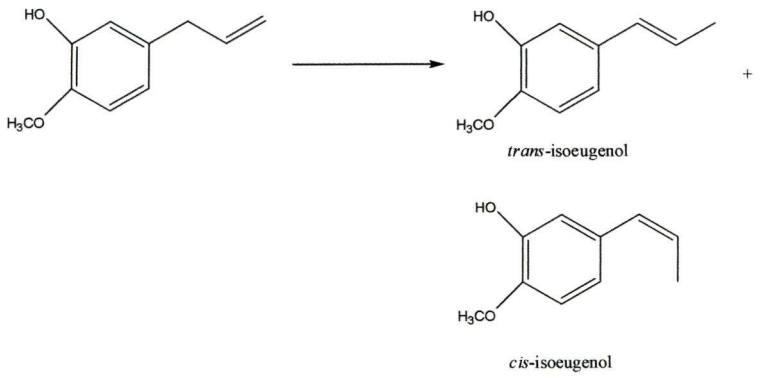

Reaction Scheme 1.3 Conversion of Eugenol to isoeugenol using M^{II}/M^{III} LDHs (where M^{II} was Mg, Ni, Co, Cu, Zn and M^{III} was Al, Fe, Cr, La, V)

A further application of using unmodified LDHs as catalysts is discussed in work carried out during the course of my PhD in conjunction with Dr. Robert Hetterley, then a PhD student with Prof. Ivan Kozhevnikov where different LDHs were tested in their effectiveness in the conversion of acetone to MIBK[126] an industrial solvent (see Reaction Scheme 1.4). This reaction will be discussed in depth in chapter 2.

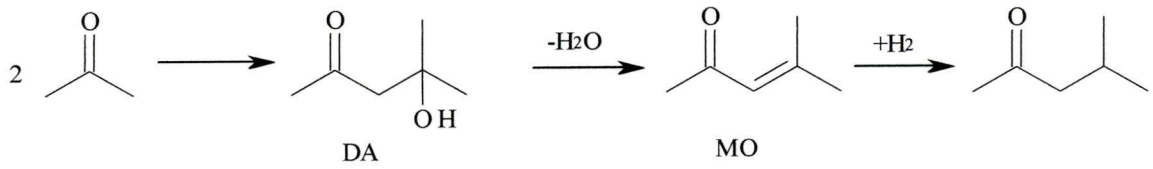

Reaction Scheme 1.4 Conversion of acetone into MIBK

1.9.3 Layered Double Hydroxides Doped with Noble Metals

The use of LDHs in catalysis is expanded upon by the doping of noble metals onto the LDH structure. This is a widely explored area, useful where a bi-functional or multi-functional catalyst is needed. An example of this application is in hydrocarbon reforming, an essential method for producing valuble chemical feedstocks. Here, Ni/Mg/Al based hydrotalcites were being deactivated in the presence of steam. Doping of the LDH with Pt solved this problem[127-128], making the process more efficient. The

use of doped LDHs can also be used for fine chemical synthesis. An example of this is the Heck reaction, catalysed by Pd-doped LDHs[129]. Gold nanoparticles can also be supported on Mg/Al-CO_3-LDH (i.e. hydrotalcite) in the green oxidation of 1,4-butanediol, giving yields and conversions of up to 99%[130] (see Reaction Scheme 1.5).

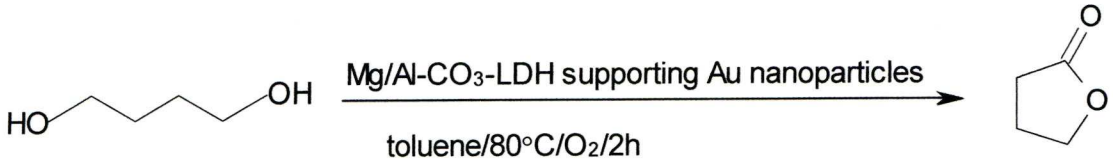

Reaction Scheme 1.5 Green oxidation of 1,4-butanediol using hydrotalcite supported Au nanoparticles

Pd supported Mg/Al-LDHs have also been found to be useful in Suzuki cross coupling reactions[131] (see Reaction Scheme 1.6). The LDH in this case appears to have no effect on the reaction itself, and is merely a support. The catalytically active complex adsorbed onto the LDH is $Pd(AcO)_2Py_2$. A possible mechanism for the reaction is shown in Reaction Scheme 1.7.

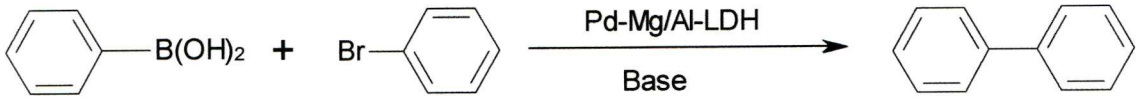

Figure 1.6 Suzuki cross coupling reaction where an aromatic molecule with a boronic acid functionality reacts with a brominated aromatic to form a biphenyl

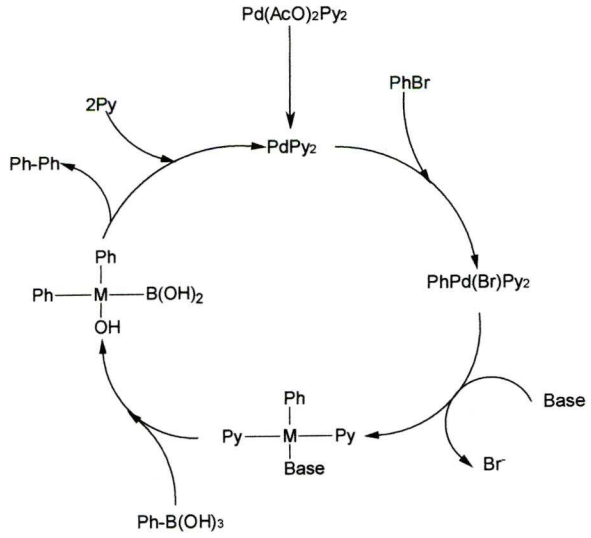

Reaction Scheme 1.7 Proposed mechanism[131] for Suzuki coupling using $Pd(AcO)_2Py_2$ supported on Mg/Al-LDH

It has also been possible to synthesise Mg/Al-LDHs doped with Pd, using a micellar method[132], where a surfactant (Sodium dodecylsulphate, NaDS)) was employed to produce a micellar aqueous solution of $Pd(OAc)_2$ which had previously been dissolved in chloroform. The surfactant is then oriented such that the hydrophobic alkyl groups point towards the micelles, and the hydrophilic ends point outwards into the aqueous solution. When aqueous hydrazine is added to this it allowed Pd nanoparticles to form, stabilised by the surfactant molecules by both steric and electrostatic effects. The surfactant molecules also form a dense layer around the nanoparticles, thus preventing aggregation. The Mg/Al-NO_3-LDH suspension was then added, leading to the exchange of NO_3^- ions for DS^- ions. This released the Pd nanoparticles and also made the LDH hydrophobic, making the material more suited to reactions carried out in organic solvents. Using this method, a large proportion of the Pd is found on the surface of the LDH, increasing its reactivity. This proved particularly useful for the semi-hydrogenation of alkynes in the liquid phase under mild conditions.

1.9.4 Pillaring of Layered Double Hydroxides

The use of pillars to open up the interlamellar space in LDHs has been explored for some time[133-134], with the intention of making LDHs with rigid pore sizes which would be analogous to zeolites but with greater control over the synthesis as well as being able to tune the catalytic activity by choice of the pillaring anion[135]. Keggin type anions (discussed in detail in Chapter 5) are frequently used as pillars in layered materials, and as Keggin ions have multiple charges, it is possible again by choice of anion to control the numbers of interlayer anions. Keggin ions also have various catalytic functions, allowing the LDH to be tuned as required to the functionalities necessary for the catalyst. As Keggin anions can be incredibly bulky, it is occasionally necessary to intercalate anions such as terephthalate to open up the layers and facilitate intercalation of the bigger Keggin ions[136-137]. Examples of catalysis by pillared LDHs are the dehydration reactions such as conversion of isopropanol into propene and acetone[135] using Mg/Al-LDHs pillared with the polytungstate $PW_{12}O_{40}^{3-}$ and the use of pillaring decavanadate[138] ($V_{10}O_{28}^{6-}$) in a Zn/Al-LDH to carry out a photo-oxidation of isopropanol to acetone. The oxidation of acetaldehyde to acetic acid has also been explored[139] using Keggin ion pillared LDHs such as Co/Al and Ni/Al-XW_{11}-Z where $X=B^{3+}$, Si^{4+}, Ge^{4+} and As^{5+} and $Z=Cu^{2+}$, Co^{2+} and Ni^{2+}. It was found that the immobilised catalysts had activities of up to nine times their homogeneous potassium $XW_{11}Z$ salt analogues. A Co substituted POM $[\alpha\text{-}SiW_9O_{37}(Co(H_2O)_3)]^{10-}$ has also been intercalated into a Mg/Al-LDH and used as a catalyst for the liquid phase oxidation of cyclohexanol to cyclohexanone[140]. The photocatalytic degradation of hexachlorocyclohexane (HCH) using Zn/Cr-POM-LDHs has also been studied[141], where the most effective POMs were the Keggin ions $[SiW_{11}O_{39}Mn(H_2O)]^{6-}$ and $[SiW_{11}O_{39}Ni(H_2O)]^{6-}$ were found to be the most effective. In the study it

was proposed that the $OH^{\cdot}$ radical was the species responsible for the decomposition, as shown in Reaction Scheme 1.8.

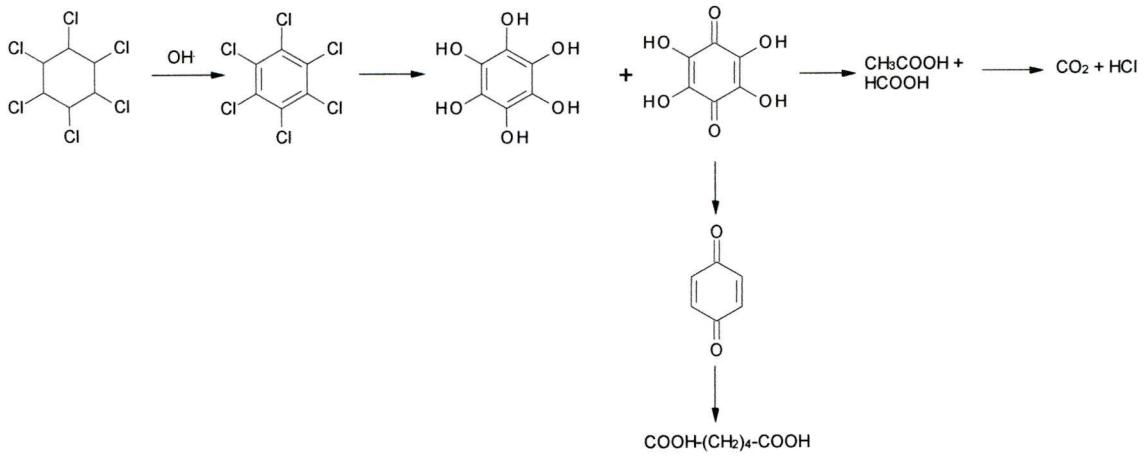

Reaction Scheme 1.8 Decomposition pathway for the pesticide hexachlorocyclohexane (HCH). The intercalated Keggin ions $[SiW_{11}O_{39}Mn(H_2O)]^{6-}$ and $[SiW_{11}O_{39}Ni(H_2O)]^{6-}$ cause the photochemical production of $OH^{\cdot}$, which is the species responsible for the decomposition.

1.9.5 Layered Double Hydroxides Supporting Catalytically Active Anions

The use of layered double hydroxides to support catalytically active anions has been relatively well studied in recent years. Organic reactions such as the Heck reaction, which uses a platinum based catalyst (see Reaction Scheme 1.9) can be performed using layered double hydroxide supported nanoplatinum[142]. Gold based catalysts can also be supported using layered double hydroxides to allow coupling reactions[143] as shown in Reaction Scheme 1.10. Oxidation reactions are commonly studied reactions catalysed by LDHs, for example, porphyrins have been shown to be immobilised on LDHs and used in the oxidation of alkenes[144], immobilised Cu on Zn/Al-LDH in the form of Cu-BDC (2,2'-bipyridine-5,5'-dicarboxylate) can oxidise organic substrates[145] (Reaction Scheme 1.11).

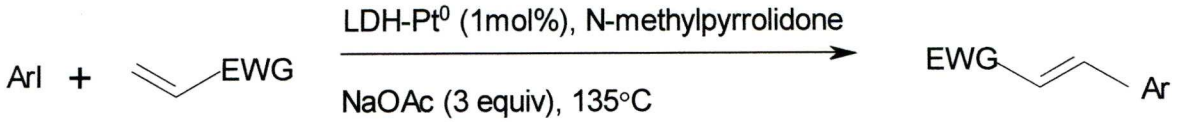

Reaction Scheme 1.9 Heck Reaction using Pt supported on LDH

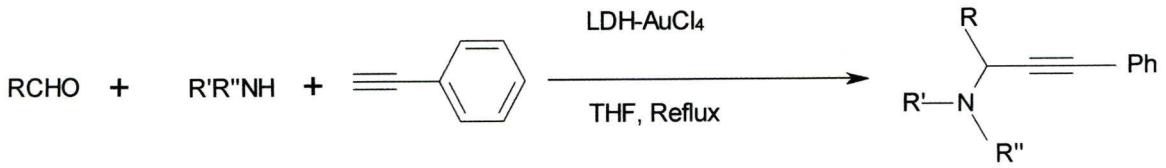

Reaction Scheme 1.10 Gold Catalysed aldehyde, amine, alkyne coupling

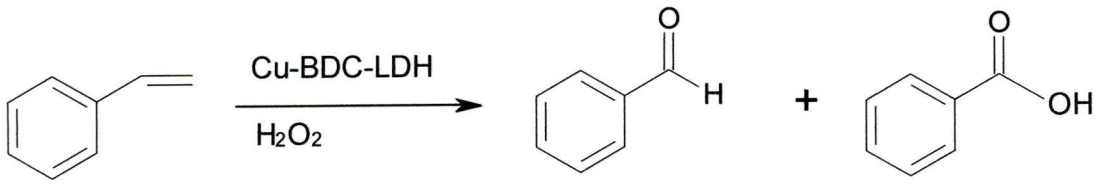

Reaction Scheme 1.11 Oxidation of styrene using Cu-BDC-LDH as a catalyst and H_2O_2 as an oxidant. The reaction is difficult to stop at the aldehyde product which is easily oxidised further to the carboxylic acid

Clearly if the interlayer anions are performing the catalysis, it is necessary to know how the reaction is occurring. The possibilities are either the organic substrate is going into the layers before the reaction occurs, swelling the layers before the product comes out again, or, it is simply the edge sites the are doing the catalysis, with the anions further in the layers having relatively little effect upon the reaction (see Figure 1.22). Evidence towards only the edge site anions doing the reactions is found when a study of Co-porphyrin immobilised on an LDH compared to being immobilised on a clay, the LDH is significantly more active due to the greater accessibility of the edge site[146]. Further evidence for edge site performing catalysis is found when a halide exchange reaction between a LDH and an alkyl halide is carried out (see Section 1.8). Kinetics data shows that the size of the alkyl halide has little effect upon the reaction rate which gives further evidence to the hypothesis that it is only the anions on the edge sites which have an effect[95].

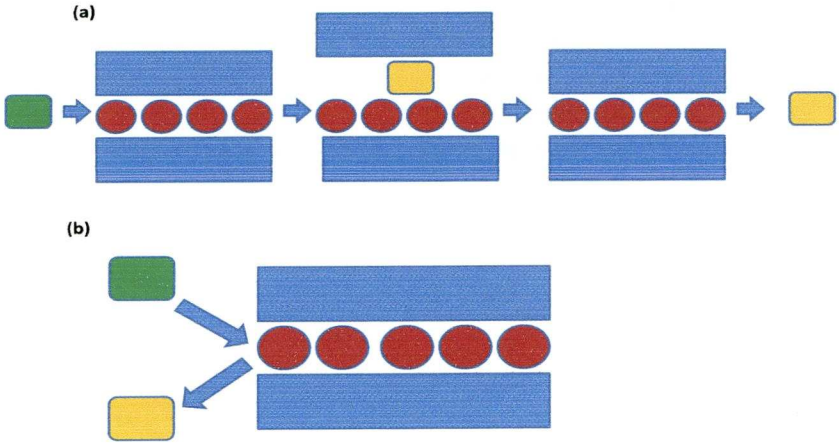

Figure 1.22 Possible ways for reaction to occur between organic substrate and interlayer anions

(a) Substrate (green) goes between layers, swelling the interlayer separation before product (yellow) comes out from the layers

(b) Reaction only occurs with interlayer anions on the edge sites

1.10 Biomimetic Catalysis

Nature has been a source of inspiration in the field of catalysis for many years. For example, the fermentation of sugar to alcohol by yeast has been carried out for millennia. Research intensified in this field towards the end of the nineteenth century when it was noted that certain parts of animal tissues were able to oxidise alcohols[147]. After further research in the twentieth century, the process became better understood and what we now know to be enzymes were successfully crystallised and studies into the structure found that most enzymes were molecules which usually contained a transition metal at the centre surrounded by various proteins. Work on harnessing the power of enzymes to efficiently catalyse reactions under mild conditions was then undertaken, such as the haloperoxidases, a mimic of which will be discussed at length in this thesis. Biological catalysis is incredibly important in industry, for example vitamin C is synthesised on a large scale from glucose. A vital step in this reaction is a selective oxidation of sorbitol, which has six alcohol groups. No known chemical reagent exists which is selective enough to oxidise just one of these, so the step is carried out using the bacterium *Acetobacter suboxydans*[148] (see Reaction Scheme 1.12). Layered double hydroxides, can also act as biomimetic catalysts when supporting anions such as tungsate. This will form one of the chapters in this thesis.

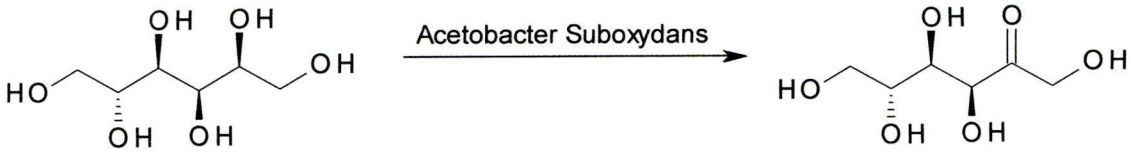

Reaction Scheme 1.12 Selective oxidation of sorbitol using the bacterium *Acetobacter suboxydans* in a key step in the industrial synthesis of ascorbic acid

There is also evidence that catalysis by LDHs could have been conducive to the formation of life on earth[149]. For example, a possibly crucial reaction in the pre-biotic atmosphere, necessary to start the beginnings of life is that of cyanide self addition[150-151] (Reaction Scheme 1.13). It is however necessary for the reaction to occur at reasonably high cyanide concentrations[152]. The LDH could be quite reasonably expected to concentrate the cyanide, with the intercalation of CN^-, thereby helping the early synthesis of amino acid and purines. As can be inferred from Reaction Scheme 1.13, if the concentration of cyanide is not high enough in aqueous systems, the resulting product is simply formamide.

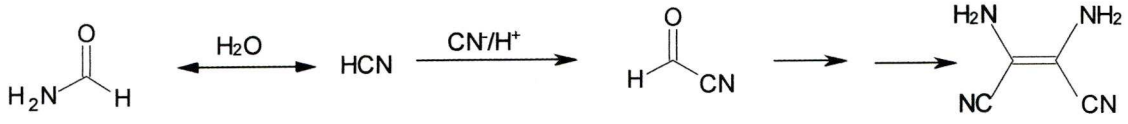

Reaction Scheme 1.13 Cyanide self addition reactions showing the formation of diaminomaleonitrile, a likely precursor to amino acids in the pre-biotic atmosphere[150]. Should the cyanide concentration be too low, the reaction goes to form formamide under aqueous conditions.

1.11 Other Applications of Layered Double Hydroxides

1.11.1 Layered Double Hydroxides and Drug Delivery

LDHs have been explored as agents for therapeutic drug delivery, as they readily intercalate many negatively charged drug molecules. The LDH-drug is then stable before the drug is released on contact with the strong acid found in the stomach. Many drug molecules (see Figure 1.23) have been successfully incorporated by ion-exchange, such as the anti-cancer drugs methotrexate[153] and camptothecin[154], and the anti-inflammatory ibuprofen[155] into Mg/Al-LDHs It has also been possible

to incorporate the anti-inflammatory drug fenbufen[156] into Mg/Al and Li/Al-LDHs during the synthesis of the LDH via the co-precipitation process.

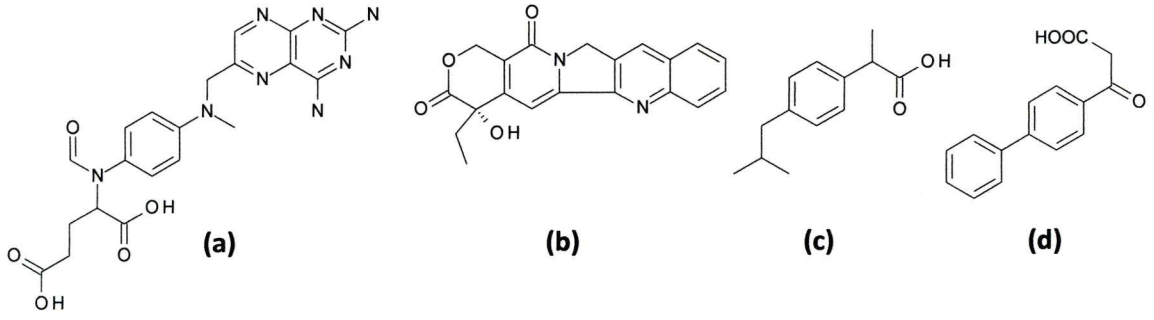

Figure 1.23 Examples of drug molecules intercalated into LDHs for drug delivery (a) methotrexate; (b) campothecin; (c) ibuprofen and (d) fenbufen

1.11.2 Layered Double Hydroxides and Isomer Separation

A surprising feature of LDH chemistry is the ability of LDHs to separate different isomers of organic compounds. Furthermore, it is possible to tune this separation according to temperature[86]. For example, if an equimolar mixture of 1,5-naphthalenedisulfonate and 2,6-naphthalenedisulfonate is stirred with $[LiAl_2(OH)_6]Cl.H_2O$ at 100°C, the 1,5-NDS isomer is preferentially intercalated over the 2,6-NDS isomer by a ratio of 98:2. However, if the reaction is repeated at 20°C, the preference is reversed with the ratio of 1,5-NDS to 2,6-NDS now being 27:73. Changing of the solvent was also found to have an effect, with the reaction repeated at 100°C with 50:50 acetonitrile:water, the ratio was 40:60 1,5:2,6 isomer, which is possibly due to the differing solvation enthalpies of the organic guests[157].

1.11.3 Trends in Layered Double Hydroxides

Recently, the focus of research into applications of layered double hydroxides has been the intercalation of materials of biological interest such as porphyrins[158], nucleosides[159], fatty acids[80], amino acids[160] and pharmaceutical molecules[161]

The first example of porphyrin intercalation into a layered double hydroxide was by Park *et al.*[162] where 5,10,15,20-Tetra(4-sulfanatophenyl)porphyrin (TSSP) was intercalated into hydrotalcite (Mg/Al-CO_3-LDH). Analysis of the interlayer separation of the material showed that the porphyrin was situated with the plane of the molecule perpendicular to the layers. This was a step forward as it had only been possible to intercalate cationic porphyrin compounds into clays whereas intercalation into LDHs allows for intercalation of anionic porphyrins. Porphyrins are compounds with interesting photochemical properties, where they can be used to induce photochemical transformations. The

use of porphyrin-intercalated LDHs was further explored by Bonnet *et al.*[158] where *meso*-Tetrakis(*p*-carboxyphenyl) porphyrin (*p*TCPP) was exchanged for the interlayer chloride in $Zn_3Al(OH)_8Cl.nH_2O$ (Zn_3Al-LDH). The thermal stability of these compounds is excellent, with analysis showing stability up to 300°C. Again, the interlayer porphyrins were situated perpendicular to the layers where other isomers intercalated, such as the *o*-carboxyphenyl porphyrin (*o*-TCPP) were situated parallel, as shown in Figure 1.24.

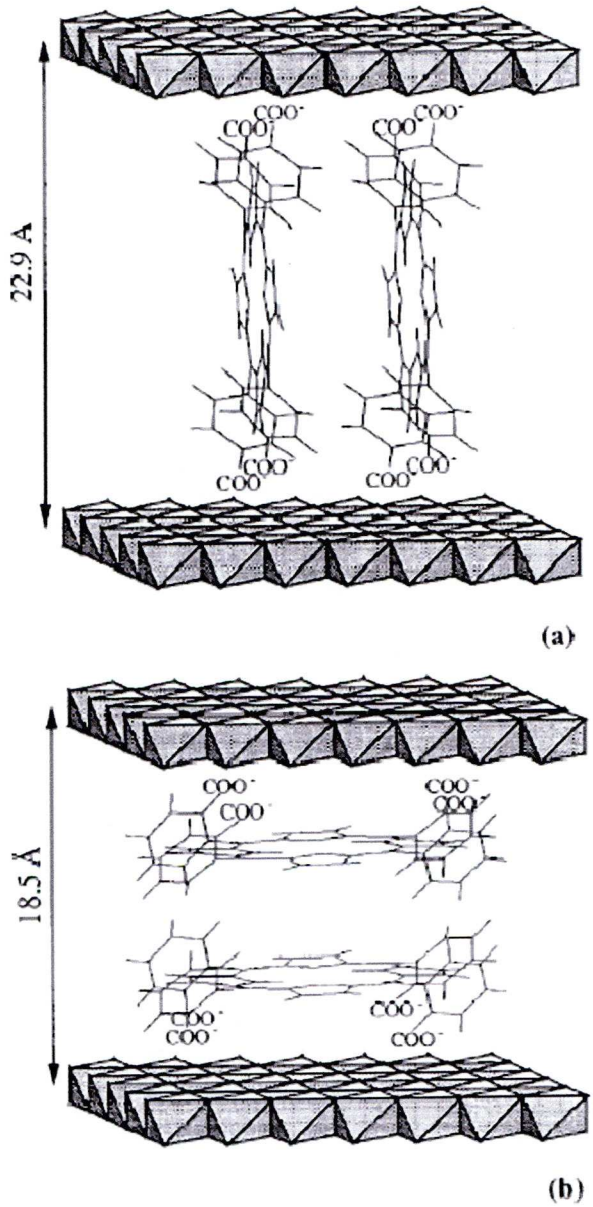

Figure 1.24[158] Orientation of porphyrin compounds between the layers of $Zn_3Al(OH)_8Cl.nH_2O$, as explored by Bonnet *et al.* (a) *meso*-Tetrakis(*p*-carboxyphenyl) porphyrin (*p*TCPP) which is oriented perpendicular to the layers, and (b) *meso*-Tetrakis(*o*-carboxyphenyl) porphyrin (*o*TCPP) oriented parallel to the layers

Intercalation of biological molecules into LDHs is also proving to be a widely studied area. Molecules such as DNA and nucleoside monophosphates are negatively charged[163], making them ideal candidates for LDH intercalation. Work by Choy *et al.*[164] has focused upon intercalation of adenosine-5'-monophosphate (AMP), guanosine-5'-monophosphate (GMP), and cytidine-5'-monophosphate (CMP) by an exchange of the interlayer nitrate in $Mg_2Al(NO_3)$-LDH. Analysis of the crystal structure shows that the biological molecules are sat perpendicular to the layers[159]. Labelling experiments using ^{32}P demonstrated the high efficiency of using the biological molecule intercalates as transfer vehicles into cells, as compared to the biological molecules alone. Another study by Lotsch *et al.*[165] showed that it was also possible to separate nucleoside monophosphates using preferential anion exchange into layered double hydroxides.

Other biological molecules such as amino acids have also been intercalated[160] into Mg/Al-NO_3-LDHs via an anion exchange method, in this case with the negative charges on glutamic acid and aspartic acid being used to hold them in place. Aisawa *et al.* have also achieved[166] intercalation of the amino acid phenylalanine into various LDHs via a co-precipitation method, finding that during the synthesis, the amount of amino acid intercalated was highly dependant on the pH of the solution. X-ray analysis shows that the amino acids were aligned perpendicular to the layers, which then allows for hydrophobic interactions such as π-π stacking to confer further stability to the interlayer amino acids.

1.12 Aims of this Thesis

This thesis aims to explore the catalytic properties of novel LDHs synthesised from gibbsite, [γ-$Al(OH)_3$], both from a point of view of the LDHs as synthesised and dispersed with Pd (as in Chapter 2) where example reactions will include the formation of MIBK from acetone in the gas phase. Previous work carried out has shown that Pd doped mixed oxide catalysts can efficiently catalyse the conversion, however, the catalysts in the literature require long and sometimes difficult syntheses. LDHs are easily synthesised and so could offer advantages in this field should they compare favourably with those already found in the literature.

Other catalytic reactions explored will be heterogeneous in nature and involve LDHs containing catalytically active anions. Tungstate will be shown to catalyse an oxidative bromination reaction, which will be discussed in depth with regards to its characterisation and reaction kinetics. A molybdate containing LDH will catalyse the oxidation of an organic molecule, citronellol. The molybdate immobilised on the LDH will be shown to be a more effective catalyst than that of

homogeneous molybdate in solution. Part of this thesis will also concern the synthesis of inorganic/organic hybrid materials, where calculations have suggested that organic molecules such as DABCO (1,4-diazabicyclo[2.2.2]octane) could act as templating molecules in the synthesis of microporous tungsten oxide[67, 167].

1.13 References

1. G. Vitins, K. West, *J. Electrochem. Soc.*, 144, **1997,** 2587-2592

2. W. Fujita, K. Awaga, *Inorg. Chem.*, 35, **1996,** 1915-1917

3. R. Clement, J.J. Girerd, I. Morgensternbadarau, *Inorg. Chem.*, 19, **1980,** 2852-2854

4. T. Matsuda, M. Udagawa, I. Kunou, *J. Catal.* , 168, **1997,** 26-34

5. D.W. Bruce, D. O'Hare, *Inorganic materials*, Wiley, 1996.

6. P.W. Stephens, L. Mihaly, P.L. Lee, R.L. Whetten, S.M. Huang, R. Kaner, F. Deiderich, K. Holczer, *Nature*, 351, **1991,** 632-634

7. G.R. Darling, A.Y. Ganin, M.J. Rosseinsky, Y. Takabayashi, K. Prassides, *Phys. Rev. Lett.*, 101, **2008,**

8. A.Y. Ganin, Y. Takabayashi, P. Jeglic, D. Arcon, A. Potocnik, P.J. Baker, Y. Ohishi, M.T. McDonald, M.D. Tzirakis, A. McLennan, G.R. Darling, M. Takata, M.J. Rosseinsky, K. Prassides, *Nature*, 466, **2010,** 221-U293

9. Y. Takabayashi, A.Y. Ganin, P. Jeglic, D. Arcon, T. Takano, Y. Iwasa, Y. Ohishi, M. Takata, N. Takeshita, K. Prassides, M.J. Rosseinsky, *Science*, 323, **2009,** 1585-1590

10. Q. Zhu, D.E. Cox, J.E. Fischer, K. Kniaz, A.R. McGhie, O. Zhou, *Nature*, 355, **1992,** 712-714

11. A.F. Hebard, M.J. Rosseinsky, R.C. Haddon, D.W. Murphy, S.H. Glarum, T.T.M. Palstra, A.P. Ramirez, A.R. Kortan, *Nature*, 350, **1991,** 600-601

12. J. Chaussy, P. Haen, J.C. Lasjaunias, P. Monceau, G. Waysand, A. Waintal, A. Meerschaut, P. Molinié, J. Rouxel, *Solid State Commun.*, 20, **1976,** 759-763

13. R.E. Thorne, *Physics Today*, 49, **1996,** 42-47

14. J.L. Hodeau, M. Marezio, C. Roucau, R. Ayroles, A. Meerschaut, J. Rouxel, P. Monceau, *J. Phys. C Solid State*, 11, **1978,** 4117-4134

15. Y.N. Xia, P.D. Yang, Y.G. Sun, Y.Y. Wu, B. Mayers, B. Gates, Y.D. Yin, F. Kim, Y.Q. Yan, *Adv. Mater.*, 15, **2003,** 353-389

16. E. Dagotto, T.M. Rice, *Science*, 271, **1996,** 618-623

17. D.C. Johnston, J.W. Johnson, D.P. Goshorn, A.J. Jacobson, *Phys. Rev. B: Condens. Matter*, 35, **1987,** 219

18. R.C. Finn, J. Zubieta, *J. Phys. Chem. Solids*, 62, **2001,** 1513-1523

19. L. Venkataraman, C.M. Lieber, *Phys. Rev. Lett.*, 83, **1999,** 5334-5337

20. J.M. Tarascon, G.W. Hull, F.J. DiSalvo, *Mater. Res. Bull.*, 19, **1984,** 915-924

21. J.H. Golden, F.J. DiSalvo, J.M.J. Frechet, J. Silcox, M. Thomas, J. Elman, *Science*, 273, **1996,** 782-784

22. F. Ribeiro, D. Roundy, M. Cohen, *Phys. Rev. B: Condens. Matter*, 65, **2002,** 153401

23. E.A.M. Lesley E. Smart, *Solid state chemistry: An introduction*, 3 ed., CRC Press, 2005.

24. Y. Koike, H. Suematsu, K. Higuchi, S. Tanuma, *Solid State Commun.*, 27, **1978,** 623-627

25. P. Marceau, L. Gautreau, F. Beguin, G. Guillaumet, *J. Organomet. Chem.*, 403, **1991,** 21-27

26. C. Herold, A. Herold, P. Lagrange, *J. Phys. Chem. Solids*, 57, **1996,** 655-662

27. L.E. Smart, E.A. Moore, *Solid state chemistry: An introduction*, 3 ed., CRC Press, 2005.

28. K.A.C. Scott M. Auerbach, Prabir K. Dutta, *Handbook of layered materials*, Marcel Dekker, Inc., 2004.

29. J.T. Kloprogge, *J. Porous. Mat.*, 5, **1998,** 5-41

30. H. Ming-Yuan, L. Zhonghui, M. Enze, *Catal. Today*, 2, **1988,** 321-338

31. M.L. Occelli, R.A. Innes, F.S.S. Hwu, J.W. Hightower, *Appl. Catal.*, 14, **1985,** 69-82

32. K. Urabe, H. Sakurai, Y. Izumi, *J. Chem. Soc., Chem. Commun.*, **1986,** 1074-1076

33. T. Matsuda, M. Matsukata, E. Kikuchi, Y. Morita, *Appl. Catal.*, 21, **1986,** 297-306

34. T. Cseri, S. Békássy, F. Figueras, S. Rizner, *J. Mol. Catal. A: Chem.*, 98, **1995,** 101-107

35. R. Burch, C.I. Warburton, *J. Catal.* , 97, **1986,** 511-515

36. G. Rytwo, D. Tropp, C. Serban, *Appl. Clay Sci.* , 20, **2002,** 273-282

37. R.L. Glass, *J. Agric. Food Chem.*, 35, **1987,** 497-500

38. A. Weidenhaupt, C. Arnold, S.R. Muller, S.B. Haderlein, R.P. Schwarzenbach, *Environ. Sci. Technol.*, 31, **1997,** 2603-2609

39. H. Babich, G. Stotzky, *Appl. Environ. Microbiol.*, 33, **1977,** 696-705

40. G. Suraj, C.S.P. Iyer, M. Lalithambika, *Appl. Clay Sci.* , 13, **1998,** 293-306

41. B.M.L. Rao, R.W. Francis, *J. Phys. Chem. Solids*, 37, **1976,** 345-345

42. E.J. Frazer, S. Phang, *J. Power Sources*, 6, **1981,** 307-317

43. M.B. Dines, *Mater. Res. Bull.*, 10, **1975,** 287-291

44. N.N. Greenwood, A. Earnshaw, *Chemistry of the elements*, 2 ed., Butterworth Heinemann, 2002.

45. S.J. Hibble, P.G. Dickens, J.C. Evison, *J. Chem. Soc., Chem. Commun.*, **1985,** 1809-1810

46. G.T. Kokotailo, S.L. Lawton, D.H. Olson, W.M. Meier, *Nature*, 272, **1978,** 437-438

47. S. Kitagawa, R. Kitaura, S. Noro, *Angew. Chem., Int. Ed.*, 43, **2004,** 2334-2375

48. J.L.C. Rowsell, O.M. Yaghi, *Microporous Mesoporous Mater.*, 73, **2004,** 3-14

49. M. Eddaoudi, H.L. Li, O.M. Yaghi, *J. Am. Chem. Soc.*, 122, **2000,** 1391-1397

50. K. Iwanami, H. Seo, J.C. Choi, T. Sakakura, H. Yasuda, *Tetrahedron*, 66, **2010,** 1898-1901

51. C.-D. Wu, A. Hu, L. Zhang, W. Lin, *J. Am. Chem. Soc.*, 127, **2005,** 8940-8941

52. P.B. Weisz, V.J. Frilette, *J. Phys. Chem. B*, 64, **1960,** 382-382

53. S. Altwasser, R. Gläser, J. Weitkamp, *Microporous Mesoporous Mater.*, 104, **2007,** 281-288

54. C.E. Gounaris, C.A. Floudas, J. Wei, *Chem. Eng. Sci.* , 61, **2006,** 7933-7948

55. S.M. Csicsery, *J. Org. Chem.* , 34, **1969,** 3338-&

56. S.M. Csicsery, *Zeolites*, 4, **1984,** 202-213

57. J. Lee, O.K. Farha, J. Roberts, K.A. Scheidt, S.T. Nguyen, J.T. Hupp, *Chem. Soc. Rev.*, 38, **2009,** 1450-1459

58. J. Coronas, *Chem. Eng. J.*, 156, **2010,** 236-242

59. M.E. Davis, R.F. Lobo, *Chem. Mater.*, 4, **1992,** 756-768

60. N.L. Rosi, J. Eckert, M. Eddaoudi, D.T. Vodak, J. Kim, M. O'Keeffe, O.M. Yaghi, *Science*, 300, **2003,** 1127-1129

61. M. Eddaoudi, J. Kim, N. Rosi, D. Vodak, J. Wachter, M. O'Keeffe, O.M. Yaghi, *Science*, 295, **2002,** 469-472

62. B. Panella, M. Hirscher, H. Putter, U. Muller, *Adv. Funct. Mater.*, 16, **2006,** 520-524

63. J. Li, R. Kuppler, H. Zhou, *Chem. Soc. Rev.*, 38, **2009,** 1477-1504

64. S. Bourrelly, P. Llewellyn, C. Serre, F. Millange, T. Loiseau, G. Ferey, *J. Am. Chem. Soc.*, 127, **2005,** 13519-13521

65. M.E. Straumanis, *J. Am. Chem. Soc.*, 71, **1949,** 679-683

66. K.A. Muller, J.G. Bednorz, *Science*, 237, **1987,** 1133-1139

67. F. Cora, D.W. Lewis, C.R.A. Catlow, *Chem. Commun.*, **1998,** 1943-1944

68. E.O. Brimm, J.C. Brantley, J.H. Lorenz, M.H. Jellinek, *J. Am. Chem. Soc.*, 73, **1951,** 5427-5432

69. A.R. Sweedler, C.J. Raub, B.T. Matthias, *Phys. Lett.*, 15, **1965,** 108-&

70. L.E. Conroy, G. Podolsky, *Inorg. Chem.*, 7, **1968,** 614-&

71. P.J. Wiseman, P.G. Dickens, *J. Solid State Chem.*, 17, **1976,** 91-100

72. F. Takusagawa, R.A. Jacobson, *J. Solid State Chem.*, 18, **1976,** 163-174

73. A. Ramanan, J. Gopalakrishnan, M.K. Uppal, D.A. Jefferson, C.N.R. Rao, *Proc. R. Soc. A*, 395, **1984,** 127-139

74. H. Saalfeld, M. Wedde, *Zeitschrift Fur Kristallographie*, 139, **1974,** 129-135

75. G. Yamaguchi, K. Sakamoto, *Bull. Chem. Soc. Jpn.*, 31, **1958,** 140-141

76. H.J. Bosmans, *Acta Crystallogr., Sect. B: Struct. Sci.* , B 26, **1970,** 649-&

77. G.Y. Chao, J. Baker, A.P. Sabina, A.C. Roberts, *Can. Mineral.*, 23, **1985,** 21-28

78. H.Z. Liu, J.S. Tse, J.Z. Hu, Z.X. Liu, L.H. Wang, J.H. Chen, D.K. Weidner, Y. Meng, D. Hausermann, H.K. Mao, *J. Phys. Chem. B*, 109, **2005,** 8857-8860

79. *Acta Crystallogr., Sect. B: Struct. Sci.* , 24, **1968,** 972-977

80. M. Meyn, K. Beneke, G. Lagaly, *Inorg. Chem.*, 29, **1990,** 5201-5207

81. M.R. Weir, J. Moore, R.A. Kydd, *Chem. Mater.*, 9, **1997,** 1686-1690

82. A.V. Besserguenev, A.M. Fogg, R.J. Francis, S.J. Price, D. Ohare, V.P. Isupov, B.P. Tolochko, *Chem. Mater.*, 9, **1997,** 241-247

83. L. Pesic, S. Salipurovic, V. Markovic, D. Vucelic, W. Kagunya, W. Jones, *J. Mater. Chem.*, 2, **1992,** 1069-1073

84. G.W. Brindley, S. Kikkawa, *Am. Mineral.* , 64, **1979,** 836-843

85. P.J. Sideris, U.G. Nielsen, Z.H. Gan, C.P. Grey, *Science*, 321, **2008,** 113-117

86. A.I. Khan, D. O'Hare, *J. Mater. Chem.*, 12, **2002,** 3191-3198

87. C.J. Serna, J.L. White, S.L. Hem, *Clays Clay Miner.*, 25, **1977,** 384-391

88. A.M. Fogg, G.R. Williams, R. Chester, D. O'Hare, *J. Mater. Chem.*, 14, **2004,** 2369-2371

89. W.T. Reichle, *Solid State Ionics*, 22, **1986,** 135-141

90. B.F. Sels, D.E. De Vos, M. Buntinx, P.A. Jacobs, *J. Catal.* , 216, **2003,** 288-297

91. F. Cavani, F. Trifiro, A. Vaccari, *Catal. Today*, 11, **1991,** 173-301

92. V. Rives, *Layered double hydroxides: Present and future*, Nova Science Publishers, 2001.

93. A.M. Fogg, A.J. Freij, G.M. Parkinson, *Chem. Mater.*, 14, **2002,** 232-234

94. T.J. Pinnavaia, *Science*, 220, **1983,** 365-371

95. K.J. Martin, T.J. Pinnavaia, *J. Am. Chem. Soc.*, 108, **1986,** 541-542

96. E. Suzuki, M. Okamoto, Y. Ono, *Chem. Lett.*, **1989,** 1485-1486

97. E. Lopez-Salinas, N. Tomita, T. Matsui, E. Suzuki, Y. Ono, *J. Mol. Catal. A: Chem.*, 81, **1993,** 397-405

98. B.F. Sels, D.E. De Vos, P.A. Jacobs, *Catal. Rev. - Sci. Eng.* , 43, **2001,** 443-488

99. D. Tichit, M.H. Lhouty, A. Guida, B.H. Chiche, F. Figueras, A. Auroux, D. Bartalini, E. Garrone, *J. Catal.* , 151, **1995,** 50-59

100. W. Kagunya, Z. Hassan, W. Jones, *Inorg. Chem.*, 35, **1996,** 5970-5974

101. F. van Laar, D.E. De Vos, F. Pierard, A.K. De Mesmaeker, L. Fiermans, P.A. Jacobs, *J. Catal.* , 197, **2001,** 139-150

102. C.M. Jinesh, C.A. Antonyraj, S. Kannan, *Catal. Today*, 141, **2009,** 176-181

103. F. Li, X.R. Jiang, D.G. Evans, X. Duan, *J. Porous. Mat.*, 12, **2005,** 55-63

104. A. Guida, M.H. Lhouty, D. Tichit, F. Figueras, P. Geneste, *Appl. Catal., A*, 164, **1997,** 251-264

105. F. Trifirò, A. Vaccari, O. Clause, *Catal. Today*, 21, **1994,** 185-195

106. J.P. Jacobs, A. Maltha, J.G.H. Reintjes, J. Drimal, V. Ponec, H.H. Brongersma, *J. Catal.* , 147, **1994,** 294-300

107. Y.G. Chen, J. Ren, *Catal. Lett.*, 29, **1994,** 39-48

108. H. Shimada, T. Ogoshi, *Bull. Chem. Soc. Jpn.*, 78, **2005,** 937-939

109. S. Velu, C.S. Swamy, *Appl. Catal., A*, 119, **1994,** 241-252

110. S. Velu, C.S. Swamy, *Appl. Catal., A* 162, **1997,** 81-91

111. J. Santhanalakshmi, T. Raja, *Appl. Catal., A* 147, **1996,** 69-80

112. J.J. Yu, Y.X. Tao, C.C. Liu, Z.P. Hao, Z.P. Xu, *Environ. Sci. Technol.*, 41, **2007,** 1399-1404

113. K.K. Rao, M. Gravelle, J.S. Valente, F. Figueras, *J. Catal.* , 173, **1998,** 115-121

114. M.J. Climent, A. Corma, S. Iborra, J. Primo, *J. Catal.* , 151, **1995,** 60-66

115. D. Tichit, M.N. Bennani, F. Figueras, R. Tessier, J. Kervennal, *Appl. Clay Sci.* , 13, **1998,** 401-415

116. D. Tichit, B. Coq, S. Cerneaux, R. Durand, *Catal. Today*, 75, **2002,** 197-202

117. S. Abelló, F. Medina, D. Tichit, J. Pérez-Ramírez, X. Rodríguez, J.E. Sueiras, P. Salagre, Y. Cesteros, *Appl. Catal., A* 281, **2005,** 191-198

118. F. Malherbe, C. Depege, C. Forano, J.P. Besse, M.P. Atkins, B. Sharma, S.R. Wade, *Appl. Clay Sci.* , 13, **1998,** 451-466

119. E. Dumitriu, C. Guimon, A. Cordoneanu, S. Casenave, T. Hulea, C. Chelaru, H. Martinez, V. Hulea, *Catal. Today*, 66, **2001,** 529-534

120. K.Z. Zhu, C.B. Liu, X.K. Ye, Y. Wu, *Appl. Catal., A*, 168, **1998,** 365-372

121. C.B. Liu, X.K. Ye, R.Y. Zhan, Y. Wu, *J. Mol. Catal. A: Chem.*, 112, **1996,** 15-22

122. R. Prihod'ko, M. Sychev, I. Kolomitsyn, P.J. Stobbelaar, E.J.M. Hensen, R.A. van Santen, *Microporous Mesoporous Mater.*, 56, **2002,** 241-255

123. S. Ueno, K. Yamaguchi, K. Yoshida, K. Ebitani, K. Kaneda, *Chem. Commun.*, **1998,** 295-296

124. D. Kishore, S. Kannan, *Appl. Catal., A*, 270, **2004,** 227-235

125. Q. Wang, Y. Yang, Y. Li, W. Yu, Z.H. Hou, *Tetrahedron*, 62, **2006,** 6107-6112

126. R.D. Hetterley, R. Mackey, J.T.A. Jones, Y.Z. Khimyak, A.M. Fogg, I.V. Kozhevnikov, *J. Catal.* , 258, **2008,** 250-255

127. K. Takehira, *J. Nat. Gas Chem.*, 18, **2009,** 237-259

128. D. Li, Y. Zhan, K. Nishida, Y. Oumi, T. Sano, T. Shishido, K. Takehira, *Appl. Catal., A*, 363, **2009,** 169-179

129. S.Y. Liu, X.Z. Jiang, G.L. Zhuo, *J. Mol. Catal. A: Chem.*, 290, **2008,** 72-78

130. T. Mitsudome, A. Noujima, T. Mizugaki, K. Jitsukawa, K. Kaneda, *Green Chem.* , 11, **2009,** 793-797

131. M. Mora, C. Jiménez-Sanchidrián, J.R. Ruiz, *J. Colloid Interface Sci.*, 302, **2006,** 568-575

132. Á. Mastalir, Z. Király, *J. Catal.* , 220, **2003,** 372-381

133. J. Wang, Y. Tian, R.C. Wang, A. Clearfield, *Chem. Mater.*, 4, **1992,** 1276-1282

134. J. Evans, M. Pillinger, J. Zhang, *J. Chem. Soc., Dalton Trans.*, **1996,** 2963-2974

135. J.D. Wang, G. Serrette, Y. Tian, A. Clearfield, *Appl. Clay Sci.* , 10, **1995,** 103-115

136. M.A. Drezdzon, *Inorg. Chem.*, 27, **1988,** 4628-4632

137. H.C. Greenwell, W. Jones, S.L. Rugen-Hankey, P.J. Holliman, R.L. Thompson, *Green Chem.* , 12, **2010,** 688-695

138. T. Kwon, G.A. Tsigdinos, T.J. Pinnavaia, *J. Am. Chem. Soc.*, 110, **1988,** 3653-3654

139. C. Hu, X. Zhang, L. Xu, B. Mu, W. Zu, E. Wang, *Appl. Clay Sci.* , 13, **1998,** 495-511

140. S.K. Jana, Y. Kubota, T. Tatsumi, *J. Catal.* , 255, **2008,** 40-47

141. Y. Guo, D. Li, C. Hu, Y. Wang, E. Wang, *Int. J. Inorg. Mater.*, 3, **2001,** 347-355

142. M.L. Kantam, M. Roy, S. Roy, M.S. Subhasa, B. Sreedhar, B.M. Choudary, *Synlett*, **2006,** 2266-2268

143. M.L. Kantam, B.V. Prakash, C.R.V. Reddy, B. Sreedhar, *Synlett*, **2005,** 2329-2332

144. M. Halma, K.A.D.d.F. Castro, V. Prévot, C. Forano, F. Wypych, S. Nakagaki, *J. Mol. Catal. A: Chem.*, 310, **2009,** 42-50

145. B. Monteiro, S. Gago, S.S. Balula, A.A. Valente, I.S. Gonçalves, M. Pillinger, *J. Mol. Catal. A: Chem.*, 312, **2009,** 23-30

146. M. Chibwe, L. Ukrainczyk, S.A. Boyd, T.J. Pinnavaia, *J. Mol. Catal. A: Chem.*, 113, **1996,** 249-256

147. M. Hughes, R.H. Prince, *Bioorg. Chem.*, 6, **1977,** 137-155

148. J. McMurry, *Organic chemistry*, 5 ed., Brooks/Cole, 2000.

149. J.W. Boclair, P.S. Braterman, B.D. Brister, J.P. Jiang, S.W. Lou, Z.M. Wang, F. Yarberry, *Origins of Life and Evolution of the Biosphere*, 31, **2001,** 53-69

150. J. Oro, S.S. Kamat, *Nature*, 190, **1961,** 442-&

151. J. Oro, *Nature*, 191, **1961,** 1193-&

152. R. Sanchez, J. Ferris, L.E. Orgel, *Science*, 153, **1966,** 72-&

153. J.-M. Oh, M. Park, S.-T. Kim, J.-Y. Jung, Y.-G. Kang, J.-H. Choy, *J. Phys. Chem. Solids*, 67, 1024-1027

154. K.M. Tyner, S.R. Schiffman, E.P. Giannelis, *J. Controlled Release*, 95, **2004,** 501-514

155. V. Ambrogi, G. Fardella, G. Grandolini, L. Perioli, *Int. J. Pharm.*, 220, **2001,** 23-32

156. B. Li, J. He, D. G. Evans, X. Duan, *Appl. Clay Sci.* , 27, **2004,** 199-207

157. A.M. Fogg, V.M. Green, H.G. Harvey, D. O'Hare, *Adv. Mater.*, 11, **1999,** 1466-1469

158. S. Bonnet, C. Forano, A. deRoy, J.P. Besse, P. Maillard, M. Momenteau, *Chem. Mater.*, 8, **1996,** 1962-1968

159. J. Choy, S. Kwak, J. Park, Y. Jeong, *J. Mater. Chem*, 11, **2001,** 1671-1674

160. N. Whilton, P. Vickers, S. Mann, *J. Mater. Chem*, 7, **1997,** 1623-1629

161. M. Del Arco, E. Cebadera, S. Gutierrez, C. Martin, M.J. Montero, V. Rives, J. Rocha, M.A. Sevilla, *Journal of Pharmaceutical Sciences*, 93, **2004,** 1649-1658

162. I.Y. Park, K. Kuroda, C. Kato, *Chem. Lett.*, **1989,** 2057-2058

163. J. Radler, I. Koltover, T. Salditt, C. Safinya, *Science*, 275, **1997,** 810-814

164. J. Choy, S. Kwak, J. Park, Y. Jeong, J. Portier, *J. Am. Chem. Soc.*, 121, **1999,** 1399-1400

165. B. Lotsch, F. Millange, R. Walton, D. O'Hare, *Solid State Sci.*, 3, **2001,** 883-886

166. S. Aisawa, S. Takahashi, W. Ogasawara, Y. Umetsu, E. Narita, *J. Solid State Chem.*, 162, **2001,** 52-62

167. D.W. Lewis, D.J. Willock, C.R.A. Catlow, J.M. Thomas, G.J. Hutchings, *Nature*, 382, **1996,** 604-606

Chapter 2: Pd Doped Layered Double Hydroxides as Catalysts for the One-Pot Synthesis of MIBK

2.1 Introduction

2.1.1 Layered Double Hydroxides Doped with Noble Metals

The use of LDHs in catalysis is expanded upon by the doping of noble metals onto the LDH structure. This is a widely explored area, useful where a bi-functional catalyst is needed. An example of this application is in hydrocarbon reforming, an essential method for producing valuble chemical feedstocks. Here, Ni/Mg/Al based hydrotalcites were being deactivated in the presence of steam. Doping of the LDH with Pt solved this problem[1-2], making the process more efficient. The use of doped LDHs can also be used for fine chemical synthesis. An example of this is the Heck reaction, catalysed by Pd-doped LDHs[3].

2.1.2 Synthesis of Methyl Isobutyl Ketone (MIBK)

Methyl isobutyl ketone (MIBK) is an industrial solvent used mainly in the paint industry. It is made by the condensation of two molecules of acetone, forming diacetone alcohol (DA), followed by an acid catalysed dehydration step forming mesityl oxide (MO). In the final step, the MO is then subjected to a metal catalysed hydrogenation to MIBK (see Figure 2.1).

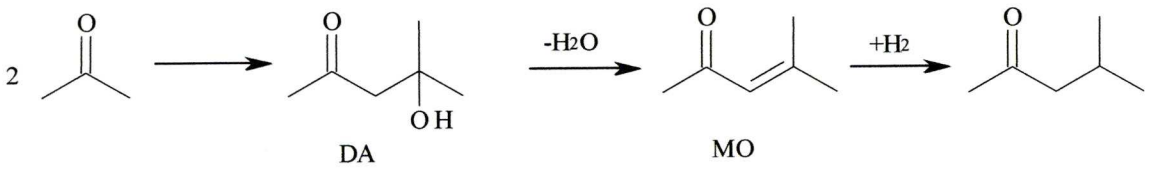

Figure 2.1 MIBK synthesis

The method used to synthesise MIBK is typically the base condensation of acetone, using $Ba(OH)_2$[4], which involves refluxing the acetone for 95-120 hours in order to obtain around an 80% yield of DA. This is followed by a distillation which takes a further 4 hours. The DA is then dehydrated by adding concentrated sulphuric acid to the DA and simultaneously heating and distilling the MO[5]. The MIBK

is then obtained by metal (e.g. Ni, Cu, Pd) catalysed hydrogenation. Clearly this process is very energy intensive. There are also problems with corrosion and salt waste disposal associated with the use and neutralisation of concentrated sulphuric acid.

Heterogeneous catalysts offer the advantages of easy separation after completion of the reaction. Significant research has been carried out into the use of multifunctional metal based catalysis where the metals provide acidic/basic functionalities and are capable of carrying out the reaction in a single step, without the need to isolate either the DA or the MO intermediates. Furthermore, such catalysts are often reusable, with the possibility of regeneration of the catalyst. Pd is frequently used in the final step as this selectively hydrogenates the C=C bond and not the C=O bond in MO[6]. Industrially, one step systems employ Pd-doped acid resins and Pd doped zirconium phosphates in the liquid phase at temperatures ranging from 120-160°C and pressures of 20-50 bar H_2. This gives MIBK selectivities of 95% at 30-40% acetone conversion[7]. Obviously these high operating pressures contribute significantly to the overall cost of the process, which has focussed the research into carrying out the reaction in the gas phase, at ambient pressure. Research in this area includes supporting Pd on heteropoly acid[8], Zn-Cr mixed oxides[9], zeolites (ZSM-5)[10], faujasites X and Y[11], $AlPO_4$-11 and SAPO-11[12], compared in Table 2.1. From these studies it is noted that the reaction temperatures are in the range 100-300°C and that the selectivities to MIBK in gas phase fixed bed type reactors are lower than those in liquid batch reactors. It is usually found that de-activation of the catalyst is also a problem. The proposed mechanism of the synthesis of MIBK is shown in Figure 2.2[13]. Acetone condensation occurs to form diacetone alcohol (DA), acid dehydration of DA then forms mesityl oxide (MO), before the C=C bond is selectively hydrogenated (over the C=O bond) to form MIBK[14]. As the reaction to form MIBK occurs, an undesirable side reaction occurs, with the Pd catalysed hydrogenation of the C=O group in acetone, giving isopropanol (IP). IP can then be dehydrated on acidic sites to propene, which can then be hydrogenated over Pd sites to form propane. Because of this side reaction, the formation of MIBK is highly dependant on the relative rates of both sets of reactions, and can be tuned to favour the formation of MIBK[15], by ensuring the catalyst is of the correct basicity, allowing the rate of condensation of the two acetone molecules to be greater than that of the hydrogenation of the C=O bond. Further to these two sets of reactions, it is also possible for condensation products of MIBK to form as shown in Figure 2.3, where MIBK can condense with either a further molecule of acetone, or another molecule of MIBK.

Catalyst[a]	Acetone conversion (%)[b]	Selectivity (%)		
		C_3 gases	MIBK	DIBK
0.5% Pd/CsPW [16]	13.3	2.9	82.6	8.2
1%Pd on Zn-Cr mixed oxide[17]	42.0	0.8	77.6	14.9
Pd/SAPO-11[12]	30.6	11.9	84.2	1.3

Table 2.1 Comparison of literature values for acetone conversion *vs.* selectivity for various systems in the conversion of acetone to MIBK

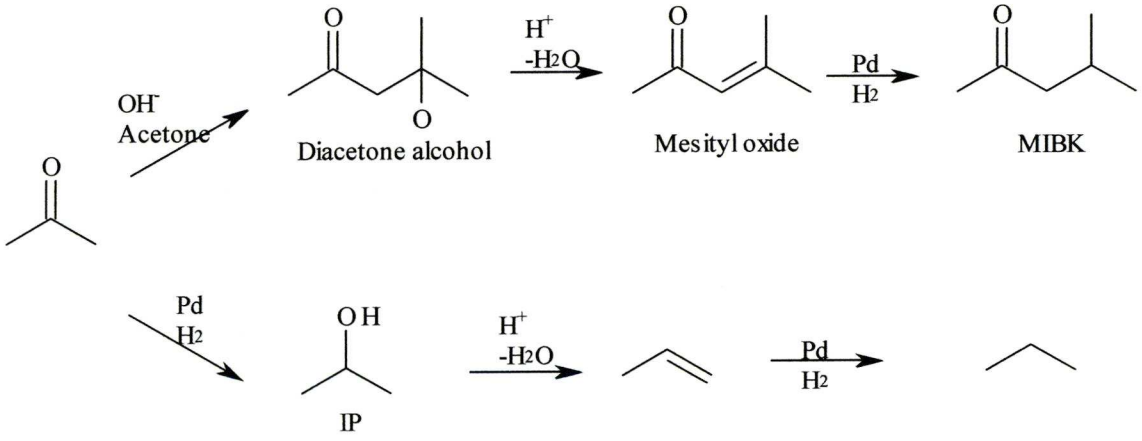

Figure 2.2 MIBK synthesis and side reaction forming propane

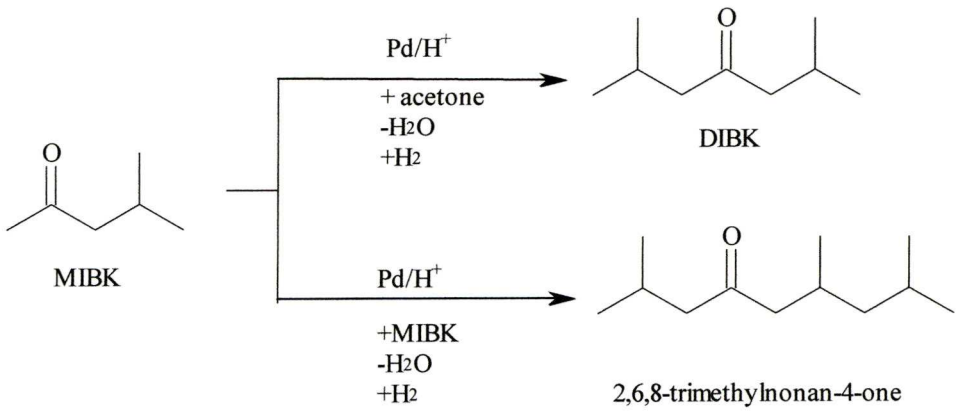

Figure 2.3 Possible condensation reactions involving MIBK

2.2 Gas Phase Reactions

2.2.1 Catalyst Characterisation

The LDH catalysts were prepared as described in Section 6.2 of the experimental chapter. After synthesis, the LDHs were ground before being impregnated with Pd by suspension in a solution of $Pd(OAC)_2$ in benzene. The doped LDHs were then reduced in a stream of H_2 at 250°C for 2 hours[17], in order to convert the Pd^{2+} to Pd^0. Following this reduction, the LDH structure changed dramatically, forming a mixed oxide structure. The resulting catalyst contained 0.65% ± 0.05% wt Pd.

Gibbsite γ-$[Al(OH)_3]$ - the starting material for all the LDHs synthesised for this study, and the LDHs themselves were initially analysed using PXRD, prior to doping with Pd. The data from which can be seen in Figure 2.4. Figure 2.4(a) shows a PXRD pattern for the batch of gibbsite used for all LDH syntheses mentioned here. Figures (b) to (g) show the LDHs as synthesised-showing successful synthesis in all cases. Each LDH as synthesised gave good agreement with literature values[18-19] on interlayer separations, with Li-OH-LDH (Figure 2.4 (b)) being 7.4 Å, Li-NO_3-LDH being 8.9 Å (Figure 2.4 (c)) and the MAl_4-LDHs (Figure 2.4 (d) to (g))having interlayer separations of 8.5 Å. In the case of the nitrate containing materials, there remains a small amount of unreacted gibbsite as is typical for these materials. In the case of Cu-LDH there was also an impurity phase in the form of $Cu(NO_3)(OH)_3$, as is typical for this synthesis[19].

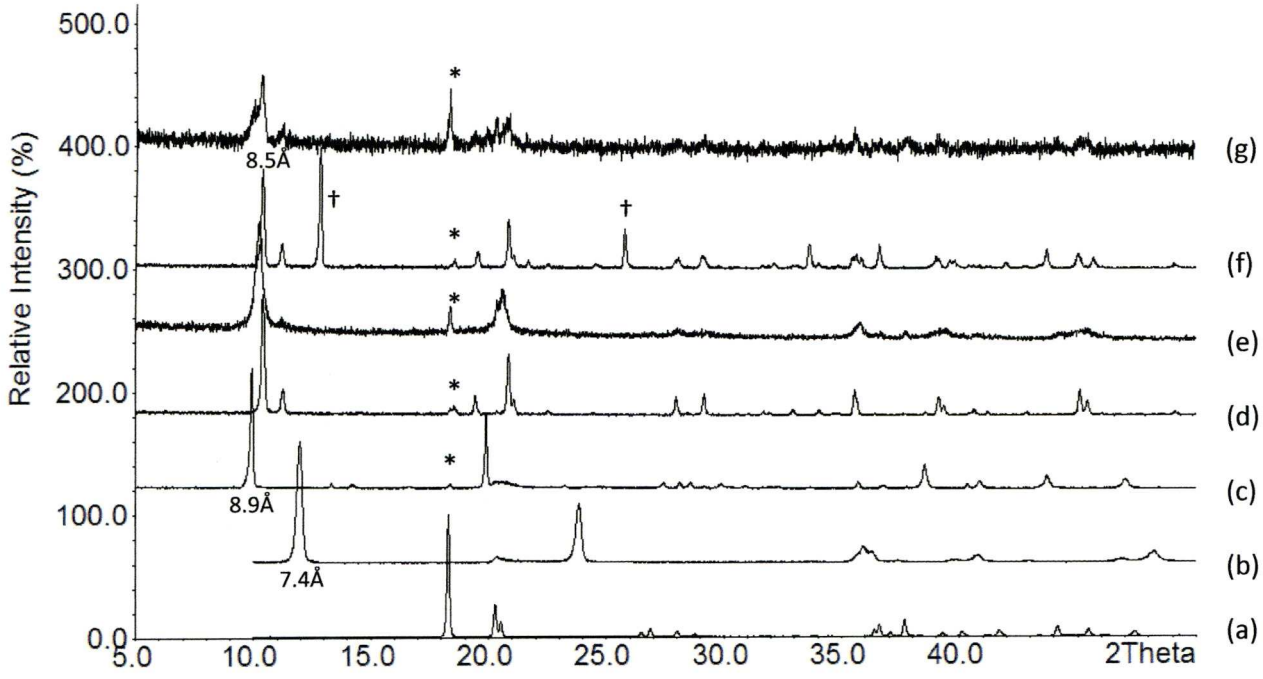

Figure 2.4 PXRD patterns for (a) gibbsite, (b) Li-OH-LDH, (c) Li-NO_3-LDH, (d) Zn-LDH, (e) Ni-LDH, (f) Cu-LDH and (g) Co-LDH

*Note: * denote small amounts of gibbsite impurities, † in Cu-LDH denote $Cu_2(NO_3)(OH)_3$ impurity phase*

Thermogravimetric analysis (TGA) was also performed on the parent LDH materials. The TGA traces for Li-NO_3-LDH (curve b) and Li-OH-LDH (curve a) are shown in figure 2.5. In the case of Li-NO3-LDH, three mass losses are observed which is characteristic of LDHs. The first mass loss occurs with the removal of interlayer water-8.3% (calculated 7.4%). Next a mass loss of 23.5% occurs (calculated 22.3%) with dehydroxylation of the layers and subsequent decomposition, leaving a mostly amorphous material with nominal composition $0.5Li_2O + Al_2O_3$ with a mass loss of 20.2% (calculated 22.2%). Further heating to 1000°C gives the crystalline phases $LiAl_5O_8$ and $LiAlO_2$[20]. The mass losses for the Li-OH-LDH were somewhat less distinct, however it is possible to see that a total loss of 44.4% (calculated 45.9%) had occurred by 600°C.

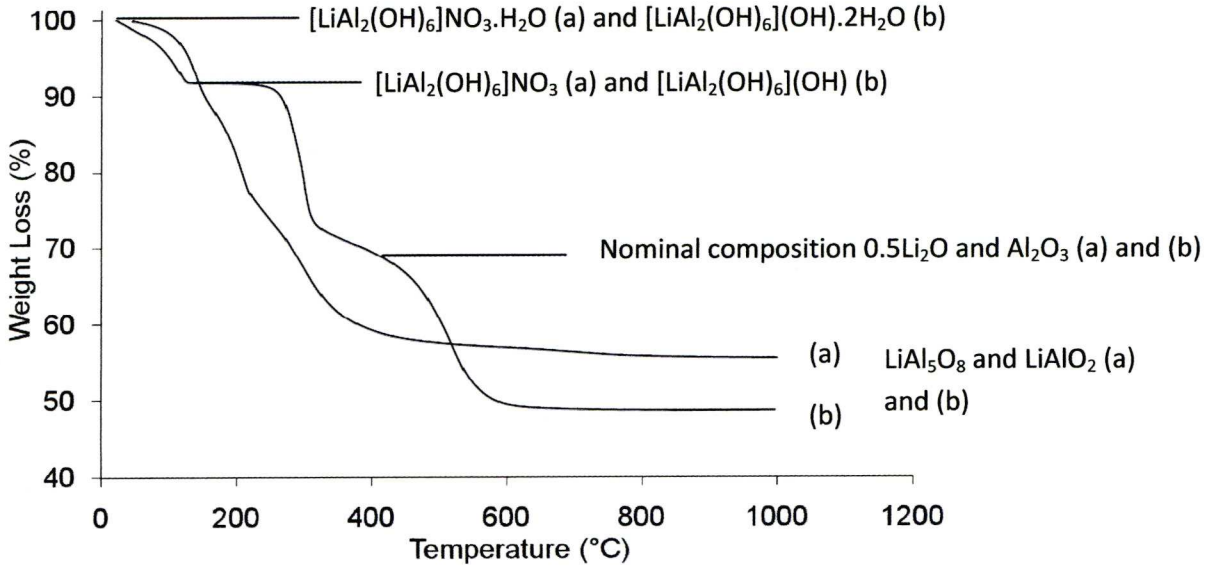

Figure 2.5 TGA Traces for (a) Li-OH-LDH and (b) Li-NO_3-LDH

Catalysts prepared by suspension in a solution of $Pd(OAc)_2$ were analysed by PXRD and were found to have no changes to their bulk structure, as shown in Figure 2.6 for the Li/Al-NO_3-LDH based catalyst. The peak at around 10° 2Θ in the Li/Al-NO_3-LDH pattern (Figure 2.6 (b)) is the interlayer separation for Li/Al-LDH with a nitrate ion between the layers. This does not change in the pattern taken after impregnation with Pd by stirring in $Pd(OAC)_2$, indicating that no anion exchange has occurred and that nitrate is still between the layers. This strongly indicates that only surface adsorption takes place. Upon reduction under H_2 at 250°C for 2 hours, a large loss of crystallinity is noted (as shown in Figure 2.6 (e)), this is consistent with the Pd^{2+} being simultaneously reduced along with the LDH after the capture of H_2. When the parent LDH is calcined at 250°C, it is found that along with a largely amorphous material, crystalline $LiNO_3$ is also present[21]. The presence of Pd as a dopant appears to suppress this. Elemental analyses were conducted on both the pristine Li-NO_3-LDH and the Pd doped sample after reduction, results of which are shown in Table 2.2, with similar analyses completed for Ni-LDH and the Pd-doped sample (Table 2.3). This indicated a near total loss of nitrogen from the sample upon reduction. This is further evidence towards the collapse of the LDH structure under the reducing conditions employed here, with the formation of a mixed oxide containing Pd metal. As can also be seen from Figure 2.6 ((e) and (f)), little bulk structural change takes place during the catalytic process, with calcination products such as $LiAl_5O_8$ and $LiAlO_2$ (as well as PdO for doped catalysts) not forming until much high temperatures Figure 2.6 (g).

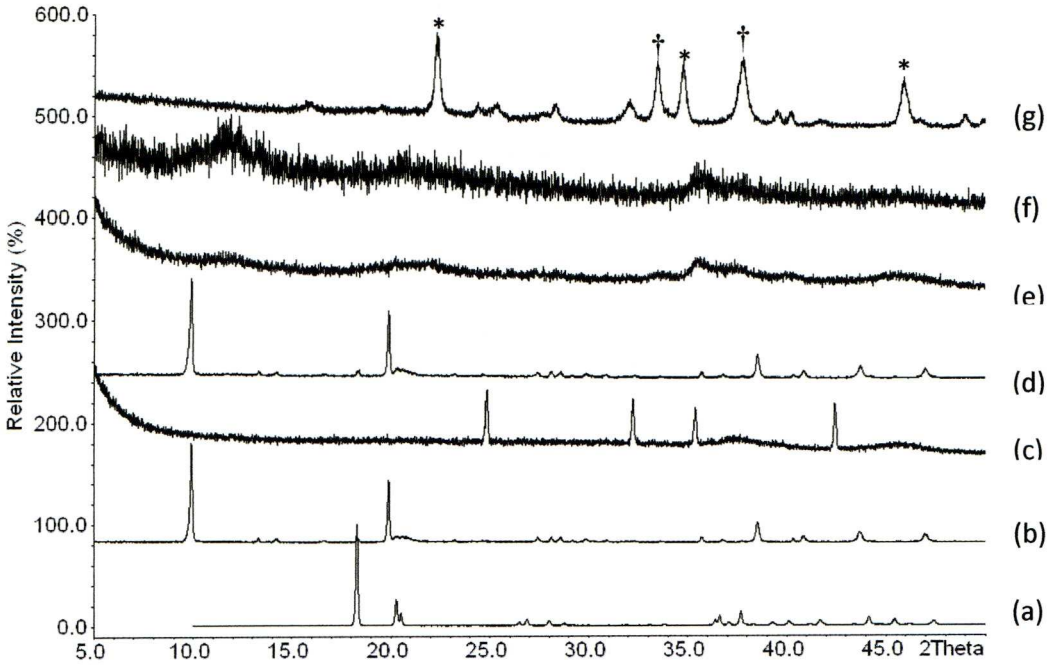

Figure 2.6 PXRD patterns of (a) gibbsite, (b)Li-NO_3-LDH as synthesised, (c) Li-NO_3-LDH calcined at 250°C, (d) Pd doped Li-NO_3-LDH, (e) Pd doped Li-NO_3-LDH after reduction in H_2 for 2 hours at 250°C, (f)Pd doped Li-NO_3-LDH after use for gas phase conversion of acetone to MIBK (6 hours on stream, 250°C), (g) Pd doped Li-NO_3-LDH after use in catalysed reaction, calcined in air at 1000°C

Note: corresponds to $LiAl_5O_8$ phase*

† corresponds to $LiAlO_2$ phase

LDH	**$[LiAl_2(OH)_6]NO_3.H_2O$ [(a)]**		**$[LiAl_2(OH)_6]NO_3.H_2O$ doped with 0.65% Pd[(b)].**	**$[LiAl_2(OH)_6]NO_3.H_2O$ doped with 0.65% Pd[(b)].**
Element	**Calculated**	**Found**	**Calculated**	**Found**
Li	2.8	3.4	4.1	4.2
Al	21.4	26.4	24.1	24.3
N	5.6	6.4	0.11	0.12
H	3.6	1.4	0.99	1.0

Table 2.2 Elemental Analysis for (a) Pristine Li/Al-NO_3-LDH and (b) Li/Al-NO_3-LDH after being doped with Pd and reduced under H_2 at 250°C. Calculated values based on formula of nominal composition $Pd_{0.012}(Li_2O)_{0.5}Al_2O_3\ (NO_3)_{0.017}(OH)_2CO_3$

LDH	$[NiAl_4(OH)_{12}](NO_3).H_2O$ [a]		Ni-LDH-LDH doped with 0.65% Pd[b]	Ni-LDH-LDH doped with 0.65% Pd[b]
Element	**Calculated**	**Found**	**Calculated**	**Found**
Ni	10.7	10.27	15.58	15.58
Al	19.7	18.96	26.49	26.88
N	5.1	5.06	0	0
H	3.3	3.08	1.43	1.47
C	0	1.05	1.32	1.35

Table 2.3 Elemental Analysis for (a) Pristine Ni-LDH and (b) Ni-LDH after being doped with Pd and reduced under H_2. Calculated values based on formula of nominal composition $Pd_{0.012}(NiO)_{0.5}Al_2O_3(CO_3)_{0.22}(OH)_{2.5}$

Further catalyst characterization was possible using ^{27}Al MAS NMR. A ^{27}Al NMR of the starting material for the LDH structure, gibbsite, as shown in Figure 2.7 (a) gave two resonances at -2.8 and 7.7ppm. This is consistent with the fact that gibbsite has two distinct aluminium sites[20, 22]. Further NMR studies were then conducted on the Li-NO_3-LDH material both before and after impregnation with $Pd(OAc)_2$ showing great similarities with a resonance at 8.4ppm indicating the presence of octahedral Al sites (Figure 2.7 (b) and (c)). This is consistent with the PXRD results showing no change to the bulk material after doping with $Pd(OAc)_2$. After reduction under H_2, the NMR shows an addition broad line at 74ppm, indicative of tetrahedrally coordinated Al. Broadening of the octahedral Al peak was also noted (Figure 2.7 (e)) consistent with PXRD data showing an amorphous phase forming upon collapse of the LDH structure. Upon testing of the used catalyst, it was noted that there were an increased proportion of tetrahedral Al sites, due to the formation of $LiAl_5O_8$, which, having an inverse spinel structure has 2 Al cations on tetrahedral sites[20]. In agreement with the PXRD, these sites are much more prevalent after calcination at 1000°C. ^7Li NMR spectra all exhibited single peaks at 0.16ppm (Figure 2.8).

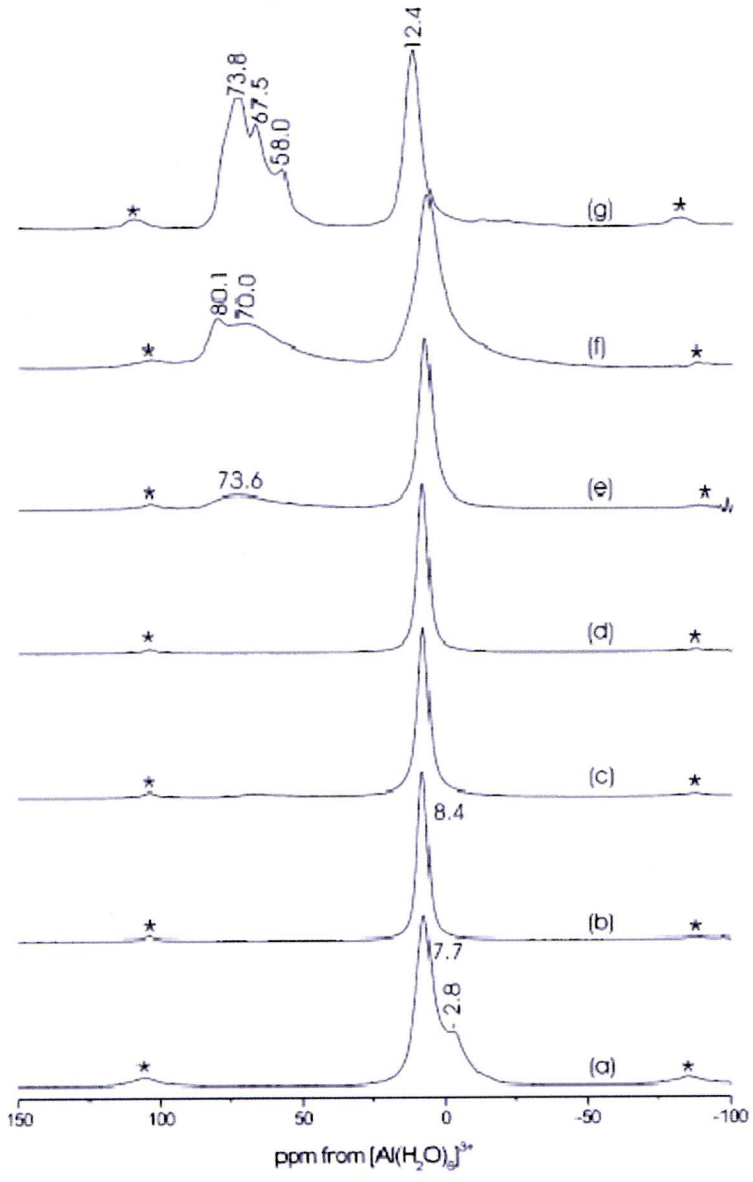

Figure 2.7 ^{27}Al MAS NMR spectrum of (a) gibbsite, (b) Li-NO_3-LDH as synthesised, (c) Li-NO_3-LDH, calcined at 250°C in air, (d) Pd doped Li-NO_3-LDH as synthesised, (e) Pd-doped Li-NO_3-LDH after reduction in H_2 for 2 hours at 250°C, (f) Pd doped Li-NO_3-LDH after use in gas phase conversion of acetone to MIBK (6 hours on stream at 250°C), (g)) Pd doped Li-NO_3-LDH after use in gas phase conversion of acetone to MIBK (6 hours on stream at 250°C) and then calcination in air at 1000°C.

*Note: * denote spinning side bands*

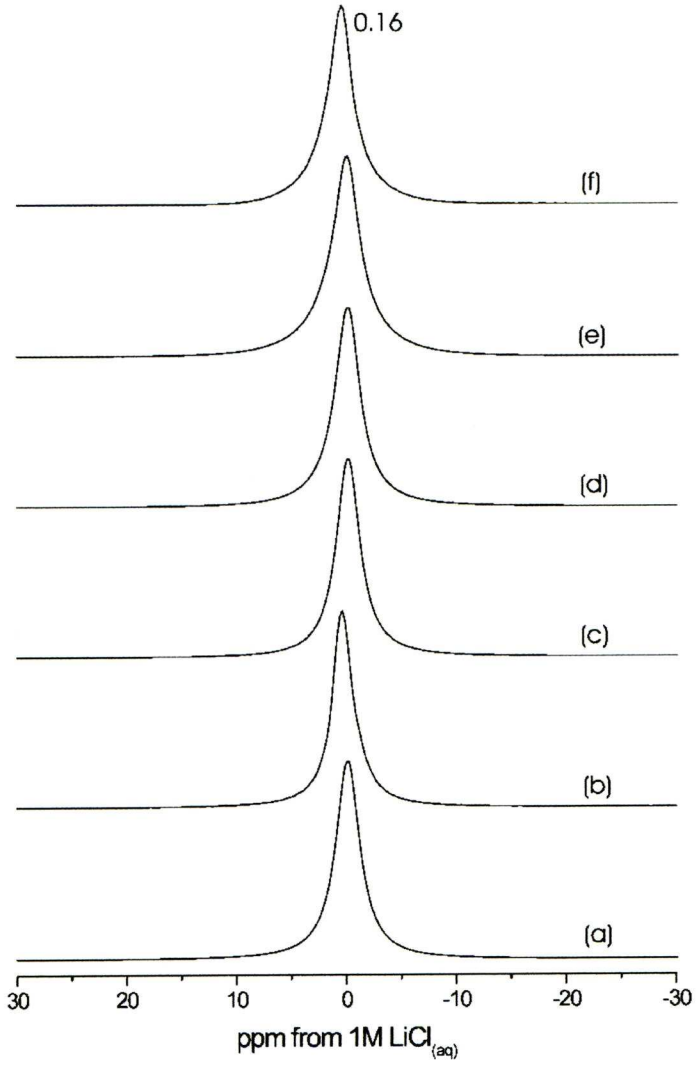

Figure 2.8 ^{7}Li MAS NMR spectrum of (a) gibbsite, (b) Li-NO_3-LDH as synthesised, (c) Li-NO_3-LDH, calcined at 250°C in air, (d) Pd doped Li-NO_3-LDH as synthesised, (e) Pd-doped Li-NO_3-LDH after reduction in H_2 for 2 hours at 250°C, (f) Pd doped Li-NO_3-LDH after use in gas phase conversion of acetone to MIBK (6 hours on stream at 250°C), (g)) Pd doped Li-NO_3-LDH after use in gas phase conversion of acetone to MIBK (6 hours on stream at 250°C) and then calcination in air at 1000°C.

Surface area measurements were also carried out both upon the LDHs and Pd-doped catalysts, as shown in Figure 2.12. It can be seen that the as synthesized LDHs had low surface areas and pore volumes, however, once reduced in H_2 at 250°C both surface areas and pore volumes increased dramatically. Pd dispersion in the catalysts, D, obtained from H_2 chemisorption is also shown in Table 2.4. In the absence of Pd, none of the materials absorbed and H_2, however in the case of Pd dispersed Co-LDH, an unusually high Pd dispersion figure was noted (D=2.35) indicating the

reduction of Co^{2+} to Co metal, the slightly larger than average for Pd/Ni-LDH can also be explained in the same way.

Catalyst	S_{BET} (m^2/g)	Pore Diamater[b] (Å)	Pore Volume[c] (cm^3/g)	D[d]
As synthesised[a] Li/Al-NO_3-LDH	7	81	0.01	-
0.65% Pd/Li/Al-NO_3-LDH	131	88	0.29	0.19
0.65% Pd/Li/Al-OH-LDH	76	83	0.16	0.12
0.65% Pd/Co/Al-LDH	266	36	0.19	2.35[f]
0.65% Pd/Cu/Al-LDH	130	26	0.08	-
Zn/Al-LDH	6	72	0.01	-
0.65% Pd/Zn/Al-LDH	262	26	0.17	0.40
0.65% Pd/Ni/Al-LDH	341	34	0.29	0.58
0.65% Pd/γ-$Al(OH)_3$	328	24	0.19	0.43

Table 2.4 Catalyst texture and Pd Dispersion

(a) All catalysts were treated at 250°C in H_2 for 2 h apart from entry 1, Li/Al-NO_3-LDH.
(b) Average pore diameter by BET.
(c) Single point total pore volume.
(d) Palladium dispersion: $D = Pd_s/Pd_{total}$. The ratio of the amount of H_2 chemisorbed by the sample to the total amount of Pd found by elemental analysis
(e) Disproportionately large dispersion indicates reduction of Co^{2+} to Co metal.

2.2.2 Catalyst Testing

The gas phase synthesis of MIBK was studied in collaboration with Robert Hetterley, a PhD student with Prof. Ivan Kozhevnikov. A fixed bed flow reactor (Figure 2.9) was used to conduct the experiments under the following conditions: 120-300° and ambient pressure. The combined gas flow rates were 4ml/min H_2, 6ml/min N_2 flowing through the acetone saturator heated to 37 °C resulting in a gas feed volume ratio [acetone]:[H_2]:[N_2] = 50:20:30. The gas feed leads to a catalyst contact time ranging from 1.7-3.0 s (gas hourly space velocity (GHSV) of 1200-2000 h^{-1}) depending on the identity of the multifunctional mixed oxide catalyst. The GHSV and contact times for each catalyst are presented in Table 2.5. Before use, the catalysts were treated *in-situ* at 250°C under a hydrogen flow for 1 hour.

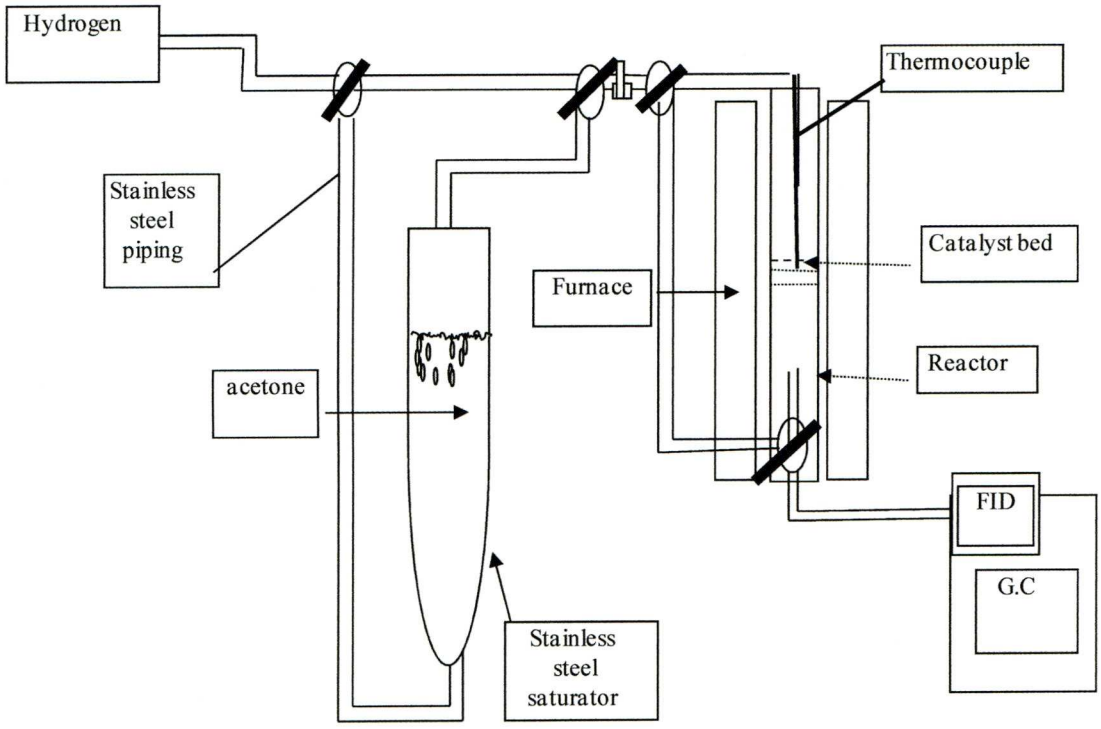

Figure 2.9 Experimental setup for gas phase conversion of acetone into MIBK

Catalyst[a]	Catalyst volume (cm^3)	GHSV (h^{-1})	Contact time (s)
Pd/Li-LDH-NO_3	0.3	2000	1.8
Pd/Li-LDH-OH	0.36	1667	2.2
Pd/Co-LDH-NO_3	0.45	1333	2.7
Pd/Cu-LDH-NO_3	0.38	1579	2.3
Pd/Zn-LDH-NO_3	0.41	1463	2.5
Pd/Ni-LDH-NO_3	0.5	1200	3.0
Pd/Al $(OH)_3$	0.29	2069	1.7

Table 2.5 GSHV and Contact Times for Pd doped LDH Catalysts

(a) Standard gas flow feed: N_2+H_2 flow rate 10 mL/min and acetone saturator temperature 37 °C, leading to [acetone]:[H_2]:[N_2] 5:2:3 molar ratio flowing over 0.2 g catalyst bed. Reactor pressure = 1 bar

Initially, the gas feed ratio for the experiment was that used for previous systems, such as the $Pd/Cs_{2.5}PW$: $[H_2]$:[acetone] of approximately 2:1[16]. A preliminary reaction was tried at 160°C using the 0.65% Pd impregnated Ni-LDH catalyst. This particular temperature was chosen as it was found from the literature to be within the optimum range[23]. These preliminary experiments showed that with this gas feed, the acetone conversion was high (at 50%), but the corresponding MIBK selectivity was low at only 10% owing to a high isopropanol (IP) selectivity of 83%. From this, it was decided that the $[H_2]$:[acetone] ratio should be decreased, but with the same gas flow rate, in an attempt to lower the direct hydrogenation of acetone to IP and thus allowing higher MIBK selectivity. This new gas feed ratio of [acetone]:$[H_2]$:$[N_2]$ of 5:2:3 lowered the IP selectivity to 52%, and raised the MIBK selectivity to 34%. This new feed rate was then used in further studies.

Table 2.6 and 2.7 show the catalytic properties of the LDH with no Pd, then with impregnation of 0.65 wt% Pd respectively. The LDHs were dried and reduced in the same manner as the Pd impregnated the catalysts. The performance of each catalyst was then tested at 120°C. From these studies, it is clear that the Pd is necessary-with the conversion of acetone being very low in the absence of the Pd (0.3-3.4%), with mesityl oxide (i.e. the product of a base condensation reaction between two molecules of acetone) being the major product (at 60-90% selectivity) with a trace amount of MIBK being formed. This shows that even the Co and Ni based LDHs had low hydrogenation activity. This is due to the temperature and relative concentration of H_2 used. Ni based catalysts can hydrogenate at 1atm pressure in the gas phase, but only at elevated temperatures and higher relative concentrations of H_2[24].

Catalyst[a]	Acetone conversion (%)[b]	Selectivity (%)							
		C_3 gases	IP	Mesityl oxide	MIBK	DIBK	Mesitylene	C_6	C_{9+}
Li/Al-LDH-NO_3	0.3	8.8	0	63.1	0	0	0	17.7	10.4
Co/Al-LDH-NO_3	5.4	0.6	0	87.7	0.2	0	0	4.0	6.9
Zn/Al-LDH-NO_3	2.4	0.6	0	77.4	18.8	0	0	3.3	0
Ni/Al-LDH-NO_3	3.5	1.0	0	94.4	0	0	0	4.7	0
Ni/Al-LDH-NO_3[c]	5.8	0.7	0	88.6	0	0	0	6.3	4.4

Table 2.6 Catalytic activities of LDHs without supported Pd at 120°C. Results obtained after 3 hours on stream.

(a) feed - H_2+N_2 flow rate 10 mL/min, [Acetone]:[H_2]:[N_2] 5:2:3, 0.2 g catalyst.
(b) Results obtained from gas chromatography after 3h of catalyst being on stream
(c) Reaction temperature 160 ºC, H_2 flow 10 mL/min, H_2:acetone 2:1, GHSV 2297 h^{-1}, contact time 1.57 s, 0.2 g catalyst.

Catalyst[a]	Acetone conversion (%)[b]	Selectivity (%)							
		C_3 gases	IP	Mesityl Oxide	MIBK	DIBK	Mesitylene	C_6	C_{9+}
Pd/Li-LDH-NO_3	20.0	0.2	7.5	0.3	70.0	16.1	2.0	0	4.0
Pd/Li-LDH-OH	15.5	0.3	33.6	2.8	54.2	8.5	0.6	0	0
Pd/Co-LDH-NO_3	21.6	0.4	82.0	1.7	15.4	0.4	0	0	0
Pd/Cu-LDH-NO_3	23.4	0.4	74.3	1.9	22.5	0.9	0	0	0
Pd/Zn-LDH-NO_3	20.2	0.2	22.9	2.8	63.2	8.9	0.6	0	0
Pd/Ni-LDH-NO_3	26.5	0.3	67.3	2.4	28.4	1.5	0.1	0	0
Pd/Al $(OH)_3$	12.9	0.5	46.5	3.1	48.8	0.7	0	0	0.4

Table 2.7 Catalytic Activities of LDHs Supported with Pd at 120°C. Results obtained after 3 hours on stream.

(a) feed - H_2+N_2 flow rate 10 mL/min, [Acetone]:[H_2]:[N_2] 5:2:3, 0.2 g catalyst.
(b) Results obtained from gas chromatography after 3h of catalyst being on stream

From these results, we can see that the best performing catalysts were the Pd doped Li-NO_3-LDH and the Pd doped Zn-NO_3-LDH, giving MIBK as the major product with excellent selectivities, with siginifcant amounts of DIBK being formed.

Analysis of the chromatogram also showed that by-products included isopropanol (IP), mesityl oxide (MO), C_{9+} acetone condensation products (mainly DIBK together with mesitylene) and small amounts ($\leq$1% selectivity) of propene and propane (C_3).

These results can be contrasted against the other transition metal based LDHs (Ni, Co, Cu), which gave IP as the main product-indicating the direct hydrogenation of acetone possibly by the metals contained in the LDH, as already mentioned. Pd supported on gibbsite showed poor activity, giving approximately equal amounts of MIBK and IP, indicating the role of the intercalated metal is significant, it should also be noted that there is no correlation between the performance of the catalysts and the Pd dispersion.

Pd/Li-NO_3-LDH was found to be the most efficient catalyst at 120°C, with 70% MIBK selectivity and 86% MIBK+DIBK combined selectivity at 20% acetone conversion, whilst also giving excellent stability (Figure 2.10), with no deactivation being noted after 15 hours of continuous operation. The catalyst took 1 hour to reach a steady state, and after that gave constant activity and selectivity. Upon increasing the temperature, MIBK and DIBK selectivities remained largely constant, with the acetone conversion going up (Figure 2.11). A further temperature increase to 300°C caused a drop in catalyst activity possibly due to structural changes in the catalyst due to dehydration.

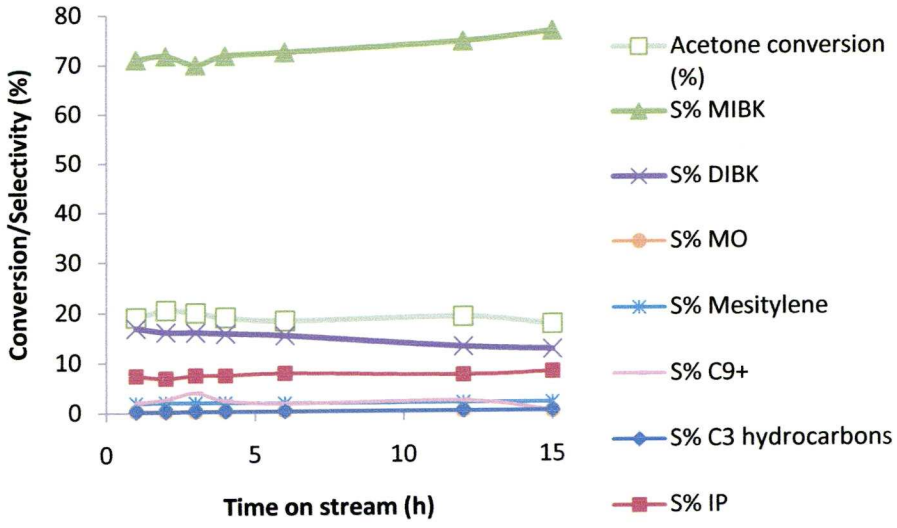

Figure 2.10 Comparison of acetone conversion vs. selectivity for Pd/Li-NO_3-LDH at 120°C over 15 hours on stream

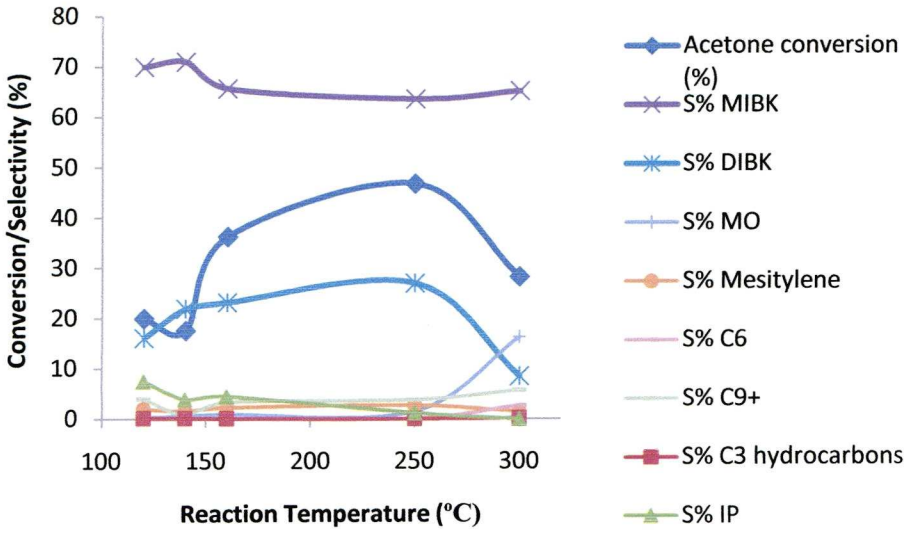

Figure 2.11 Effect of temperature on stability of Pd/Li-NO_3-LDH catalyst

Table 2.8 shows the study of the performance of the catalyst at the optimal temperature of 250°C. Here the acetone conversion is high, up to 77%. For all catalysts tested, MIBK was found to be the major product (47-91% selectivity) with high MIBK/DIBK selectivities (82% up to 98%). This is in good agreement with previous studies[6, 11-12, 16-17, 25-32]. As opposed to the catalyst performance at 120°C, the most active catalysts at 250°C were those containing Co and Ni, which also had the largest surface areas (266 and 341m^2/g respectively-see Figure 2.12). These catalysts also had the largest metal dispersions. Pd/Co-LDH gave the best performance (77% conversion and the highest MIBK yield at 44% and an MIBK+DIBK combined yield of 69%). Pd/Li-OH-LDH gave the best selectivity for MIBK of 91% and the best combined MIBK and DIBK selectivity of 98%, this, however was with a very low acetone conversion of 15%. Reasonable stability was also noted for the catalysts at 250°C, as can be seen in Figure 2.12. The catalyst reached a steady state after 2 hours, after which time it exhibited constant MIBK+DIBK selectivity with a relatively slow decrease in acetone conversion from 73-60% over the course of 16 hours.

Catalyst	Acetone conversion (%)	Selectivity (%)							
		C_3 gases	IP	Mesityl oxide	MIBK	DIBK	Mesitylene	C_6	C_{9+}
Pd/Li-LDH-NO_3	46.8	0.04	1.2	1.5	63.6	27.0	2.7	0.1	3.8
Pd/Li-LDH-OH	15.1	0.3	0	0.4	90.9	7.2	1.2	0	0.1
Pd/Co-LDH-NO_3	76.5	0.7	2.2	1.3	57.9	32.6	1.8	0	3.6
Pd/Cu-LDH-NO_3	37.7	7.9	3.5	1.6	60.9	20.9	2.4	0.3	2.5
Pd/Zn-LDH-NO_3	67.2	2.9	2.3	1.4	53.5	30.5	2.8	0.2	6.6
Pd/Ni-LDH-NO_3	72.2	0.9	3.8	1.4	47.2	36.9	2.9	0	6.9

Table 2.8 Catalytic Activities of LDHs Supported with Pd at 250°C. Results obtained after 3 hours on stream.

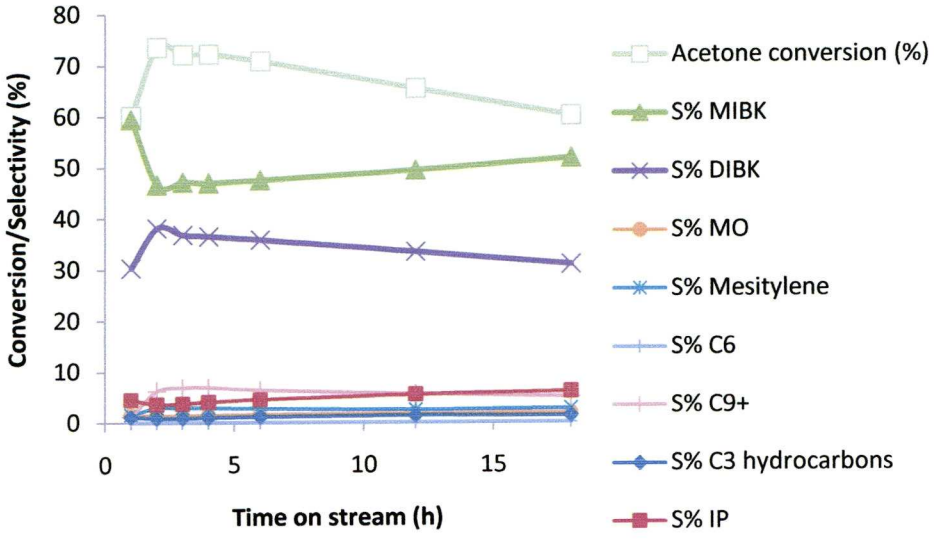

Figure 2.12 Catalytic performance of Pd/Ni-LDH over the course of 18 hours on stream

2.3 Conclusions

Pd doped, gibbsite based layered double hydroxides have been successfully synthesised and fully characterised and have been shown to be excellent precursors to bifunctional metal oxide catalysts used for the one step conversion of acetone to MIBK. At the relatively low temperature of 120°C, the Pd/Li-NO_3-LDH catalyst proved to be the most effective with MIBK selectivity of 70% at a 20% conversion rate of acetone. The catalyst was used at atmospheric pressure for over 15h without notable deactivation. At the optimum reaction temperature of 250°C, the best performing catalyst was Pd/Ni-LDH giving up to 77% acetone conversions coupled with 91% MIBK+DIBK combined selectivity. The Pd/Ni-LDH catalyst outperformed the catalysts found in the literature described at the beginning of the chapter, with the conversions being nearly double the Zn-Cr mixed oxide

system (77% for the LDH as opposed to 42.0% for the mixed oxide). The selectivity for the Pd/Li-NO_3-LDH however was lower (70% for MIBK for the Pd/Li-NO_3-LDH system compared to values of around 80% for the systems found in the literature.

2.4 References

1. K. Takehira, *Journal of Natural Gas Chemistry*, 18, **2009,** 237-259

2. Y. Zhan, D. Li, K. Nishida, T. Shishido, Y. Oumi, T. Sano, K. Takehira, *Applied Clay Science*, 45, **2009,** 147-154

3. S. Liu, X. Jiang, G. Zhuo, *Journal of Molecular Catalysis A: Chemical*, 290, **2008,** 72-78

4. J.B. Conant, N. Tuttle, *Organic Syntheses*, Coll. Vol. 1, **1941,**

5. L.P. Kyriakides, *J. Am. Chem. Soc.*, 36, **1914,** 530-537

6. F. Delbecq, P. Sautet, *J. Catal.* , 152, **1995,** 217-236

7. H.J.A. K. Weissermel, *Industrial organic chemistry, 3rd edition*, VCH, Weinheim, 1997.

8. R.D. Hetterley, E.F. Kozhevnikova, I.V. Kozhevnikov, *Chemical Communications*, **2006,** 782-784

9. E.F. Kozhevnikova, I.V. Kozhevnikov, *Journal of Catalysis*, 238, **2006,** 286-292

10. N.S. Chang, C.C. Chen, S.J. Chu, P.Y. Chen, T.K. Chuang, Acidity effect of zsm-5 zeolites on phenol methylation reaction, in: H.G. Karge, J. Weitkamp (Eds.) *Studies in surface science and catalysis*, Elsevier, 1989, pp. 223-230.

11. C.O. Veloso, J.L.F. Monteiro, E.F. Sousaaguiar, Aldol condensation of acetone over alkali cation-exchanged zeolites, in: *Zeolites and related microporous materials: State of the art 1994*, 1994, pp. 1913-1920.

12. S.M. Yang, Y.M. Wu, *Appl. Catal., A*, 192, **2000,** 211-220

13. L. Melo, P. Magnoux, G. Giannetto, F. Alvarez, M. Guisnet, *J. Mol. Catal. A: Chem.*, 124, **1997,** 155-161

14. R. Ruiz, C. Pesquera, F. Gonzalez, C. Blanco, *Appl. Catal., A*, 257, **2004,** 165-175

15. L. Melo, A. Llanos, L. Garcia, P. Magnoux, F. Alvarez, M. Guisnet, G. Giannetto, *Catal. Lett.*, 51, **1998,** 207-212

16. R.D. Hetterley, E.F. Kozhevnikova, I.V. Kozhevnikov, *Chem. Commun.*, **2006,** 782-784

17. E.F. Kozhevnikova, I.V. Kozhevnikov, *J. Catal.* , 238, **2006,** 286-292

18. A.V. Besserguenev, A.M. Fogg, R.J. Francis, S.J. Price, D. Ohare, V.P. Isupov, B.P. Tolochko, *Chem. Mater.*, 9, **1997,** 241-247

19. A.M. Fogg, G.R. Williams, R. Chester, D. O'Hare, *J. Mater. Chem.*, 14, **2004,** 2369-2371

20. X. Hou, R.J. Kirkpatrick, *Inorg. Chem.*, 40, **2001,** 6397-6404

21. K.R. Poeppelmeier, S.J. Hwu, *Inorg. Chem.*, 26, **1987,** 3297-3302

22. H. Saalfeld, M. Wedde, *Zeitschrift Fur Kristallographie*, 139, **1974,** 129-135

23. D. Tichit, C. Gerardin, R. Durand, B. Coq, *Topics in Catalysis*, 39, **2006,** 89-96

24. L.M. Gandía, M. Montes, *Appl. Catal., A* 101, **1993,** L1-L6

25. PY Chen, NS Chang,TK Chuang,SJ Chu,LY Chen, *Zeolites as catalysts, sorbants and detergent builders*, Elsevier Science Publishers B.V., Amsterdam, 1989.

26. R. Unnikrishnan, S. Narayanan, *J. Mol. Catal. A: Chem.*, 144, **1999,** 173-179

27. N. Das, D. Tichit, R. Durand, P. Graffin, B. Coq, *Catal. Lett.*, 71, **2001,** 181-185

28. M.D. Martinez-Ortiz, D. Tichit, P. Gonzalez, B. Coq, *J. Mol. Catal. A: Chem.*, 201, **2003,** 199-210

29. N.N. Das, S.C. Srivastava, *Bull. Mater. Sci.*, 25, **2002,** 283-289

30. A.A. Nikolopoulos, B.W.L. Jang, J.J. Spivey, *Appl. Catal., A*, 296, **2005,** 128-136

31. F. Winter, A.J. van Dillen, K.P. de Jong, *J. Mol. Catal. A: Chem.*, 219, **2004,** 273-281

32. D. Tichit, C. Gerardin, R. Durand, B. Coq, *Top. Catal.*, 39, **2006,** 89-96

Chapter 3: The Oxidative Bromination of Phenol Red by Tungstate Supported Layered Double Hydroxides

3.1 Introduction

3.1.1 Introduction to Haloperoxidases

Up until the late 1950s few examples of halogenated bio-organic compounds were known, with exceptions such as the ancient dye Tyrian purple (6,6'-dibromoindigo), obtained from certain species of shellfish. An important breakthrough came in 1959 when it was reported that the fluid from the uterus of pregnant dogfish *Squalas acanthias* was able to brominate the organic dye phenol red (see Figure 3.1), forming bromophenol blue[1]. At this stage it was unknown how the reaction was proceeding, however several years later, the family of enzymes which were catalysing this reaction – the haloperoxidases – were being studied[2].

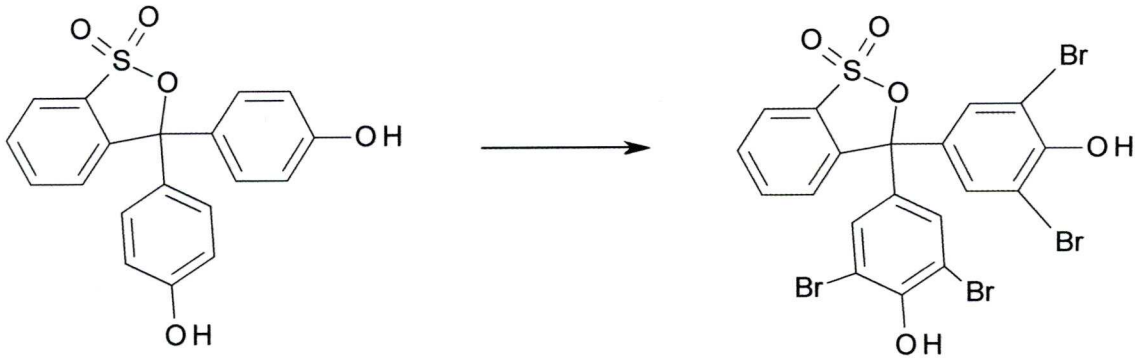

Figure 3.1 - Bromination of the Organic Dye Phenol Red

The haloperoxidases are enzymes which catalyse the oxidation of a halide anion (i.e. chloride, bromide or iodide but not fluoride) by hydrogen peroxide, with the result being an organic substrate being halogenated. The nomenclature of the haloperoxidase being studied is based on the most electronegative halide which it is able to oxidise, i.e. chloroperoxidases can catalyse the oxidation of chloride, bromide and iodide, whereas bromoperoxidases can catalyse only the oxidation of bromide and iodide etc[3].

3.1.2 Studies into Peroxidases

Early studies of vanadium haloperoxidase (VBPO) activity involved the oxidation of iodide to triiodide (I_3^-) using H_2O_2,[4] followed spectrophotometrically at 353nm (ε=26400$M^{-1}cm^{-1}$). This reaction, however, is of limited use due to the presence of competing side reactions such as the oxidation of iodide by H_2O_2 without the use of the VBPO and also the reduction of triiodide by H_2O_2[5]. Following this, the standard way to measure the activity of a haloperoxidase was to follow the bromination of the molecule monochlorodimedone (mcd), (2-chloro-5,5-dimethyl-1,3-dimedone), using H_2O_2 along with the haloperoxidase to oxidise the halide[6], as shown in Figure 3.2. The reaction can be followed spectrophotometrically at 290nm as the mcd starting material has a large (ε=20000 $M^{-1}cm^{-1}$) absorption coefficient whereas that of the product is very small (ε=100$M^{-1}cm^{-1}$).

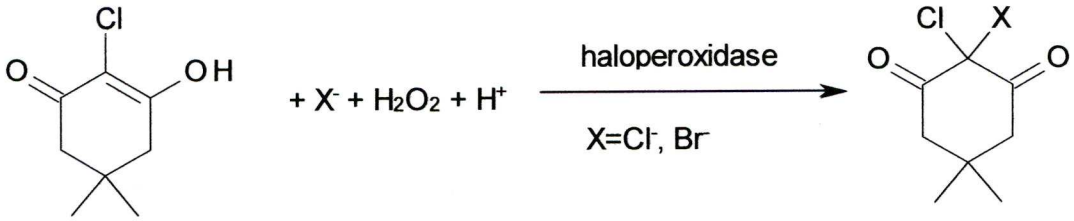

Figure 3.2 The reaction of monochlorodimedone with halide anions as an assay for VBPO activity

3.1.3 Peroxidase Structures

Bromoperoxidases have been isolated from various marine algae[7] with chloroperoxidases being isolated from moulds such as *Caldariomyces Fumago*[2, 8]. Haloperoxidase enzymes are mainly found in marine life, and fall into two general classes; non-heme Vanadium bromoperoxidases (VBPO), found in many types of red[9] and brown[10] algae, and FeHeme bromoperoxidase (Fe-Heme BPO), found in red algae[11] and marine worms[12]. A structure for a chloroperoxidase isolated from a fungus, *C. Inaequalis* is shown in Figure 3.3. The vanadium(V) site shown here is similar for all Vanadium containing haloperoxidases[13], with the histidine residue being a ligand to the vanadate. The vanadate is located at the top of a broad channel, one side of which contains polar residues making it hydrophilic, whereas the other side is predominantly hydrophobic[3]. For comparison, a structure

for the active site of a haem containing CPO is shown in Figure 3.4, containing a Fe(III) containing porphyrin moiety. This structure has two channels that lead to the main active site, and here, the organic substrate, 1,3-cyclopentanedione is located in the broader of the two channels[13]. The Heme based peroxidases function as redox catalysts[13] and as in the current discussion, we are mainly concerned with the V containing haloperoxidases where the V centre stays in the +5 oxidation state, as can be seen in proposed catalytic cycles for each peroxidase enzyme discussed in detail later in this chapter.

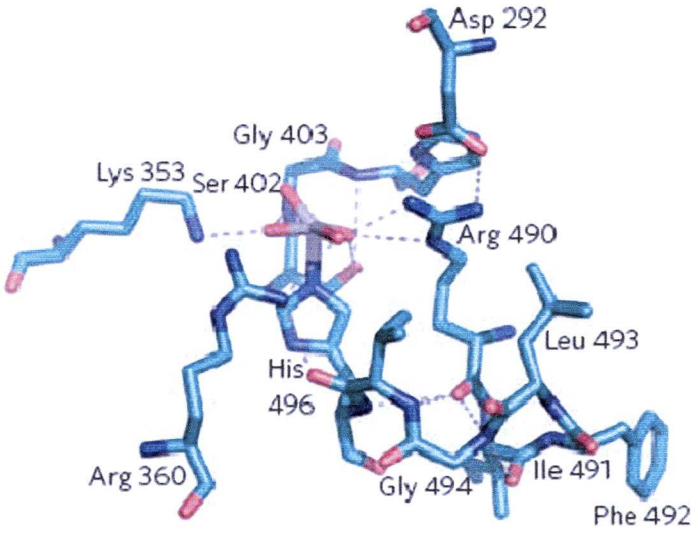

Figure 3.3 Enzyme structure for a chloroperoxidase isolated from the fungus *C. Inaequalis*[13] as solved by Messerschmidt *et al*[14]. Note the His residue being a ligand to the vanadate. The vanadate is trigonal bipyramidially coordinated by hydroxide and His 496 in the axial positions and by three non protein atoms in the equatorial plane[3]. The carbon backbone is green, oxygen red, nitrogen blue, and the V(V) centre in grey. Dashed lines indicate hydrogen bonding.

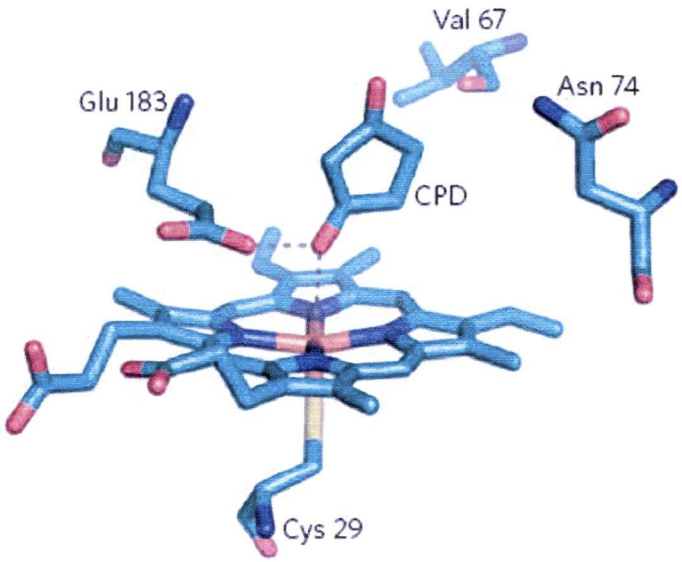

Figure 3.4[13] Structure of the active site from a haem CPO isolated from the fungus *C. Fumago*. The active site is a Fe(III) containing porphyrin moiety, coordinated by the thiolate side chain of Cysteine in the proximal position. The 1,3-cyclopentanedione was located in the broader channel, with the halide anions found in the narrower channel[15]

The vanadate site in VClPO is shown more clearly in Figure 3.5. Here it is shown to be in a trigonal bipyramidial geometry. In the axial positions, we can see hydroxide and His_{496} coordinated, with three non-protein oxygen atoms in the equatorial positions. The vanadate (V) coordination to the proteins is stabilised by multiple hydrogen bonds between the equatorial coordinated oxygen atoms, and the protonated protein residues Lys353, Arg360, Arg390 and Ser402 as well as the amide proton on Gly403.

A study of the X-ray structure of the peroxo form of the VClPO[16] reveals the vanadium(V) in a tetragonal pyramidial geometry, as shown in Figure 3.6. The peroxide is coordinated in an η^2 manner, with the His496 and an oxygen atom in the basal plane, with an oxo ligand in the axial position. The His404 is now no longer bonded to the vanadate. One of the peroxide oxygen atoms is also hydrogen bonded to Lys353.

Structural features of the VBPO are almost identical[17], which raises the issue of why some haloperoxidases are only able to oxidise the halides with lower electronegativities. A closer comparison to the protein backbone of the chloro and bromoperoxidases reveals slight differences, allowing one of the residues in the VBPO to act as a proton acceptor/donor in catalysis, which would affect the stability of the V(v) centre[18].

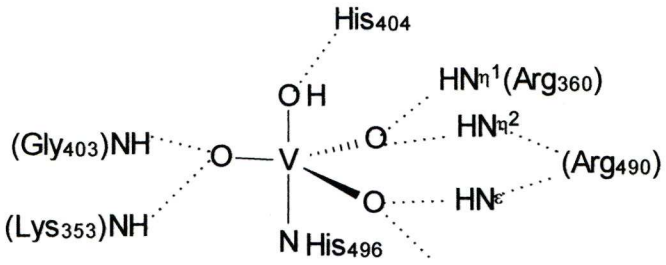

Figure 3.5 The vanadate site in VClPO

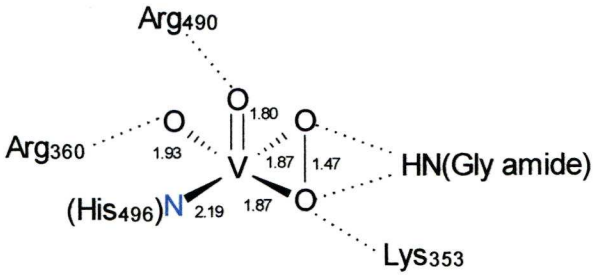

Figure 3.6 The vanadate site in peroxo VClPO

3.1.4 Advantages of Peroxidases

Clearly, VBPO enzymes offer an excellent alternative to traditional bromination methods, such as the use of elemental bromine[19], with its associated toxicity; and reagents such as N-Bromosuccinimide[20], which generate stoichiometric amounts of organic waste. However, problems do exist with haloperoxidases, such as the high cost of purification, and the need for tight controls of pH and temperature[21]. Using the model of the VBPO, it would therefore be desirable to synthesise a mimic, which gives comparable bromination activity along with greater stability. The early mimics such as NH_4VO_3 required harshly acidic conditions (pH 0.12-0.9, using $HClO_4$)[22-23]. When lower pH values were used, it became necessary to use almost quantitative amounts of ammonium metavanadate (NH_4VO_3)[24].

3.1.5 Catalytic Cycles of Haloperoxidases

The catalytic cycles of VBPO and Fe-Heme BPO are significantly different. As the introduction to this chapter alluded to, the Fe-Heme BPO system is based around redox reactions (Figure 3.7). Initially the haem centre is oxidised by H_2O_2 to a Fe^{IV} cation radical species via a short lived peroxo-anion complex[25]. The Fe^{IV} cation radical species then proceeds to oxidise chloride by 2 electrons, which in turn reforms the Fe^{III} centre. This particular species has been discussed at length[26], where it is unclear whether the OCl^- is a ligand to the Fe^{III}-haem, whether it had been released from the active

site, or otherwise been trapped in the enzyme away from the active site. The OCl^- can then react with the organic substrate or else a further molecule of H_2O_2, producing $^1O_2$, depending on the reaction conditions.

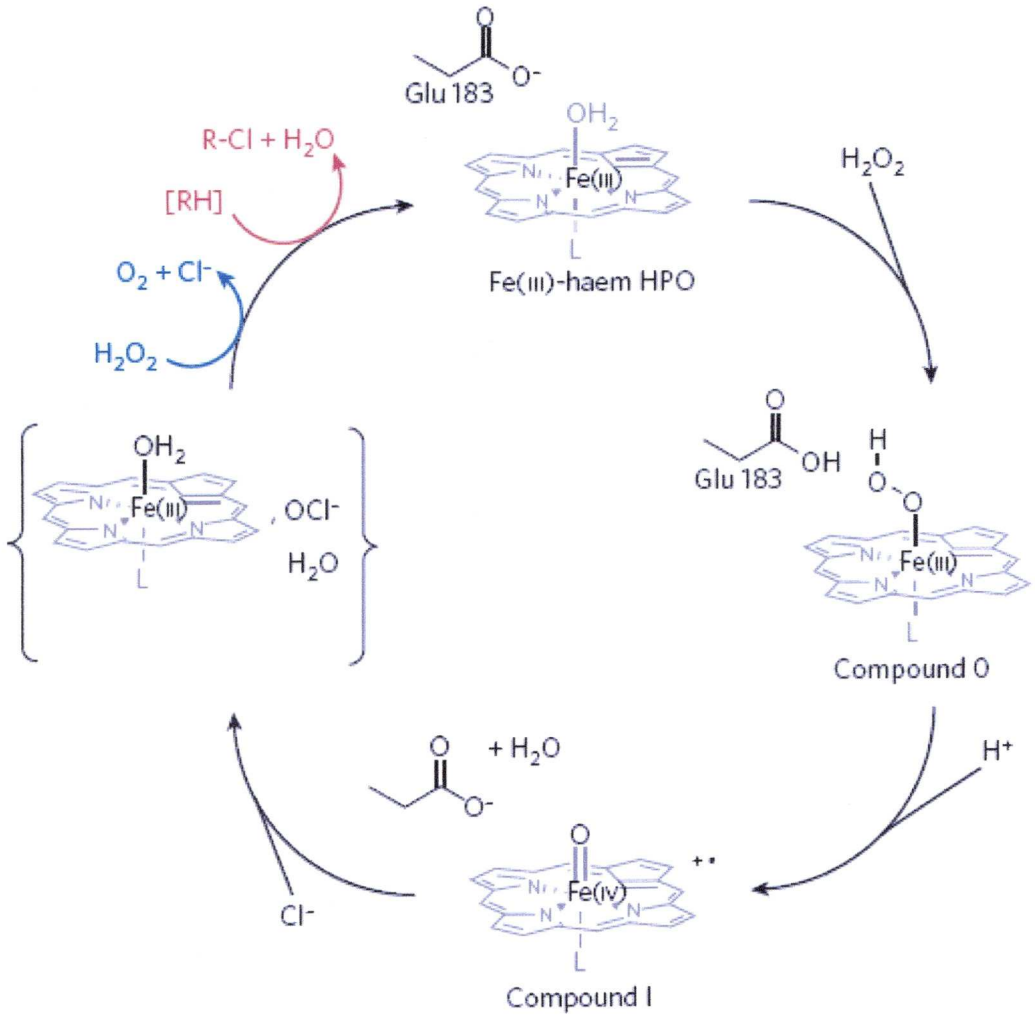

Figure 3.7 Catalytic cycle for Fe-Heme HPO[13]. Here the Fe^{III}-haem HPO is initially oxidised by H_2O_2 forming compound 0 which immediately decomposes to compound 1, a Fe^{IV} radical cation. This then oxidises Cl^-, forming OCl^-. OCl^- can then go on to chlorinate the organic substrate (red), or a further molecule of H_2O_2 (blue).

The VHPO in contrast to the Fe-Heme HPO do not function as redox catalysts but as Lewis acid catalysts (Figure 3.8). The reaction is initiated by the coordination of a molecule of H_2O_2 to the V^V centre. This oxo-peroxo complex is then able to oxidise a halide formally to X^+, but more probably OX^-, i.e., hypohalite. This then can react with an organic substrate, or a further molecule of H_2O_2, again forming $^1O_2$ and X^-[13, 27].

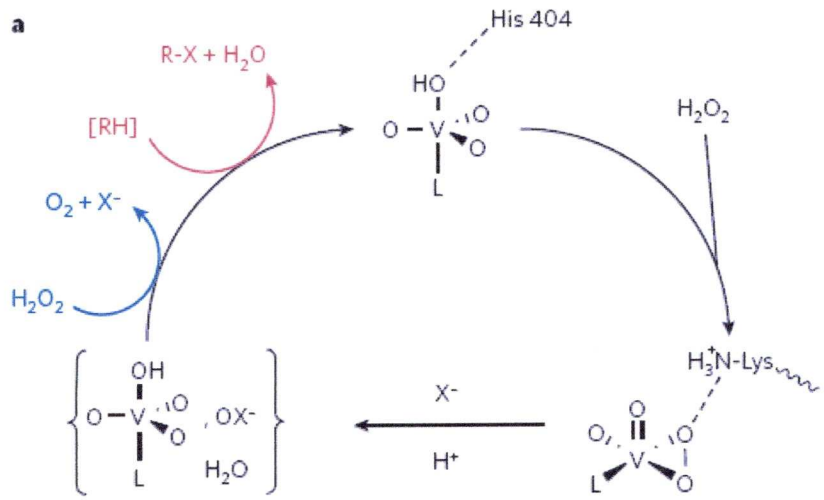

Figure 3.8 Catalytic cycle for VHPO[13]. Here the VHPO is not a redox catalyst as in the -Heme HPO system. The V centre coordinates a molecule of H_2O_2, with the H_2O_2 H-bonding to the Lys side chain. This likely causes the V^V complex to have a greater oxidation potential allowing it to then oxidise a halide anion. The oxidised anion can then go on to halogenate an organic substrate (red) or a further molecule of H_2O_2 (blue) forming singlet oxygen.

3.1.6 Haloperoxidase Mimics Based on Layered Double Hydroxides

In an attempt to mimic this, a catalyst based on tungstate (WO_4^{2-}) exchanged layered double hydroxide was developed[28]. This system gave the advantages of being stable, reusable and working under mild conditions. The system was based upon either Mg/Al or Ni/Al based LDHs. As the surface of the LDH has excess positive charge, the peroxotungstate species, which are negatively charged are more shielded, allowing high bromide oxidation rates, crucially without the need for acidic conditions[29], as the negatively charged peroxotungstate species can then react with the negatively charged bromide species in the manner suggested in the catalytic cycle (Figure 3.9). This use of shielding makes the catalyst truly biomimetic as they are then related to the structures in Figures 4.3-4.6. A comparison of many VHPO mimics used in the literature can be found in Table 3.1.

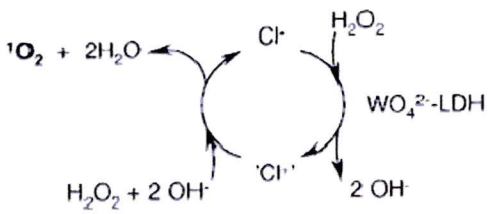

Figure 3.9 Proposed catalytic cycle for halogenation using LDH-WO_4^{2-}. Note the similarities between this and the VHPO cycle shown in Figure 4.8

Catalyst	TOF[a]	$[H^+]$	Solvent	$[H_2O_2];[Br^-]$	Ref
VO_4^{3-}	15	0.05M $HClO_4$	25% MeOH	5mM;0.43mM	[30]
V^VO-SB[b]	1.3[c]	Stoichiometric SB	DMF	4mM;0.1M	[31]
V^VO-SB[b]	2.8	0.001M $HClO_4$	DMF	4mM;0.1M	[31]
K(18-crown-6)-$VO(O_2)$heida[b]	120	0.005M Triflic acid	Acetonitrile	5mM;15mM	[32]
VO_4^{3-}	0.17	0.12M $HClO_4$	$H_2O/CHCl_3$	20mM;0.05M	[22, 33]
MoO_4^{2-}	48	0.1M $HClO_4$	25% MeOH	1.5mM;0.5M	[34]
MoO_4^{2-}	1.8	10^{-5}M (acetate buffer)	25% MeOH	0.3mM;1M	[33]
$MoO(O_2)_2(ox)^{2-}$	1.7[d]	10^{-5}M (oxalate buffer)	25% MeOH	0.5mM;1M	[34]
$MoO(O_2)_2(ox)^{2-}$	3.2	10^{-5}M (oxalate buffer)	Water	1mM;0.1M	[23]
WO_4^{2-}	95	0.5M $HClO_4$	Water	1mM;0.1M	[34]
WO_4^{2-}	24	0.01M $HClO_4$	25% MeOH	1mM;2M	[34]
CH_3ReO_3	85	1M $HClO_4$	Water	1mM	[35]
Ti-MCM-48[e]	0.16	$3x10^{-7}$M(hepes buffer)	Water	10mM;0.1M	[36]
Ti-MCM-41[e]	0.05	0	Chloroform		[28, 37-38]
Mg/Al-WO_4^{2-}LDH	33	0	H_2O/MeOH/THF	2.5mM;0.1M	[28]
Mg/Al-WO_4^{2-}LDH	71	0	H_2O/MeOH/THF	5mM;0.1M	[28]
Ni/Al-WO_4^{2-}LDH	48	0	H_2O/MeOH/THF	5mM;0.1M	[28]
$Na_2WO_4.2H_2O$	2.5	0	H_2O/MeOH/THF	2.5mM;0.1M	[28]

Table 3.1 Comparison of VBPO mimics with respect to TOF[28, 39]

(a) Turn over frequency (TOF) measured in moles Br^- oxidised per mole of catalyst per hour
(b) SB = Schiff base; heida= N-(2-hydroxyethyl)iminodiacetate
(c) In the absence of added acid, the reaction is not catalytic in the metal
(d) Stoichiometric reaction. Only one mole of product per mole of metal is formed, hence $MoO(O_2)_2(ox)^{2-}$ is not a catalyst but a reagent
(e) Ti-MCM-48 (5%wt Ti) has a three dimensional cubic structure. Ti-MCM-41 (4%wt Ti) has a hexagonal, one dimensional pore structure. Hepes=2-[4-(2-hydroxyethyl)piperazin-1-yl]ethanesulfonic acid
(f) $Febipy_2Y$ and $Mnbipy_2Y$ are *cis*-$[Febipy_2]^{2+}$ and *cis*-$[Mnbipy_2]^{2+}$ encapsulated in zeolite NaY (bipy=bipyridine)

The standard assay for measuring the activity of LDHs is however the conversion of the organic dye phenol red (λ_{max}=429nm, ε=2140$M^{-1}cm^{-1}$), which upon bromination becomes bromophenol blue (λ_{max}=598nm, ε=7040$M^{-1}cm^{-1}$), which is shown in Figure 3.1. It is this reaction to which all data concerning the use of the novel family of LDHs intercalated with tungstate will refer. Studies on this compound[27-28] reveal the bio-mimetic nature of the LDH immobilised tungstate catalysts. From measuring UV spectra of the catalyst in situ, two broad bands appear at 235 and 330nm. The 235nm band can be attributed to the formation of O_2^{2-} → W charge transfer transition of a diperoxotungstate (for example $WO_2(O_2)_2^{2-}$). The 330nm band can be attributed to O_2^{2-} → W charge transfer of tetraperoxotungstate $W(O_2)_4^{2-}$.[40-42]

3.1.7 Other Reactions of Tungstate Exchanged Layered Double Hydroxides

Tungstate exchanged LDHs are also used to catalyse other reactions. Most reactions studied use the tungstate in conjunction with H_2O_2 to exploit the ability of the tungstate to form peroxotungsten species which subsequently oxidise organic substrates. Examples include the oxidation of cyclohexene into the corresponding epoxide and then diol[43], the oxidation of thioethers[44] and thiophenes[44-45], and the oxidation of DMSO to the corresponding sulfone[46] which could be used to remove DMSO residues from wastewater as the sulfone is much more biodegradable.

3.2 Use of Li/Al-WO_4-LDHs as Catalysts

3.2.1 Materials Characterisation

The tungstate exchanged LDHs were synthesised via anion exchange. The Li/Al-NO_3-LDH starting material ($6.18x10^{-4}$ mol) was then stirred in an aqueous solution containing sodium tungstate ($1.24x10^{-3}$ mol, a 2 fold excess) in a sealed ampoule in an oil bath at 50°C overnight. The resulting solid was then filtered, washed several times with de-ionised water before being washed with acetone and dried in the air at room temperature. A PXRD pattern recorded of the solid is shown in Figure 3.11 and compared to the Li/Al-NO_3-LDH starting material. As can be seen from the pattern, a little gibbsite remains in the Li/Al-NO_3-LDH starting material, which is normal for this synthesis. The interlayer separation for the parent Li/Al-NO_3-LDH (Figure 3.10 (a)) material was 8.9Å, giving excellent agreement with the literature[47]. The tungstate exchanged LDH (Figure 3.10 (b)) had an interlayer separation of 11.6Å, in good agreement with the literature[45]. Unfortunately, during the anion exchange process, a small amount of de-intercalation of the Li^+ ions from the parent LDH took place, resulting in reformation of the gibbsite, [γ-($Al(OH)_3$] starting material, as can be seen from Figure 3.10 (b) and Figure 3.11, however complete exchange of tungstate for nitrate had occurred as

can be seen from the elemental analysis shown in Figure 3.13, with no nitrogen being found in the exchanged sample. Thermogravimetric analysis (TGA) was also conducted upon the Li/Al-WO_4-LDH material, shown in Figure 3.12. Starting with a composition of $[LiAl_2(OH)_6](WO_4)_{0.5}.3.5H_2O$ two main mass losses were observed. The first mass loss of 8.0% (calculated 8.2%) occurred at 160°C and corresponds to the loss of 3.5 molecules of coordinated water, giving $[LiAl_2(OH)_6](WO_4)_{0.5}$. The second mass loss of 24.6% (calculated 33.2%) between 160 and 500°C is due to the decomposition of the layers forming $LiAl_2O_3(WO_4)_{0.5}$. Elemental analysis was also performed on the Li/Al-WO_4-LDH sample, the results of which are shown in Table 3.2 and are shown to be in good agreement with the calculated values.

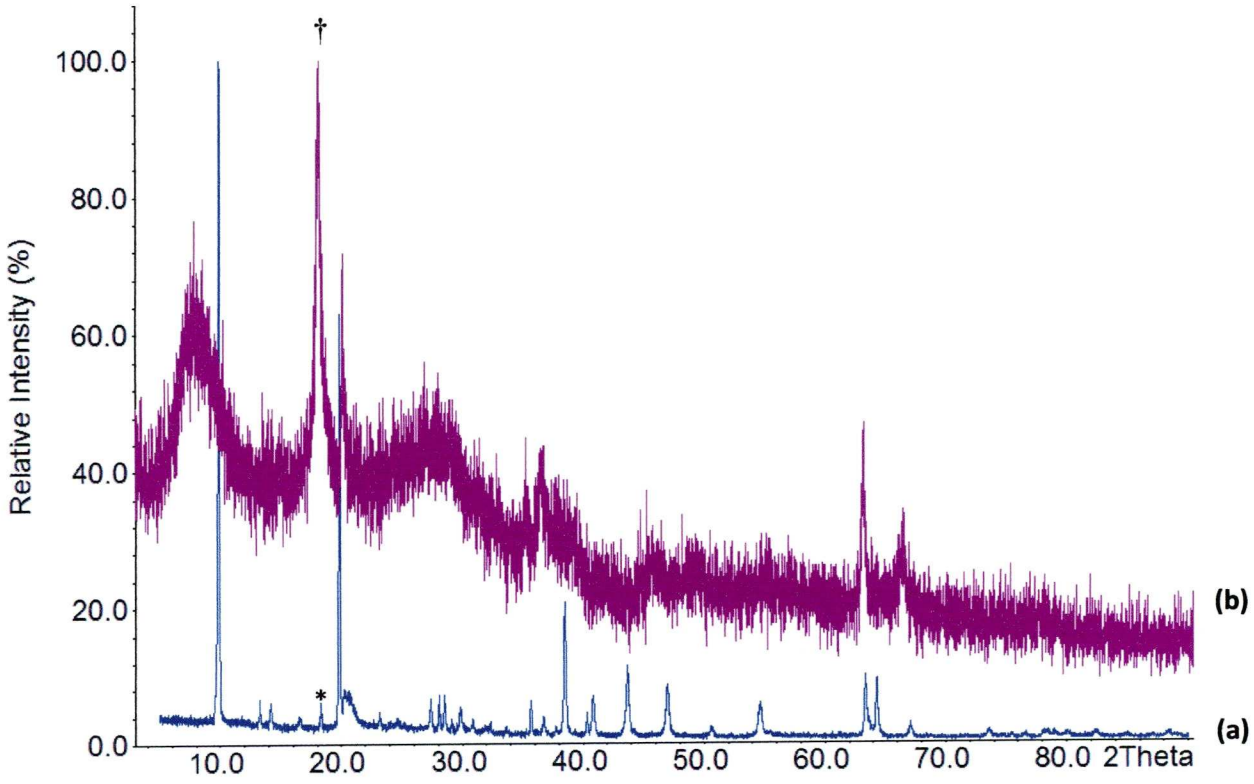

Figure 3.10 PXRD Patterns for Li/Al-LDH (a) Li/Al-NO_3-LDH as synthesised and (b) After intercalation with WO_4^{2-}.

Note * shows small amount of residual gibbsite, [γ-$Al(OH)_3$] in the parent Li/Al-NO_3-LDH
† Shows small amount of de-intercalated Li^+, forming gibbsite in tungstate exchanged material

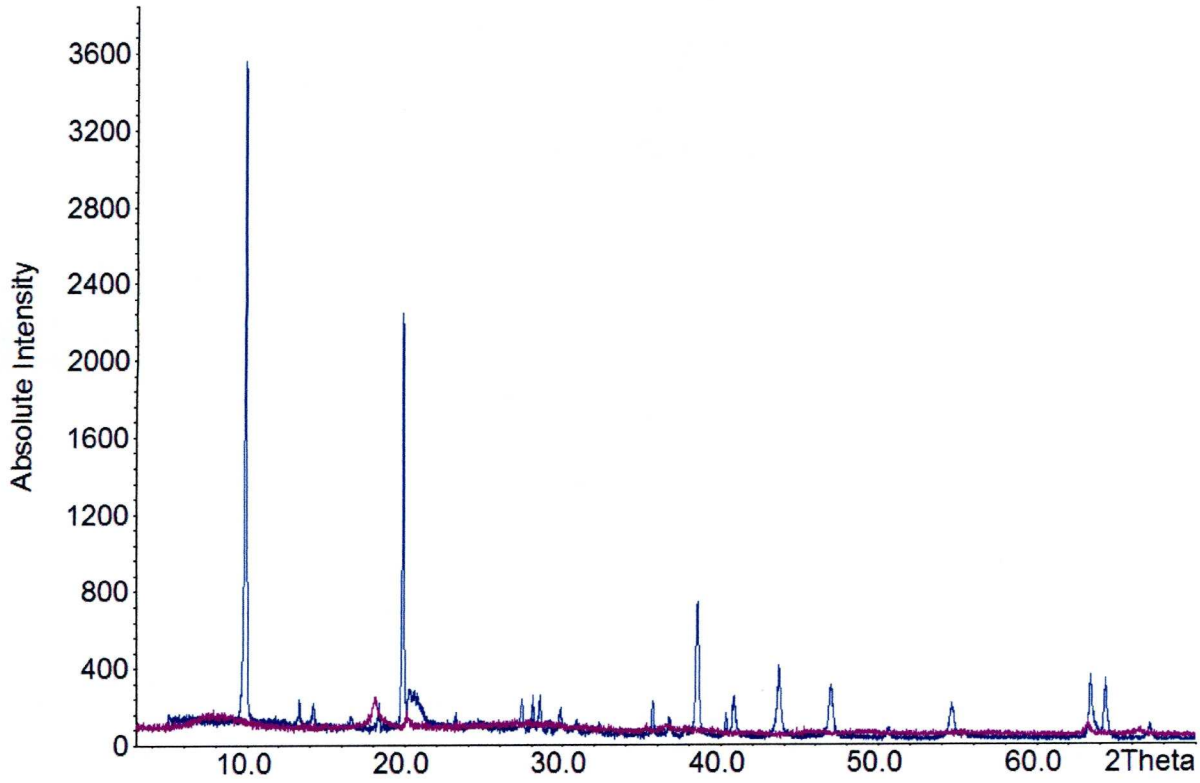

Figure 3.11 PXRD Patterns for Li/Al-NO_3-LDH (blue) and Li/Al-WO_4-LDH (purple) using an absolute intensity scale highlighting the relatively small degree of de-intercalation of Li^+ as shown by the relatively small amount of extra residual gibbsite in the Li/Al-WO_4-LDH. This agrees well with the elemental analysis.

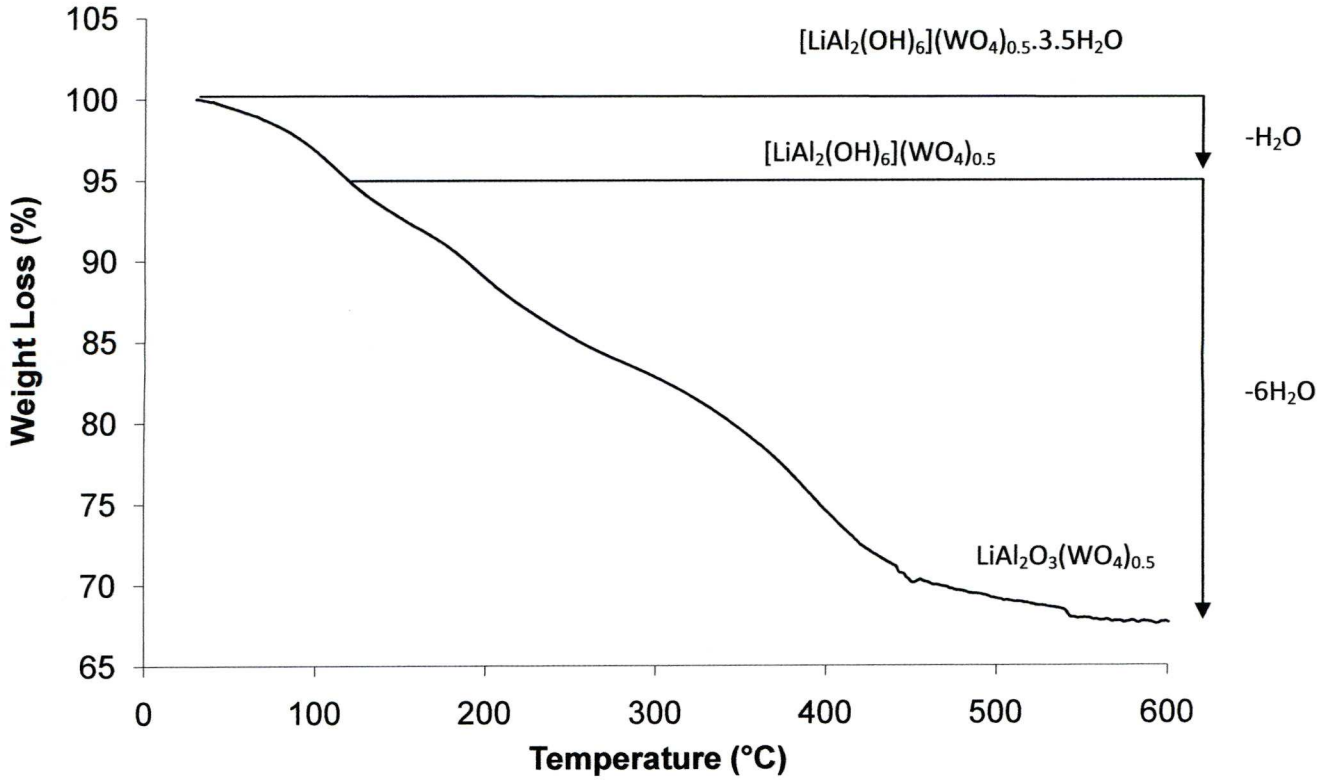

Figure 3.12 TGA curve for Li/Al-WO_4-LDH

$[LiAl_2(OH)_6](WO_4)_{0.5}.3.5H_2O$		
Element	**Calculated**	**Found**
Li	1.9	1.85
Al	15.3	14.76
N	0.00	0.00
H	3.7	3.12
W	26.3	25.00

Table 3.2 Elemental analysis data for Li/Al-WO_4-LDH, based on the formula $[LiAl_2(OH)_6](WO_4)_{0.5}.3.5H_2O$. Values for Li and Al are slightly higher due to reformation of γ-$Al(OH)_3$ as evidenced from the PXRD pattern in Figure 3.11

3.2.2 Catalyst Testing

In a typical reaction, Li/Al-WO_4-LDH (0.0607g, $2.00x10^{-4}$mol) was placed in a round bottomed flask with phenol red (0.0177g, $5.00x10^{-5}$mol) along with ammonium bromide (0.1959g, $2.00x10^{-3}$mol). To this a mixture of H_2O, methanol and tetrahydrofuran (THF) in the ratio 4:3:2 (20ml) was added and the mixture was allowed to stir for 30 minutes. After this time a UV-Visible spectrum was taken by adding 3.00ml of the H_2O, methanol and THF mixture to 35µl of the reaction mixture, using a micro-pipette. The diluted sample was then analysed by UV-Vis spectroscopy in the range of 200 to 800nm with a scan rate of 266.75 nm per minute. H_2O_2 (30%, 2.5×10^{-3} M) was then added and the reaction was allowed to proceed, with a sample from the mixture being taken every 5 minutes for spectrophotometric analysis. Once the reaction had gone to completion (as observed by the UV-Visible spectrum) the reaction mixture was worked up in order to extract the bromophenol blue for further analysis. The mixture was filtered to remove the heterogeneous Li/Al-WO_4-LDH catalyst before extracting the bromophenol blue into dichloromethane using tetra-*n*-hexylammonium chloride and evaporating to dryness. A ^{1}H NMR spectrum (Figure 3.14) was then used to confirm that bromination had indeed taken place. The ^{1}H NMR of the product shows one singlet (7.28, 4*H*), two doublets (6.85 and 8.05, 1*H* each, J = 7.5Hz), and two triplets (7.21 and 7.35, 1*H* each, J = 7.5Hz). This is in good agreement with bromophenol blue.

The bromination of phenol red, catalysed by the Li/Al-WO_4-LDH was followed spectrophotometrically. A typical reaction is shown below in Figure 3.13. As can be seen, the progress of the reaction can be monitored by following the disappearance of the phenol red peak (λ_{max}=429nm) and the appearance of the bromophenol blue peak (λ_{max}=598nm). Other features of the spectrum are the broad bands at 235 and 330nm. A search of the literature shows that the peaks can be attributed to tungsten species[40-42]. The band at 235nm can be attributed to the $O_2^{2-} \rightarrow$W charge transfer transition of a diperoxotungstate (e.g. $WO_2(O_2)^{2-}$, $W_2O_3(O_2)_2^{2-}$), with the peak at 330nm being $O_2^{2-} \rightarrow$ W charge transfer in the tetraperoxotungstate $W(O_2)_4^{2-}$. This provides good evidence of the catalyst being bio-mimetic as the Li/Al-WO_4-LDH forms a peroxo-complex as does the vanadium site in VHPO. This is in agreement with previous work done on tungstate exchanged LDHs being used as bio-mimetic catalysts[27].

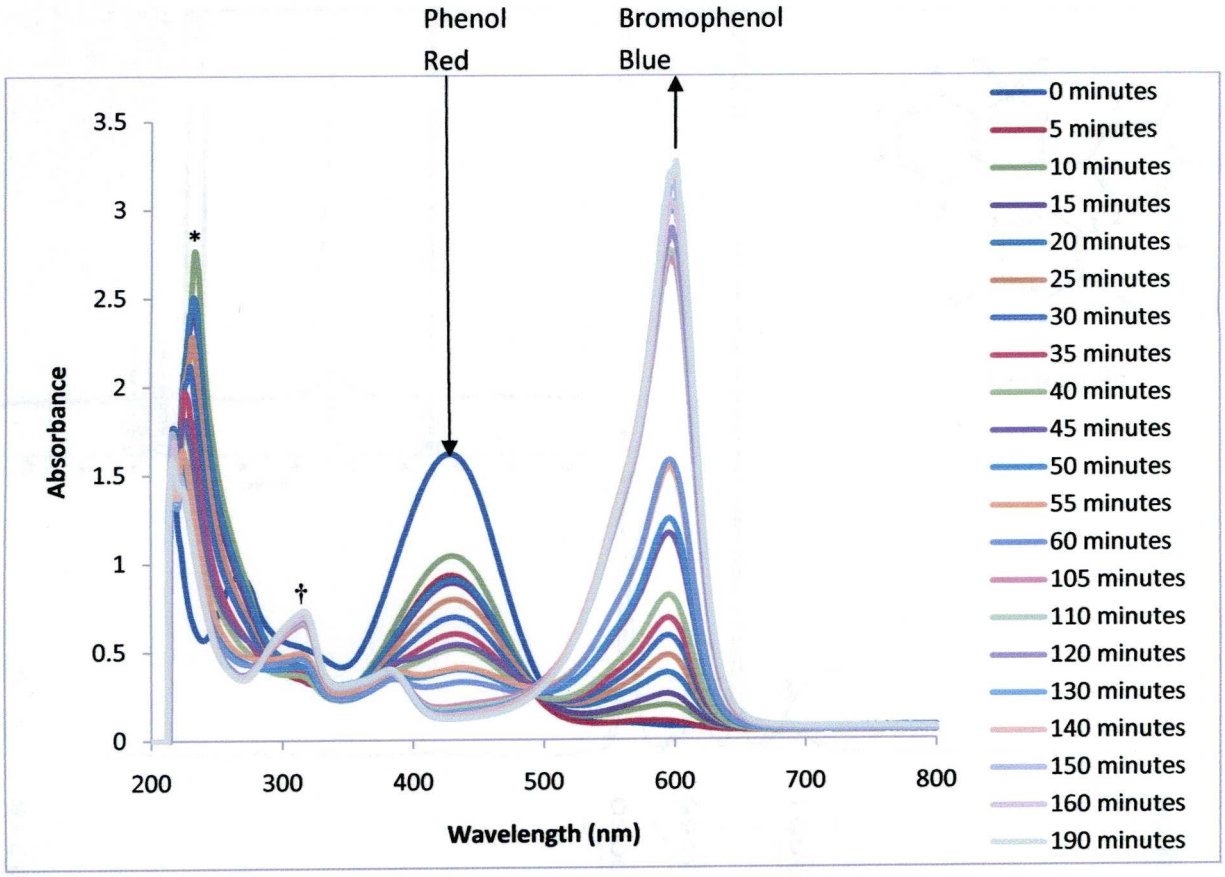

Figure 3.13 UV-Visible spectra for the conversion of phenol red into bromophenol blue in the presence of H_2O_2, using Li/Al-WO_4^{2-}.

Notes

* denotes the O_2^{2-}→ W charge transfer transition of a diperoxotungstate

† denotes the being O_2^{2-}→ W charge transfer in the tetraperoxotungstate $W(O_2)_4^{2-}$

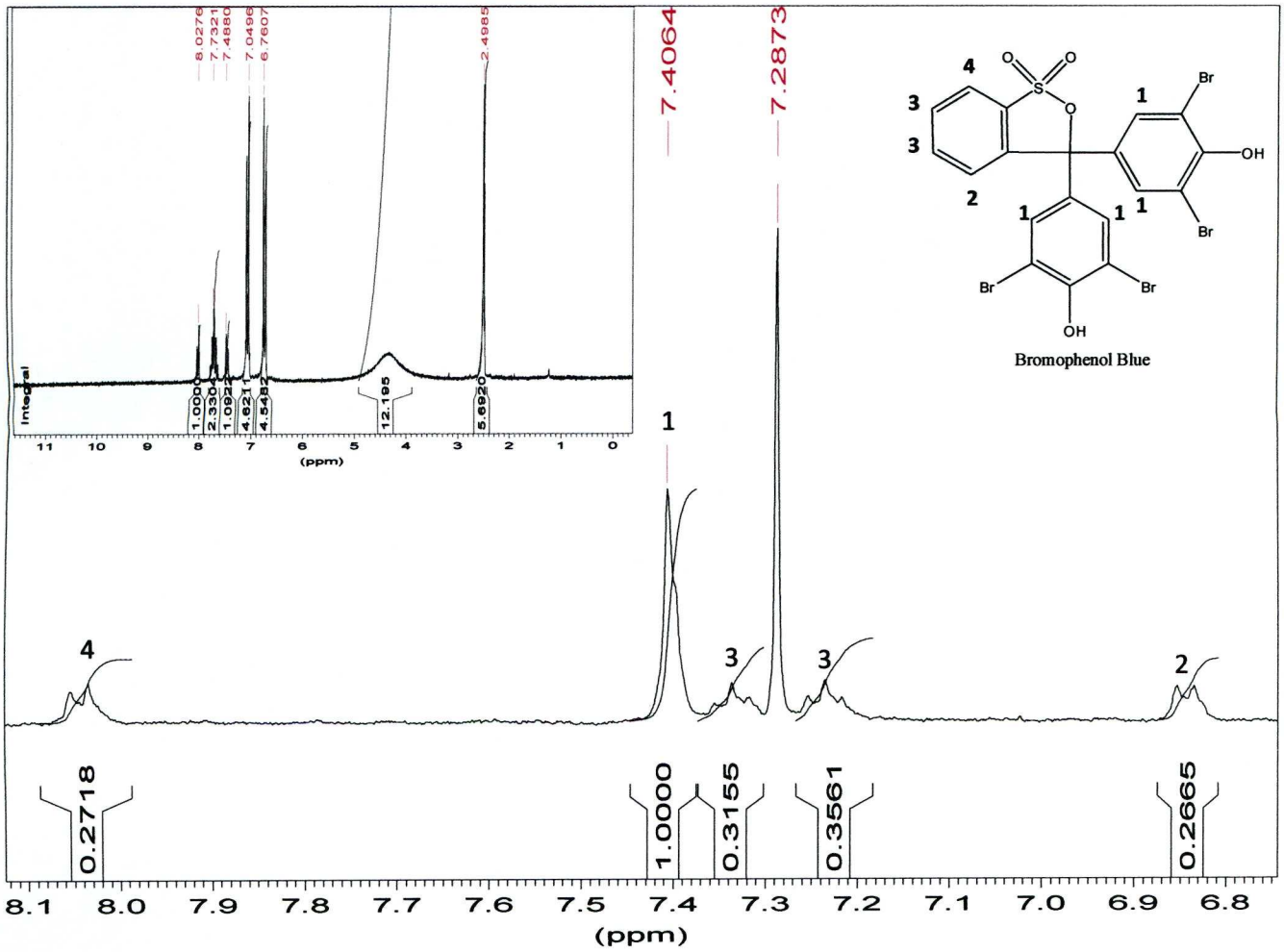

Figure 3.14 ^{1}H NMR spectrum of bromophenol blue, showing the aromatic region; inset, ^{1}H spectrum of phenol red starting material

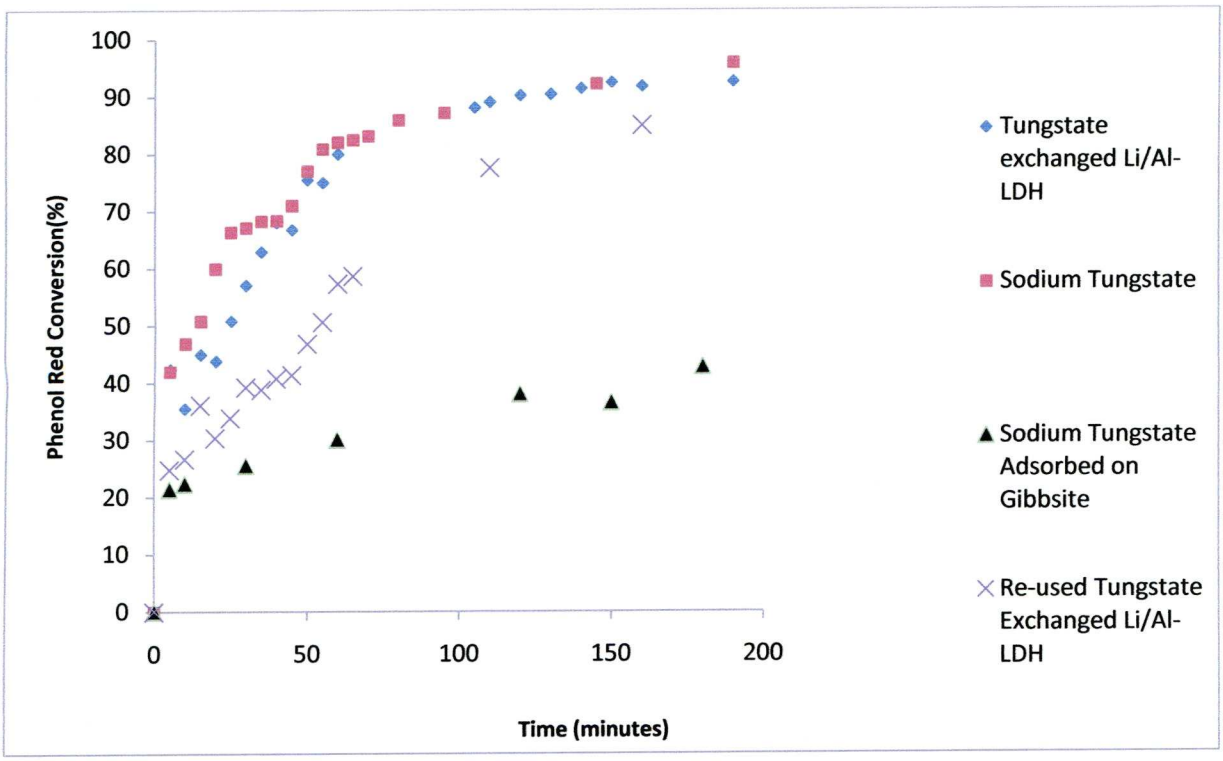

Figure 3.15 Comparison of percentage conversions of phenol red into bromophenol blue using various tungstate based catalysts

Conditions: Phenol red (0.0177g, 2.00×10^{-4}mol), NH_4Br (0.1959g, 2.00×10^{-3}mol) Li/Al-WO_4-LDH (0.0600g, 1.97×10^{-4} mol) and H_2O_2 (30%, 2.5×10^{-3} M) in H_2O, methanol and tetrahydrofuran (THF) in the ratio 4:3:2 (20ml)

From the UV-Vis Spectra concentrations of both phenol red and bromophenol blue were calculated using the Beer-Lambert law. The resulting concentrations were then used to calculate the conversion of phenol red into bromophenol blue by using Equation 1. A plot of conversion vs. time is shown in Figure 3.15, error bars have been omitted, as the maximum total errors for each measurement were less than 1%. From this it is then possible to fit a kinetic model to the reaction. The bromination appears to follow zero order reaction kinetics, as shown by approximately linear loss of substrate vs. time, until most of the reagent has been used up (at ca 80 minutes for the Li/Al-WO_4-LDH system). This is in agreement with similar Mg/Al-WO_4-LDH catalysts[27]. It is also possible to numerically compare the catalysts with literature values, using the parameters[27, 48] (see Table 3.3) bromination rate (Equation 2), turnover frequency, TOF, (Equation 3) and specific activity (Equation 4). Values for each catalyst are compared in Table 3.3. As can be seen from this table and Table 3.2 the LDH supported tungstate catalysts are among the best catalysts.

ation 1

$$\text{Conversion} = \frac{\text{Concentration of Phenol Red} - \text{Initial Concentration of Phenol Red}}{\text{Initial Concentration of Phenol Red}}$$

ation 2

$$\text{Bromination Rate} = \frac{\text{moles } Br^- \text{oxidised}}{\text{time} \,.\, \text{volume}}$$

ation 3

$$\text{TOF} = \frac{\text{moles } Br^- \text{oxidised}}{\text{moles of exchanged metal} \,.\, \text{time}}$$

ation 4

$$\text{Specific Activity} = \frac{\text{moles } Br^- \text{oxidised}}{\text{total weight of LDH} \,.\, \text{time}}$$

Catalyst	Bromination Rate (x10^6 mmol $l^{-1}s^{-1}$)	TOF (h^{-1})	Specific Activity ($mmol^{-1}g^{-1}h^{-1}$)
Na_2WO_4	3.90	0.280	1.1
Li/Al-WO_4-LDH	756	14.229	2.3
Mg/Al-WO_4-LDH(from literature[28])	300	21.60	4.0
Na_2WO_4 adsorbed onto gibbsite	0.013	0.043	0.455
Re-used Li/Al-WO_4-LDH	488	11.9	1.6
No Catalyst	0.01	0	0

Figure 3.3 Comparison between a Mg/Al-WO_4-LDH catalyst[28] from the literature and catalysts used in the current study

In an attempt to ascertain whether the effect was surface based, or whether the organic substrate was accessing the interlayer space, as described in the introduction chapter, an attempt was made to adsorb sodium tungsate onto the surface of gibbsite by suspending gibbsite in a 2 fold molar excess of an aqueous sodium tungstate and then testing its catalytic activity. The results for the oxidative bromination of phenol red are shown in Figure 3.16. The activity of the adsorbed sodium tungstate is significantly less than that of homogenous tungsate, and that of tungsate immobilised on LDH, indicating that in the case of heterogeneous catalysis, the tungstate needs to be held between the layers as well as on the surface. To rule out any activity by metals in the LDH other than tungsate (e.g. Li or Al) a test was carried out on the parent Li/Al-NO_3-LDH. Similarly, a test was carried out on the gibbsite [γ-Al(OH_3)] material, as some de-intercalation of the Li metal occurs when the tungstate anion is exchanged for nitrate in the catalyst synthesis. Both tests indicated that it was indeed the case that tungstate was necessary for the catalysis to occur, with the reaction failing to go forwards to any significant degree over the course of 1 week, due to the inactivity of both the Li/Al-NO_3-LDH and the gibbsite, as tested by taking samples of the reaction mixture every 24 hours and analysing the UV-Vis spectra. The re-usability of the catalyst was also tested. As can be seen in Figure 3.19, the second time the catalyst was used, its performance was slightly poorer. This is reflected in the lower bromination rate of 488 x10^6 mmol $l^{-1}s^{-1}$ for the recycled catalyst as compared to the initial rate of 756 x10^6 mmol $l^{-1}s^{-1}$ in Table 3.3. To test if this was due to leaching of tungstate from, the catalyst, the Li/Al-WO_4-LDH was stirred in the reaction solvent (H_2O:MeOH:THF in the ratio 4:3:2, 20ml), for 4 hours before removal of the catalyst by centrifugation. The reaction was then performed without any solid catalyst, using the catalyst soaked solvent. The reaction again did not occur to any significant degree over the course of 1 week, again as tested by taking samples of the reaction mixture every 24 hours and analysing the UV-Vis spectra.

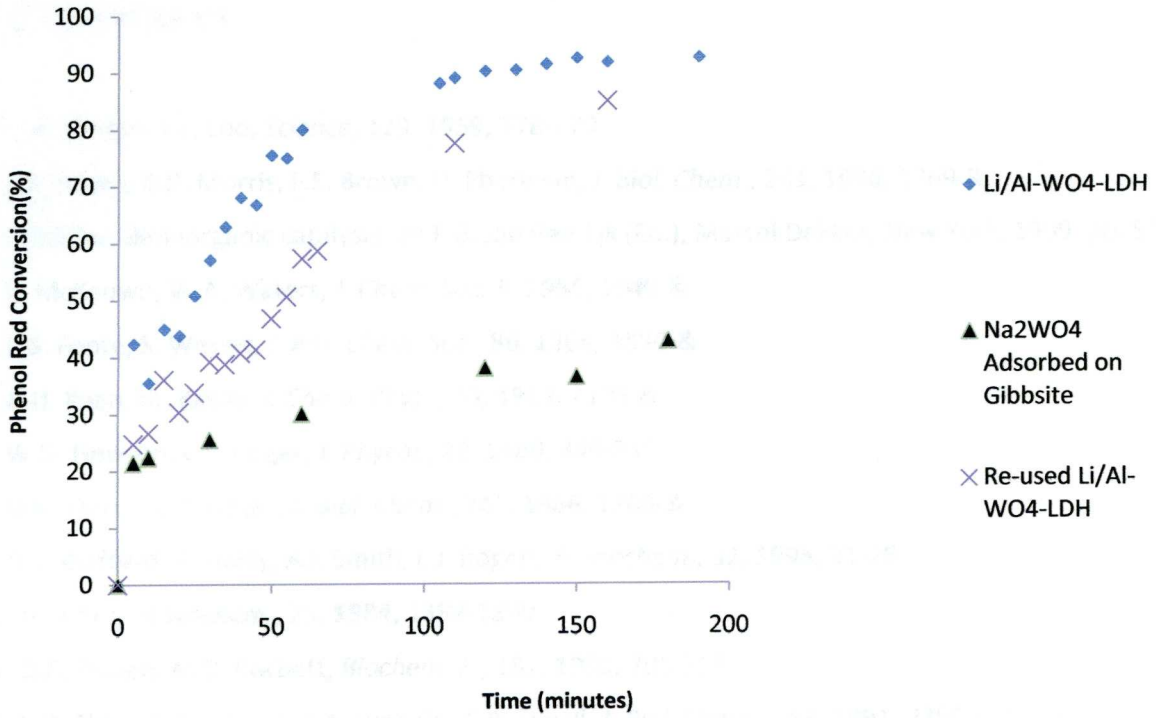

Figure 3.16 Reaction monitoring for the oxidative bromination of phenol red using Na_2WO_4 adsorbed onto gibbsite, [γ-$Al(OH)_3$], a re-used Li/Al-WO_4-LDH catalyst. Both are compared to fresh Li/Al-WO_4-LDH catalyst

3.3 Conclusions

The use of immobilised tungstate on LDHs has been shown to mimic the action of the haloperoxidases. By studying the catalytic cycles of both VHPO and tungstate exchanged LDHs, many similarities can be found, such as the way that both VHPO and the LDH mimic work not by redox, but by binding a molecule of H_2O_2. This higher energy complex then oxidises a halide anion which can then go on to halogenate an organic substrate. The test reaction, the bromination of phenol red was easily completed in 200 minutes. This compares well to the other Mg/Al-WO_4-LDH bio-mimetic catalysts previously tested. Further experimentation highlighted the need for tungstate to be present, with the reactions using Li/Al-NO_3-LDH and gibbsite proving unsuccessful with no reaction after 1 week. Leaching of tungstate from the Li/Al-WO_4-LDH catalyst was also minimal as evidenced by soaking the catalyst in reaction solvent before filtering the catalyst and attempting the reaction in that solvent. Again, no reaction occurred here. The LDH bio-mimetic system has many advantages over the standard bromination methods as it is much more mild, using more environmentally friendly reagents. It is also more useful than the VHPO enzymes in many organic syntheses, as there is no requirement for strongly acidic conditions for the reaction to proceed.

3.4 References

1. J.W. Burger, T.L. Loo, *Science*, 129, **1959,** 778-779
2. L.P. Hager, D.R. Morris, F.S. Brown, H. Eberwein, *J. Biol. Chem.*, 241, **1966,** 1769-&
3. A. Butler, Bioinorganic catalysis, in: E.B. Jan Reedijk (Ed.), Marcel Dekker, New York, 1999, pp. 55.
4. E. McKeown, W.A. Waters, *J. Chem. Soc. B*, **1966,** 1040-&
5. C.S. Foote, S. Wexler, *J. Am. Chem. Soc.*, 86, **1964,** 3880-&
6. A.U. Khan, M. Kasha, *J. Chem. Phys.* , 39, **1963,** 2105-&
7. W.D. Hewson, L.P. Hager, *J. Phycol.*, 16, **1980,** 340-345
8. D.R. Morris, L.P. Hager, *J. Biol. Chem.*, 241, **1966,** 1763-&
9. D.J. Sheffield, T. Harry, A.J. Smith, L.J. Rogers, *Phytochem.*, 32, **1993,** 21-26
10. H. Vilter, *Phytochem.*, 23, **1984,** 1387-1390
11. D.G. Baden, M.D. Corbett, *Biochem. J.* , 187, **1980,** 205-211
12. Y.P. Chen, D.E. Lincoln, S.A. Woodin, C.R. Lovell, *J. Biol. Chem.*, 266, **1991,** 23909-23915
13. A. Butler, M. Sandy, *Nature*, 460, **2009,** 848-854
14. A. Messerschmidt, R. Wever, *Proc. Natl. Acad. Sci. U. S. A.*, 93, **1996,** 392-396
15. K. Kuhnel, W. Blankenfeldt, J. Terner, I. Schlichting, *J. Biol. Chem.*, 281, **2006,** 23990-23998
16. A. Messerschmidt, L. Prade, R. Wever, *Biol. Chem.*, 378, **1997,** 309-315
17. M. Weyand, H.J. Hecht, M. Kiess, M.F. Liaud, H. Vilter, D. Schomburg, *J. Mol. Biol.*, 293, **1999,** 595-611
18. G.J. Colpas, B.J. Hamstra, J.W. Kampf, V.L. Pecoraro, *J. Am. Chem. Soc.*, 118, **1996,** 3469-3478
19. J.H. Rolston, K. Yates, *J. Am. Chem. Soc.*, 91, **1969,** 1469-&
20. M.C. Carreno, J.L.G. Ruano, G. Sanz, M.A. Toledo, A. Urbano, *J. Org. Chem.* , 60, **1995,** 5328-5331
21. N. Itoh, A. Hasan, Y. Izumi, H. Yamada, *Eur. J. Biochem.*, 172, **1988,** 477-484
22. V. Conte, F. Difuria, S. Moro, *Tetrahedron Lett.*, 35, **1994,** 7429-7432
23. M.S. Reynolds, S.J. Morandi, J.W. Raebiger, S.P. Melican, S.P.E. Smith, *Inorg. Chem.*, 33, **1994,** 4977-4984
24. C.U. Dinesh, R. Kumar, B. Pandey, P. Kumar, *J. Chem. Soc., Chem. Commun.*, **1995,** 611-612
25. H.-A. Wagenknecht, W.-D. Woggon, *Chem. Biol.*, 4, **1997,** 367-372
26. R.D. Libby, T.M. Beachy, A.K. Phipps, *J. Biol. Chem.*, 271, **1996,** 21820-21827
27. B.F. Sels, D.E. De Vos, M. Buntinx, P.A. Jacobs, *J. Catal.* , 216, **2003,** 288-297
28. B. Sels, D. De Vos, M. Buntinx, F. Pierard, A. Kirsch-De Mesmaeker, P. Jacobs, *Nature*, 400, **1999,** 855-857
29. B.F. Sels, D.E. De Vos, P.A. Jacobs, *J. Am. Chem. Soc.*, 123, **2001,** 8350-8359

30. R.I. De La Rosa, M.J. Clague, A. Butler, *J. Am. Chem. Soc.*, 114, **1992,** 760-761

31. M.J. Clague, N.L. Keder, A. Butler, *Inorg. Chem.*, 32, **1993,** 4754-4761

32. G.J. Colpas, B.J. Hamstra, J.W. Kampf, V.L. Pecoraro, *J. Am. Chem. Soc.*, 116, **1994,** 3627-3628

33. M. Andersson, V. Conte, F. Difuria, S. Moro, *Tetrahedron Lett.*, 36, **1995,** 2675-2678

34. G.E. Meister, A. Butler, *Inorg. Chem.*, 33, **1994,** 3269-3275

35. J.H. Espenson, O. Pestovsky, P. Huston, S. Staudt, *J. Am. Chem. Soc.*, 116, **1994,** 2869-2877

36. J.V. Walker, M. Morey, H. Carlsson, A. Davidson, G.D. Stucky, A. Butler, *J. Am. Chem. Soc.*, 119, **1997,** 6921-6922

37. C.T. Kresge, M.E. Leonowicz, W.J. Roth, J.C. Vartuli, J.S. Beck, *Nature*, 359, **1992,** 710-712

38. T. Maschmeyer, F. Rey, G. Sankar, J.M. Thomas, *Nature*, 378, **1995,** 159-162

39. B.F. Sels, D.E. De Vos, M. Buntinx, P.A. Jacobs, *Journal of Catalysis*, 216, **2003,** 288-297

40. A.J. Dedman, D.H. Richards, T.J. Lewis, *J. Chem. Soc.*, **1963,** 5020-&

41. W.P. Griffith, *J. Chem. Soc.*, **1963,** 5345-&

42. M.H. Dickman, M.T. Pope, *Chem. Rev.*, 94, **1994,** 569-584

43. E. Gardner, T.J. Pinnavaia, *Appl. Catal., A* 167, **1998,** 65-74

44. E. Dumitriu, C. Guimon, A. Cordoneanu, S. Casenave, T. Hulea, C. Chelaru, H. Martinez, V. Hulea, *Catal. Today*, 66, **2001,** 529-534

45. A.-L. Maciuca, E. Dumitriu, F. Fajula, V. Hulea, *Appl. Catal., A* 338, **2008,** 1-8

46. A.-L. Maciuca, E. Dumitriu, F. Fajula, V. Hulea, *Chemosphere*, 68, **2007,** 227-233

47. A.V. Besserguenev, A.M. Fogg, R.J. Francis, S.J. Price, D. Ohare, V.P. Isupov, B.P. Tolochko, *Chem. Mater.*, 9, **1997,** 241-247

48. J.M. Thomas, W.J. Thomas, *Principles and practice of heterogeneous catalysis*, VCH, 1997.

Chapter 4: The Oxidation of Citronellol by Molybdate Supported Layered Double Hydroxides

4.1 Introduction

Singlet oxygen ($^1O_2$) generation in aqueous solution was first observed in 1960 by Seliger[1] when sodium hypochlorite (NaOCl), or chlorine was added to aqueous hydrogen peroxide. Work by Khan and Kasha[2], Foote and Wexler[3] and Corey and Taylor[4], discussed this further, with the conclusion that singlet oxygen was being generated. Soon after, Yamazaki[5] used singlet oxygen to form alcohols via the oxidation of propane, with others using the species to oxidise common organic molecules[6-7]. Studies concerning the selectivities of oxidations using the various methods were also conducted[8], which concluded that the method of singlet oxygen generation did not affect the overall product yield, or distribution of products. Work was also conducted on the yield of singlet oxygen via the various generation methods[9-10]. It was also found that 1,10-diphenylanthracene peroxide was effectively a storage molecule for captured singlet oxygen, which could be released when required to oxidise organic substrates which were efficient acceptors of the species[11], for example 2, 5-diphenyl-4-methyloxazole (see Figure 4.1).

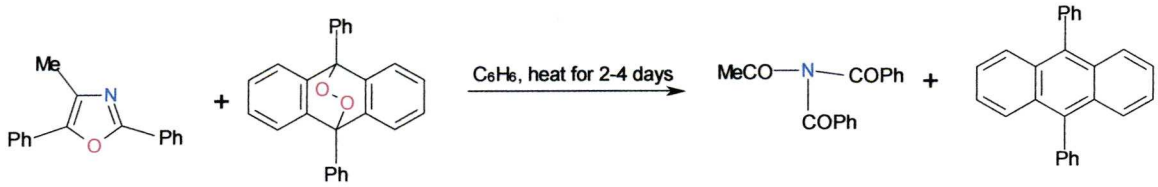

Figure 4.1 Using the molecule 1, 10-diphenylanthracene peroxide for effectively storing singlet oxygen, which can be released upon heating to oxidise organic substrates

Most methods of generating singlet oxygen from hydrogen peroxide solution were either homogeneous as in the use of hypochlorite[1], or less commonly heterogeneous as in the case of a photosensitizer such as Rose Bengal (see figure 4.2) adsorbed onto silica[12].

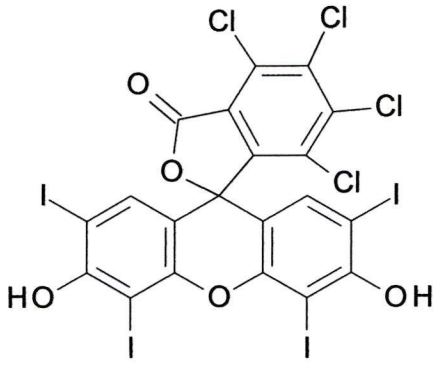

Figure 4.2 Rose Bengal, a commonly used organic photosensitiser for the generation of singlet oxygen

Another common way to produce singlet oxygen is the disproportionation of hydrogen peroxide using minerals[13], such as CeO_2[14], OH^-[15], Fe(II)[16] and also MoO_4^{2-}[17]. Other more novel methods involve the formation of peroxy-metal species such as K_3CrO_8[18] and CrO_5[19], which can then be decomposed, releasing singlet oxygen. In general, transition metals in the d^0 configuration are able to generate singlet oxygen, with niobium^V as an exception[13]. Lanthanum containing compounds have also shown promise in this area with La containing zeolites[20], Lanthanum(III) compounds[21] and La doped zinc hydroxycarbonates[22]. La containing materials have disadvantages of low activity and low H_2O_2 efficiency, however, this brings an advantage of high selectivity, with minimal amounts of epoxide and enone side products forming, which can be a problem in the Mo based system described presently.

The use of Mg/Al-LDHs to immobilise the molybdate anion has been explored[23-26]. Methods involving the immobilisation of molybdate generally include the synthesis of a Mg/Al-NO_3-LDH via a co-precipitation method and then exchange of nitrate for molybdate. The use of molybdate as a catalyst for the decomposition of H_2O_2 into singlet oxygen has been shown to be quantitiative[27]. Using molybdate immobilised on the Mg/Al-LDH, results suggested that unit activity per Mo atom was higher than that of homogeneous molybdate[25] (Figure 4.3), with LDH immobilised molybdate allowing for the use of aprotic organic solvents[28], which is not possible with free molybdate.

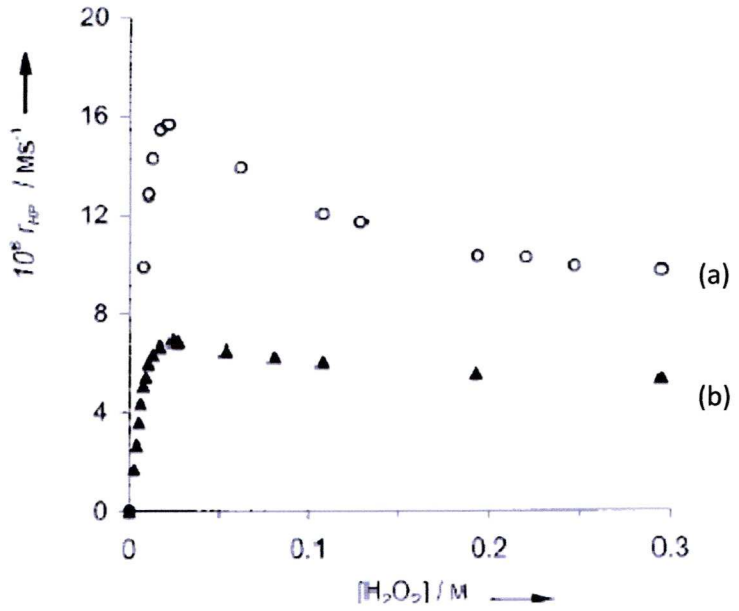

Figure 4.3 Comaprison[25] of heterogeneous molybdate in the form Mg/Al-MoO_4-LDH (a) and (b) homogeneous molybdate (Na_2MoO_4)

A chemical test for the efficiency of the molybdate catalyst is the chemical trapping of the singlet oxygen generated from the H_2O_2 solution using suitably reactive olefins[29], and in particular, β-citronellol[28], forming a hydroperoxide, which can be reduced quantitatively to its corresponding alcohol using sodium sulphite[30]. Citronellol is also an excellent substrate to use, as at the concentrations used in the oxidation reactions studied, it is well above its β-value (in methanol β=0.15M)[31], the β-value being the Foote reactivity index, i.e. the alkene concentration required to trap exactly half of the singlet oxygen in solution - implying that the vast majority of singlet oxygen released by the decomposition of hydrogen peroxide is trapped by the substrate, with a larger β-value leading to more efficient reaction conditions[32]. The oxidation of β-citronellol is also a synthetically useful reaction, with the reaction being an important step in the synthesis of the perfumery ingredient rose oxide[33] (see Figure 4.4).

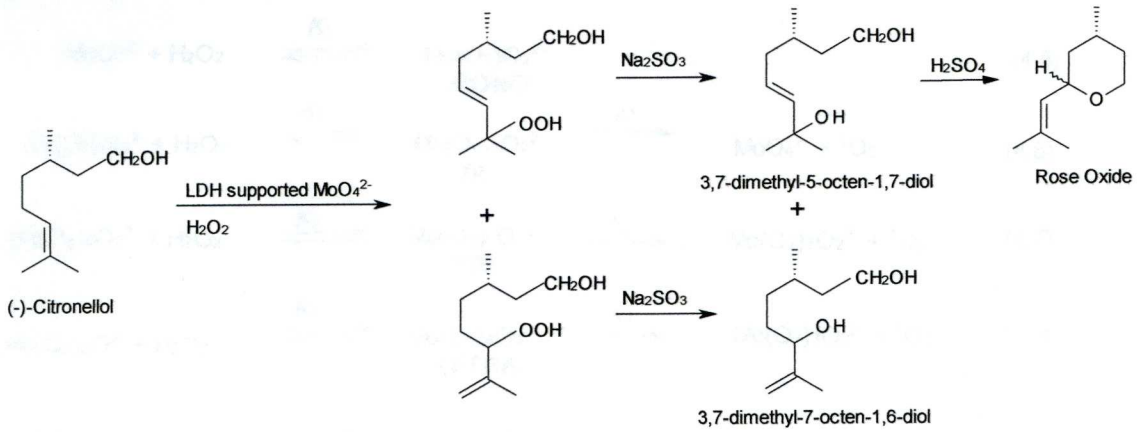

Figure 4.4 Oxidation of Citronellol to hydroperoxy species before reduction to their corresponding alcohols. The final step is the addition of H_2SO_4 forming rose oxide

A kinetic pathway for the decomposition of H_2O_2 has been proposed[25], where several peroxo-molybdate species are involved (see Figure 4.5-4.14). Reactions involving acid species can be ignored due to the inherent basicity of the LDH support[34], which reduces the initial large set of reactions to only reactions 4.5-4.8. The formation of each peroxo-species has been confirmed by Raman spectroscopy[25]. The main points of the relevant reaction schemes are the formation of various peroxo molybdate species after treatment of MoO_4^{2-} with H_2O_2 and the decomposition of the peroxo-molybdate species into singlet oxygen and oxo-molybdenum species.

$$MoO_4^{2-} + H_2O_2 \overset{K_1}{\rightleftharpoons} Mo(O_2)O_2^{2-} \quad \textbf{MONO} \qquad (4.5)$$

$$Mo(O_2)O_3^{2-} + H_2O_2 \overset{K_2}{\rightleftharpoons} Mo(O_2)_2O_2^{2-} \quad \textbf{DI} \xrightarrow{k_1} MoO_4^{2-} + {}^1O_2 \qquad (4.6)$$

$$Mo(O_2)_2O_2^{2-} + H_2O_2 \overset{K_3}{\rightleftharpoons} Mo(O_2)_3O_2^{2-} \quad \textbf{TRI} \xrightarrow{k_2} Mo(O_2)_2O_2^{2-} + {}^1O_2 \qquad (4.7)$$

$$Mo(O_2)_3O^{2-} + H_2O_2 \overset{K_4}{\rightleftharpoons} Mo(O_2)_4O_2^{2-} \quad \textbf{TETRA} \xrightarrow{k_3} Mo(O_2)_3O_2^{2-} + {}^1O_2 \qquad (4.8)$$

$$HMo(O_2)O_3^- + H_2O \rightleftharpoons Mo(O_2)O_2^{2-} + H_3O^+ \qquad (4.9)$$

$$HMo(O_2)_2O_2^- + H_2O \rightleftharpoons Mo(O_2)_2O_2^{2-} + H_3O \qquad (4.10)$$

$$HMo(O_2)_3O^- + H_2O \rightleftharpoons Mo(O_2)_3O_2^{2-} + H_3O^+ \qquad (4.11)$$

$$HMo(O_4)^- + H_2O \rightleftharpoons Mo(O_2)_4^{2-} + H_3O^+ \qquad (4.12)$$

$$2Mo(O_2)_2O_2^{2-} + 2H_3O^+ \rightleftharpoons Mo_2O_3(O_2)_4^{2-} + 3H_2O \qquad (4.13)$$

$$H_2O_2 + H_2O \rightleftharpoons HOO^- + H_3O^+ \qquad (4.14)$$

Reaction Schemes 4.5-4.14 Possible decomposition pathways for H_2O_2 in the presence of molybdate. Only reactions 4.5-4.8 are appropriate in the case of LDH supported molybdate owing to the basicity of the LDH structure

The reaction of singlet oxygen with alkenes occurs in a synthetically useful manner where substitution and rearrangement in the allylic position[35] takes place in a selective and predictable manner. OOH, formed from the reaction between the organic substrate is distinct from free radical autooxidation by triplet ($^3O_2$) oxygen. Evidence against a free radical mechanism is provided when limonene (Figure 4.15 (a)), a chiral compound, is reacted with singlet oxygen. Among other products is the chiral hydroperoxide (Figure 4.15 (b)). It would not be possible to form this should a free radical mechanism be taking place, as the intermediate would possess a plane of symmetry[36] (Figure 4.15 (c)). The auto oxidation reaction gave both enantiomers of the hydroperoxide. The rates of alkenes with differing amounts of substitution have also been studied[37], showing that the more highly substituted the alkene, the greater the reaction rate, with electron withdrawing groups having a deactivating effect. Geminal selectivity is also observed in singlet oxygen addition reactions, with alkyl substituted alkenes having the hydrogen which is geminal to the larger substituent removed[38] (see Figure 4.16).

Several mechanisms for the addition of singlet oxygen have been proposed, such as that of a concerted reaction[39], however, there is stereochemical evidence against this[40]. The most likely mechanism is that of the addition of singlet oxygen across a double bond giving a perepoxide[41] before a proton transfer[42] (see Figure 4.17).

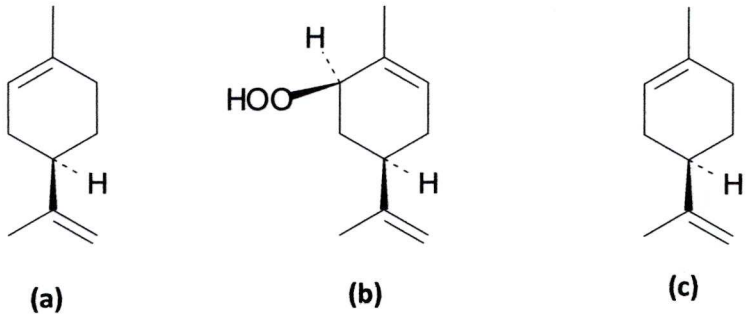

Figure 4.15 (a) Limonene, (b) Chiral hydroperoxide and (c) intermediate in free radical mechanism

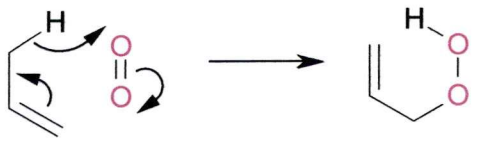

Figure 4.16 Demonstration of geminal hydrogen being more easily abstracted from a double bond

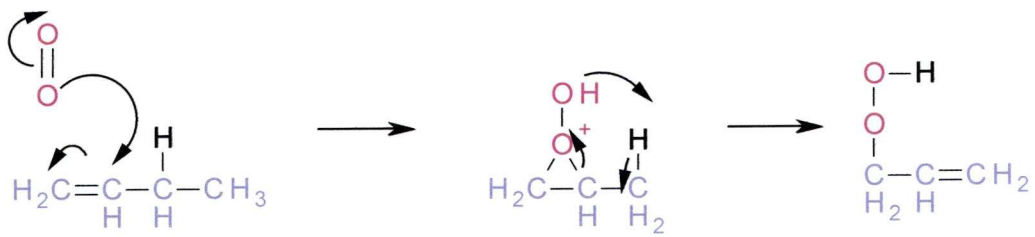

Figure 4.17 Formation of a perepoxide followed by internal proton transfer

4.2 Catalyst Preparation and Characterisation

The Li/Al-MoO_4-LDH catalysts were prepared via an anion exchange reaction of Li/Al-NO_3-LDH as described in Chapter 6. The catalyst was then characterised using PXRD, TGA, elemental analysis and IR-spectroscopy. The PXRD pattern is shown in Figure 4.18, and is compared to the parent Li/Al-NO_3-LDH. As can be seen, a small amount of nitrate is left after the exchange process. Figure (a) shows the parent Li/Al-NO_3-LDH, with an interlayer separation of 8.9Å, which agrees well with the literature[43] as does the value of 11.7Å for the Li/Al-MoO_4-LDH[44]. As can be seen, a small amount of nitrate remains in the Li/Al-MoO_4-LDH material with the peak at 8.9Å still being visible, albeit smaller. Unfortunately, a significant loss in crystallinity is also noted after the anion exchange process, as is a small amount of leaching of Li^+ ions from the parent gibbsite structure. As seen in Figure 4.19, when looked at on an absolute basis when the main gibbsite peak (at 4.8Å, 18.2° 2Θ) is compared between gibbsite and the Li/Al-MoO_4-LDH, the amount of gibbsite reformation through loss of Li^+ is relatively little. TGA was also performed on the catalyst, as shown in (Figure 4.20). There are two main mass losses, the first being around 8%, corresponding to a loss of interlayer water (calculated 8.2%), based upon a formula $[Li_{0.67}Al_2(OH)_4](MoO_4)_{0.45}(NO_3)_{0.1}.2.5H_2O$. The second mass loss of 25.5% (calculated 25.0%) between 160 and 500°C is due to the decomposition of the layers forming $LiAl_2O_3(MoO_4)_{0.45}$. Elemental analysis was also performed on the sample (see Figure 4.21), which gave reasonable agreement with the calculated values, consistent with the overall formula $[Li_{0.67}Al_2(OH)_4](MoO_4)_{0.45}(NO_3)_{0.1}.2.5H_2O$

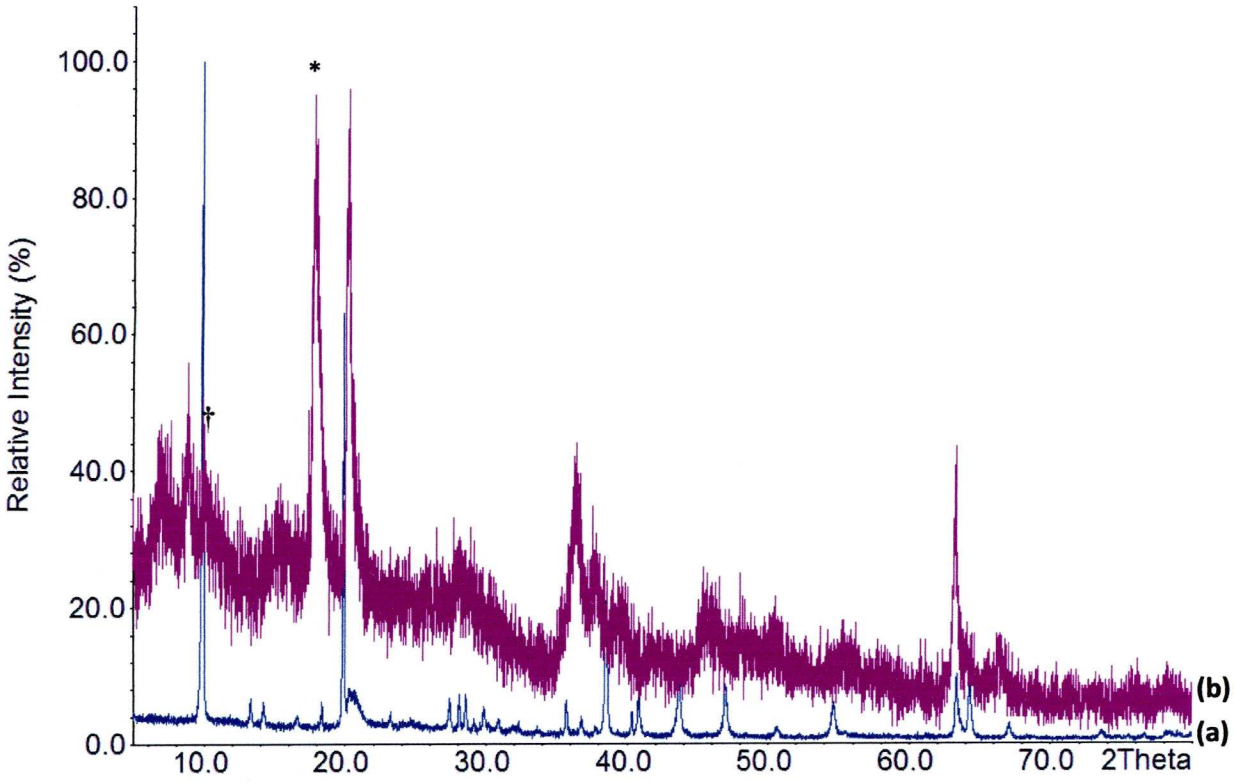

Figure 4.18 Comparison of PXRD patterns for (a) Li/Al-NO_3-LDH and (b) Li/Al-MoO_4-LDH. In the Li/Al-MoO_4-LDH pattern, a marked loss in crystallinity is observed, as is some de-intercalation of Li^+ ions from the parent gibbsite structure.

* peak attributed to gibbsite

†peak showing that a small amount of nitrate remains in the LDH

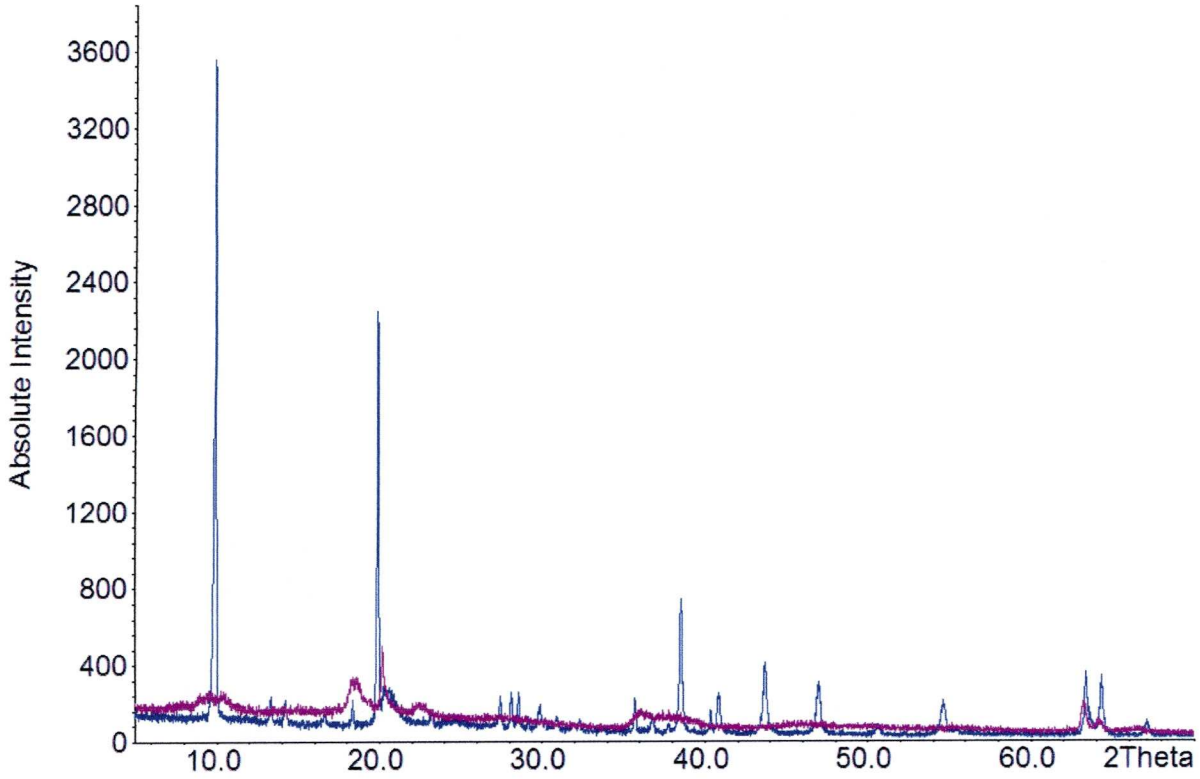

Figure 4.19 Comparison between Li/Al-NO_3-LDH (blue) and Li/Al-MoO_4-LDH (purple) PXRD patterns on an absolute scale, showing relatively little de-intercalation of Li^+, reforming gibbsite has occurred

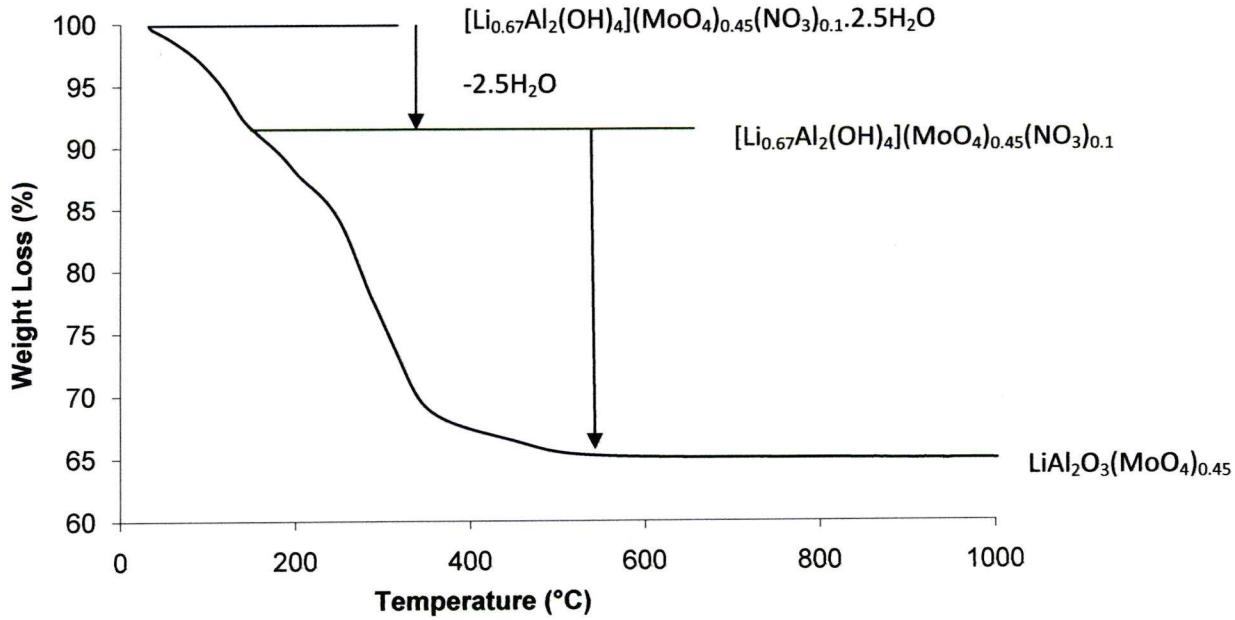

Figure 4.20 TGA curve for Li/Al-MoO_4-LDH

Nominal Composition	$[Li_{0.67}Al_2(OH)_4](MoO_4)_{0.45}(NO_3)_{0.1}.2.5H_2O$	
Element	**Calculated**	**Found**
Li	1.87	1.9
Al	21.8	21.8
N	0.5	0.5
H	2.6	2.8
Mo	17.6	16.9

Figure 4.21 Elemental analyses performed on Li/Al-MoO_4-LDH, using the nominal formula $[Li_{0.67}Al_2(OH)_4](MoO_4)_{0.45}(NO_3)_{0.1}.2.5H_2O$

4.3 Catalyst Testing

The oxidation of (-)-S-β-Citronellol was followed by gas chromatography. In accordance with the literature[28], in a typical reaction (-)S-β-Citronellol (911 µl, 0.05mol) was put in a flask along with methanol (10ml) and the Li/Al-MoO_4-LDH (0.2500 g, $9.58x10^{-4}$ mol). The mixture was stirred for 30 minutes to ensure complete dispersion of the catalyst before an initial gas chromatograph was taken. H_2O_2 (30%) was then added in 200µl portions with reduction using sodium sulphite being performed before GC being performed after each total conversion of H_2O_2. This could be observed when the colour of the reaction mixture changed from red back to yellow. Each chromatograph was analysed and the levels of (-)S-β-Citronellol and subsequent products were quantified by using the integrated values of the appropriate peaks.

The gradual addition of H_2O_2 has been shown to favour the formation of the triperoxomolybdate species (see Figures 4.5-4.14) which is the species responsible for the most efficient generation of singlet oxygen in LDHs supporting molybdate[32]. The products were then characterised using GC-MS and also ^1H NMR spectroscopy. GC-MS results showed that the products were distributed in the ratio 80:20 3,7-dimethyl-5-octen-1,7-diol: 3,7-dimethyl-7-octen-1,6-diol. The relative rates of each reaction can be followed in Figure 4.23, using the following equations to calculate the values.

$$\text{Yield} = \frac{\text{Concentration of both products}}{\text{Citronellol concentration} + \text{Concentration of both products}} \times 100$$

$$\text{Individual Product Yield} = \frac{\text{Individual Product Concentration}}{\text{Cirtonellol Concentration} + \text{Concentration of both products}} \times 100$$

$$\text{Citronellol (\%)} = \frac{\text{Citronellol concentration}}{\text{citronellol concentration} + \text{Concentration of both products}} \times 100$$

A ^{1}H NMR for the final product mixture is shown in Figure 4.24, whilst in Figure 4.25 a confirmation of the product distribution can be found by ^{1}H NMR. Upon comparison with the literature[28], the oxidation proceeds much more quickly. As can be seen in Figure 4.22, the conversion of citronellol is complete in 5 hours using the Li/Al-MoO_4-LDH system, whereas in a similar Mg/Al-LDH system, only around 90% conversion is achieved after 10 hours.

LDH	Conversion (%)	Time (hours)
Mg/Al-MoO_4-LDH[28]	90%	10
$[Li_{0.67}Al_2(OH)_4](MoO_4)_{0.45}(NO_3)_{0.1}.2.5H_2O$	>99%	5
$[Li_{0.67}Al_2(OH)_4](MoO_4)_{0.45}(NO_3)_{0.1}.2.5H_2O$ Reused	>99%	6.6

Figure 4.22 Comparison between conversions of citronellol oxidation using different LDHs

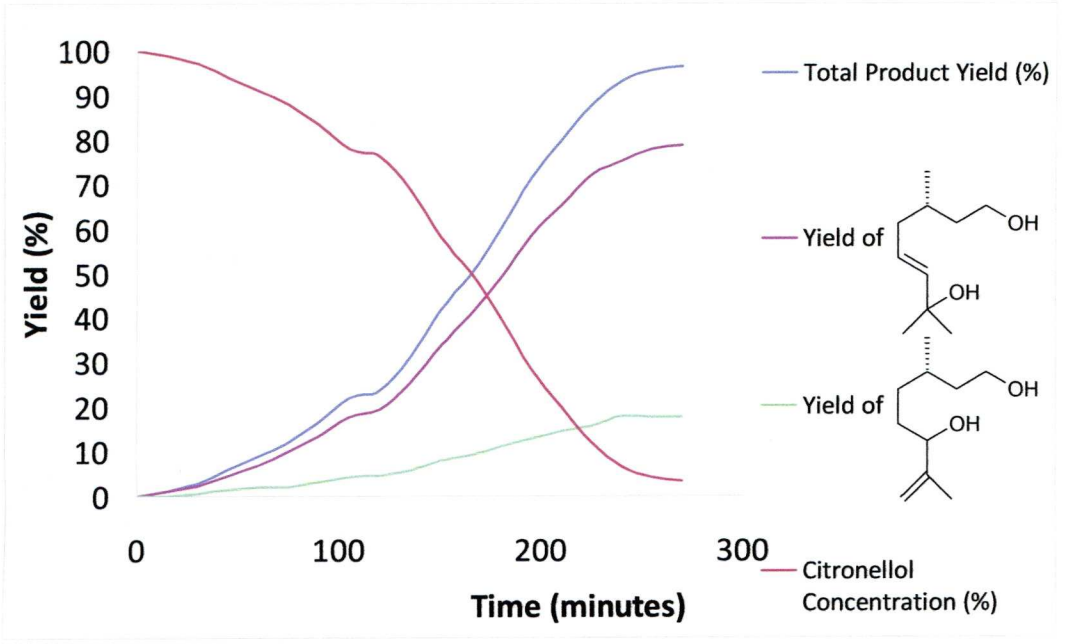

Figure 4.23 Comparison of reaction rates and product distribution for oxidation of S-Citronellol

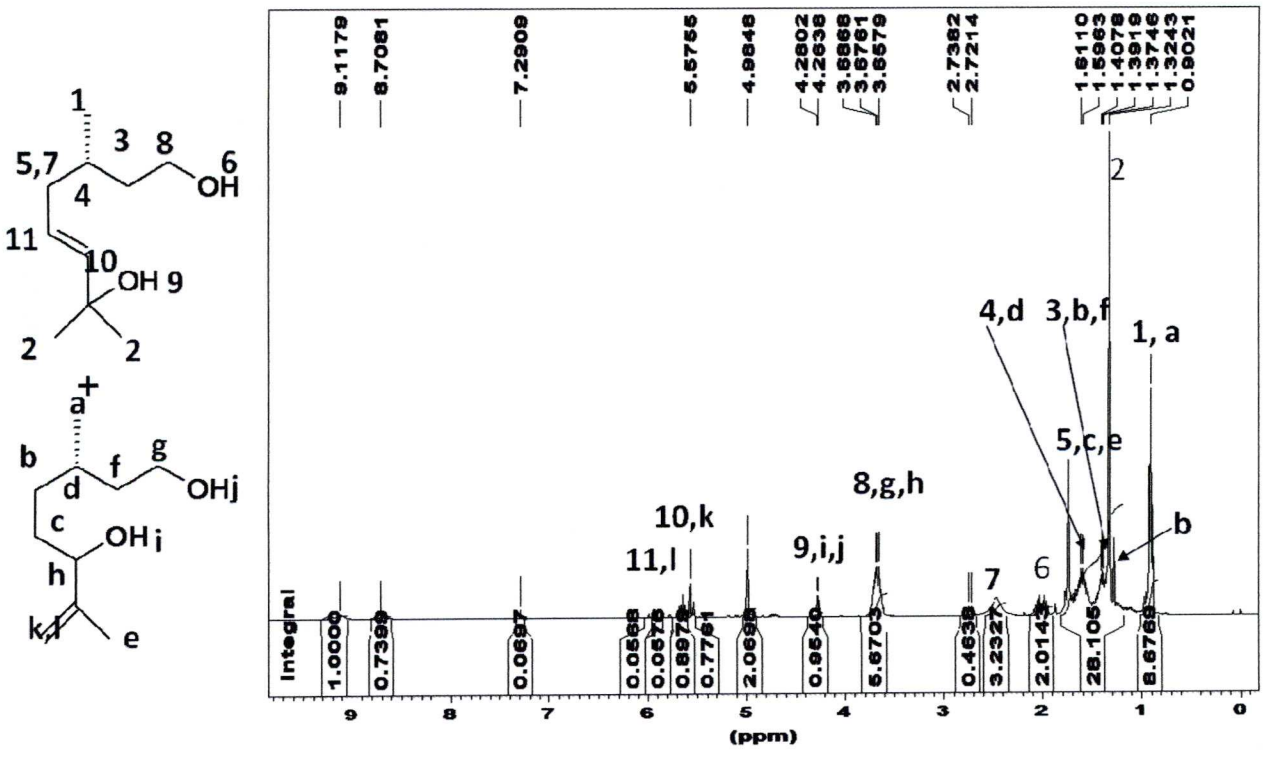

Figure 4.24 ^{1}H NMR spectrum of product mixture after oxidation of S-Citronellol

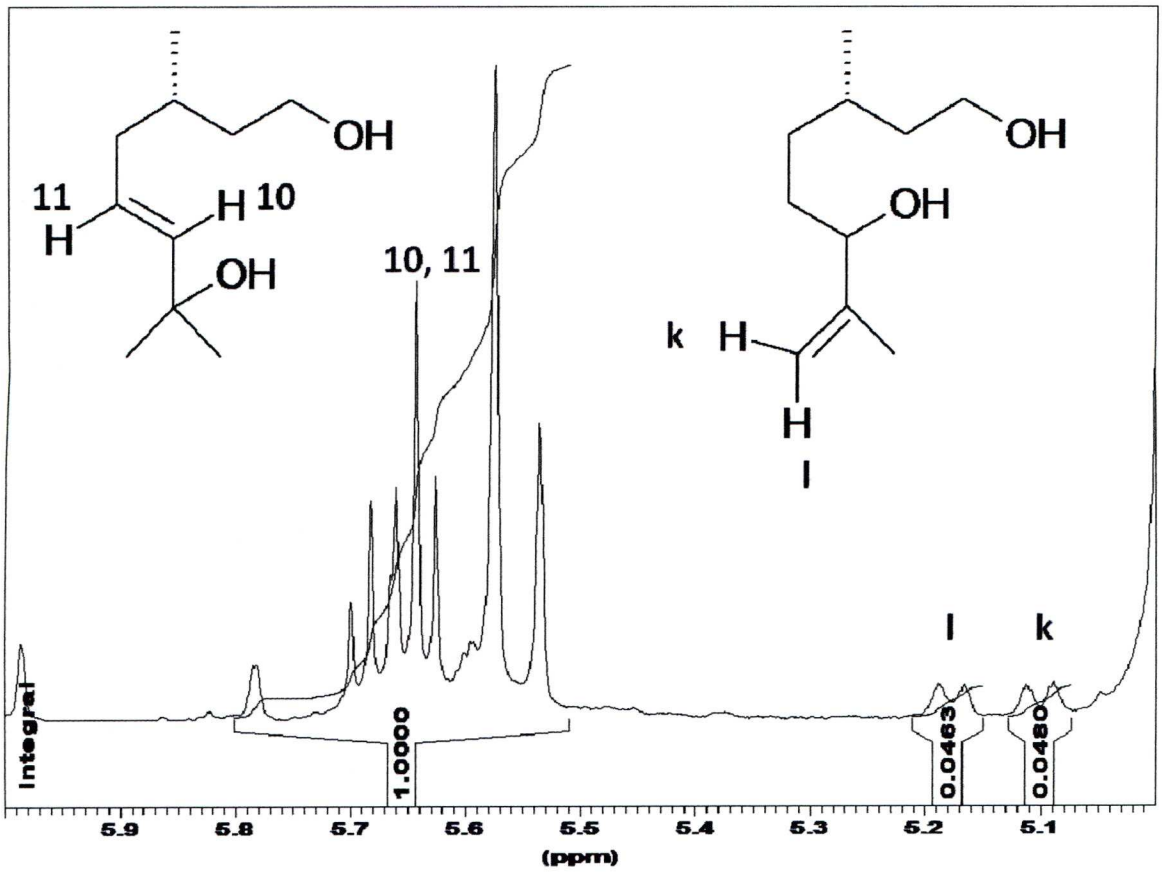

Figure 4.25 ^{1}H NMR showing product distribution after oxidation of S-Citronellol

Studies were also performed on how well the catalyst performed on subsequent runs. A full comparison between the first and second catalyst uses can be found in Figure 4.26. As can be seen, in the second use, the catalyst is less active taking over two hours more for the reaction to go to completion. However, the product distribution was very similar. To test if it was a surface phenomenon, the molybdate was adsorbed onto gibbsite by suspending gibbsite in an aqueous 3 fold molar excess solution of sodium molybdate and stirring at room temperature for 24 hours, before filtering the gibbsite. The remaining solid was not washed so as not to remove any molybdate which may have been loosely bound. Metals analysis showed there to be only 1.07% Mo present. When the oxidation was attempted, using 0.3g of the Na_2MoO_4/gibbsite , no reaction occured. The reaction was also attempted with gibbsite alone, as the PXRD pattern showed there to be some present, due to de-intercalation of the Li^+ ions and furthermore the reaction was carried out upon the parent Li/Al-NO_3-LDH. In both cases no reaction occurred. It was also decided to try the oxidation simply using a solution of sodium molybdate in methanol, which was a homogeneous

reaction. The results for this are shown in Figure 4.27. Clearly the products of this reaction are different to those in the heterogeneous oxidation using the molybdate exchanged LDH, due to their differing retention times to those in the first reaction. The reaction was therefore monitored using GC-MS, which showed the products to be citronellal hydrate and hydroxycitronellal (see Figure 4.28). This reaction occurs because by using sodium molybdate, instead of the exchanged LDH, a tetraperoxomolybdate species forms[45], which forms a dienone-hydroperoxide moiety, which upon reduction with sodium sulphite forms a hydroxyl-carbonyl compound[17]. Upon heating the hydroxy-carbonyl compound in the presence of sodium sulphite, a bisulphite addition complex forms, i.e. a sulphonic acid. This can happen in the GC, resulting in extra products being formed in situ. The Li/Al-MoO_4-LDH catalyst compares well to the literature (Figure 4.29), with excellent conversion rates observed in relatively short time periods.

The Li/Al-MoO_4-LDH catalyst was then recovered after use and a PXRD pattern was taken. As can be seen in Figure 4.30, the used catalyst had similar features as it had before the reaction, with a loss in crystallinity noted post reaction, as can be seen in the decrease in the gibbsite peak.

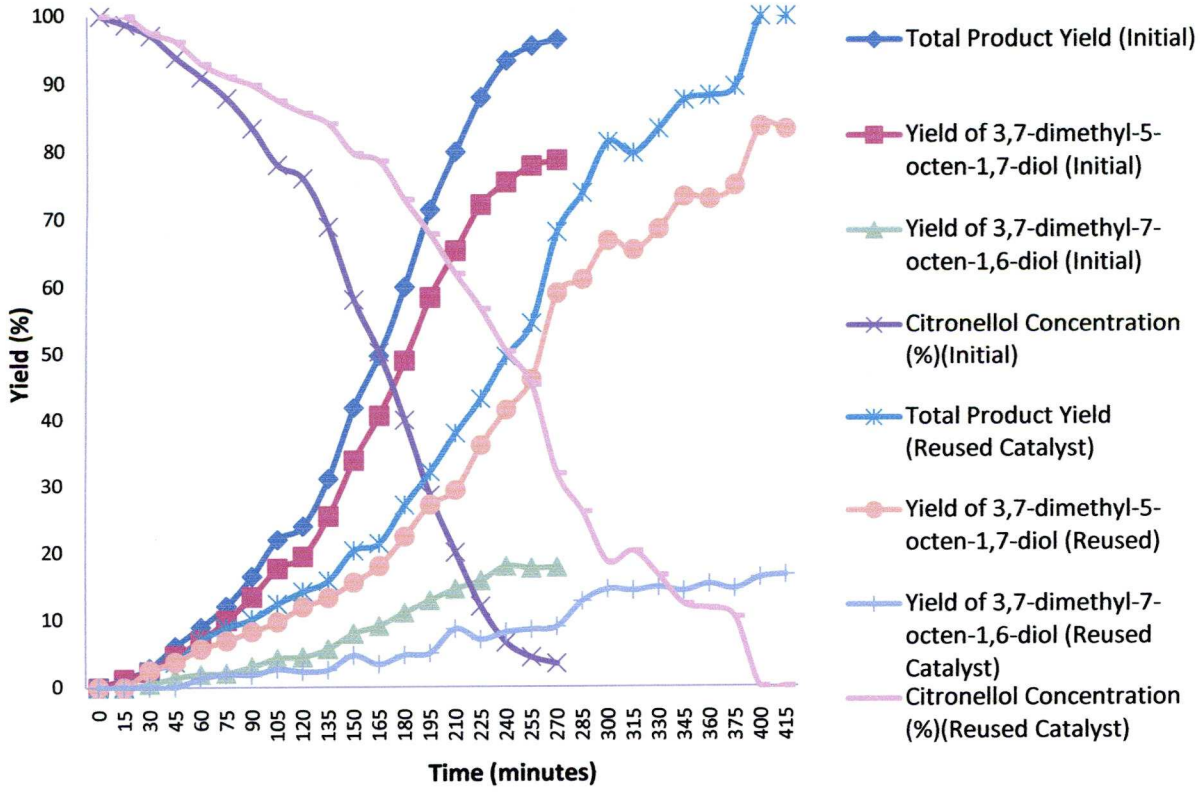

Figure 4.26 Comparison between Li/Al-$LiMoO_4$-LDH catalyst in the oxidation of S-Citronellol in first use and then subsequent re-use

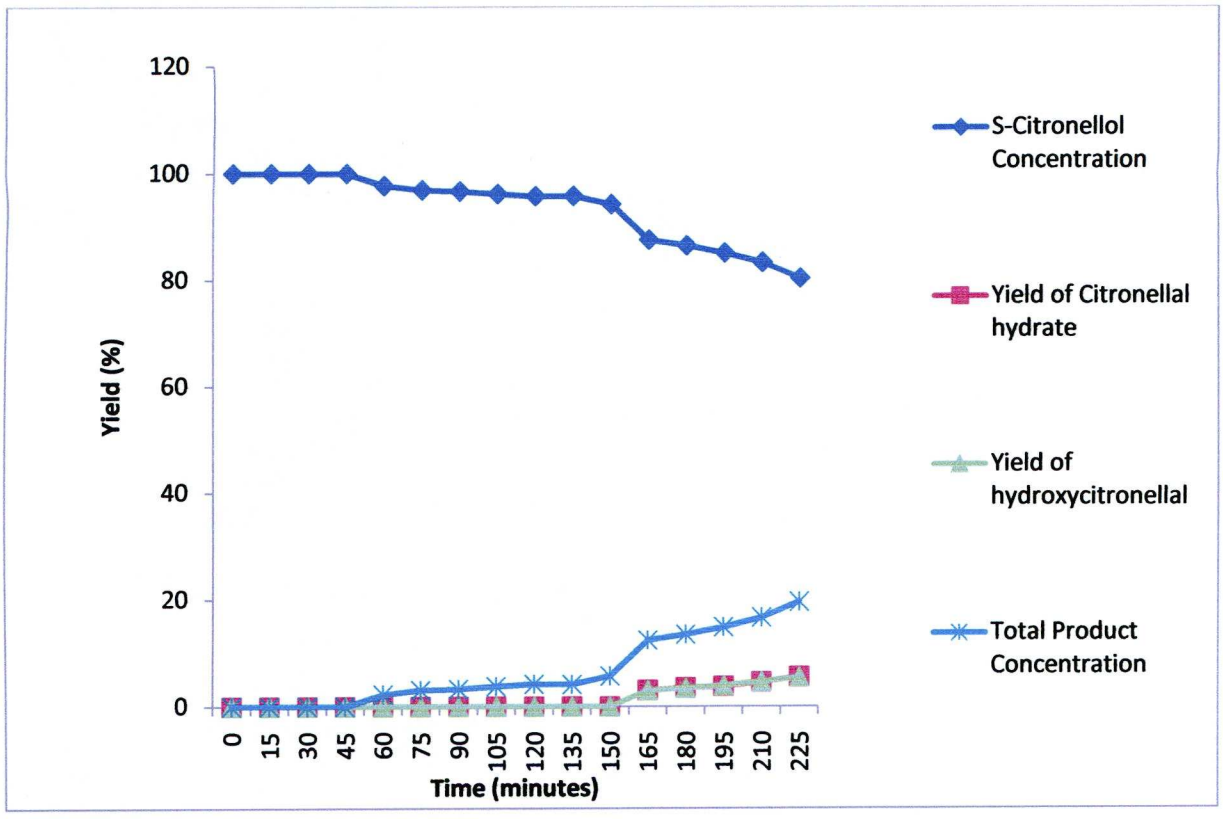

Figure 4.27 Product distribution for oxidation of S-Citronellol using Sodium Molybdate

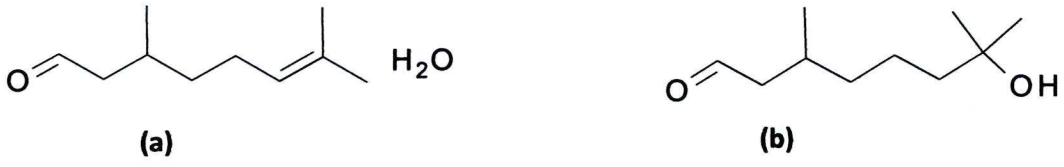

Figure 4.28 Citronellal hydrate (a) and (b) hydroxyl citronellal (7-hydroxy-3,7-dimethyloctanal)

	Product Distribution (%)				
Catalyst (Concentration) [time]	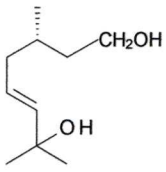	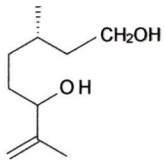	**30% [H_2O_2] mM**	**Conversion (%)**	**Selectivity (%)**
La (10%)doped Zn-hydroxycarbonate[22] (0.15mmol La)/[24h]	50	50	60-80 (50%)	90.0	97.2
$La(NO_3)_3$ [21](0.15 mmol)/[no time given]	55	45	20-50 (50%)	87	>95
Na_2MoO_4 [21] (0.15mmol)/[no time given]	54 (hydroperoxide not reduced)	46 (hydroperoxide not reduced)	18	85	>95
La-exchanged zeolite[20] (0.05mmol La)/[24h]	47	53	58	99	97
Mg/Al-MoO_4-LDH[28] (0.05mmol Mo)/[8h]	75	25[26]	40	90 (in meOH)[28]	>99
Li/Al-MoO_4-LDH (0.05mmol Mo)/[4.5h]	80	20	46	>99	>99
Na_2MoO_4 (0.5mmol)/[4h]	-	-	41	20	100
Li/Al-NO_3-LDH	0	0	50	0	0
Gibbsite	0	0	50	0	0
Re-used Li/Al-MoO_4-LDH (0.05mmol Mo)/[7h]	80	20	337	>99	>99
Na_2MoO_4 adsorbed on gibbsite	0	0	50	0	0

Figure 4.29 Comparison of catalysts in the 'dark' oxidation of (-)S-β-Citronellol

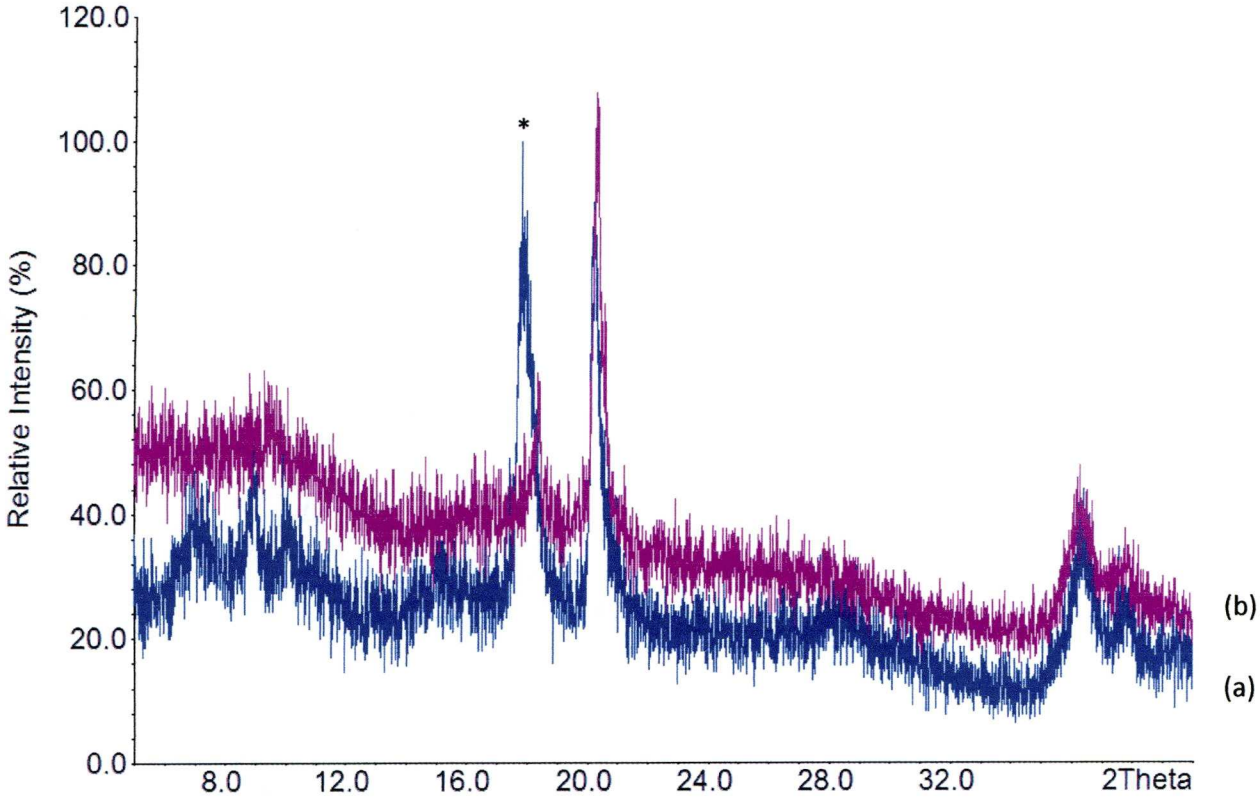

Figure 4.30 Li/Al-MoO_4-LDH (a) before, and (b) post-catalysis

* Denotes peak due to gibbsite, which has decreased in the post reaction PXRD, highlighting a loss of crystallinity of the LI/Al-MoO_4-LDH

4.4 Conclusions

The oxidation of citronellol under mild conditions using Li/Al-MoO_4-LDH proved to be successful, with the Li/Al system outperforming the Mg/Al based system found in the literature, both on initial use and upon reuse (taking 5 hours and 6.6 hours respectively compared to 10 hours for the Mg/Al system). This is a useful reaction in synthetic organic chemistry, where many syntheses require an oxidation step. Due to the mild conditions that are employed in this reaction, this could prove to be useful in sensitive molecular oxidations. A study into the product distribution was also undertaken, finding that first and second use of the Li/Al-MoO_4-LDH catalyst gave the same distributions. Na_2MoO_4 however gave totally different products based upon citronellal hydrate.

4.5 References

1. H.H. Seliger, *Anal. Biochem.* , 1, **1960,** 60-65
2. A.U. Khan, M. Kasha, *J. Chem. Phys.* , 39, **1963,** 2105-&
3. C.S. Foote, S. Wexler, *J. Am. Chem. Soc.*, 86, **1964,** 3880-&
4. E.J. Corey, W.C. Taylor, *J. Am. Chem. Soc.*, 86, **1964,** 3881-3882
5. H. Yamazaki, Cvetanov.Rj, *J. Chem. Phys.* , 41, **1964,** 3703-&
6. C.S. Foote, S. Wexler, *J. Am. Chem. Soc.*, 86, **1964,** 3879-3880
7. E. McKeown, W.A. Waters, *J. Chem. Soc. B*, **1966,** 1040-&
8. C.S. Foote, S. Wexler, W. Ando, *Tetrahedron Lett.*, **1965,** 4111-&
9. R.J. Browne, E.A. Ogryzlo, *Can. J. Chem.*, 43, **1965,** 2915-&
10. B. Stevens, B.E. Algar, *Chem. Phys. Lett.*, 1, **1967,** 58-60
11. Wasserma.Hh, J.R. Scheffer, *J. Am. Chem. Soc.*, 89, **1967,** 3073-&
12. R. Nilsson, D.R. Kearns, *Photochem. Photobiol.*, 19, **1974,** 181-184
13. J.M. Aubry, *J. Am. Chem. Soc.*, 107, **1985,** 5844-5849
14. D.H.R. Barton, P.D. Magnus, J.C. Quinney, *J. Chem. Soc., Perkin Trans. 1*, **1975,** 1610-1614
15. L.L. Smith, M.J. Kulig, *J. Am. Chem. Soc.*, 98, **1976,** 1027-1029
16. H. Sugimoto, D.T. Sawyer, *J. Am. Chem. Soc.*, 106, **1984,** 4283-4285
17. S.S. Yuji Hayashi, Masatoshi Togami, Takeo Sakan, *Chem. Lett.*, 2, **1973,** 651-654
18. J.W. Peters, J.N. Pitts, Rosentha.I, H. Fuhr, *J. Am. Chem. Soc.*, 94, **1972,** 4348-&
19. H.W.S. Chan, *J. Chem. Soc. D*, **1970,** 1550-&
20. J. Wahlen, D. De Vos, S. De Hertogh, V. Nardello, J.M. Aubry, P. Alsters, P. Jacobs, *Chem. Commun.*, **2005,** 927-929
21. V. Nardello, J. Barbillat, J. Marko, P.T. Witte, P.L. Alsters, J.M. Aubry, *Chem.--Eur. J.*, 9, **2003,** 435-441
22. J. Wahlen, D.E. De Vos, P.A. Jacobs, V. Nardello, J.M. Aubry, P.L. Alsters, *J. Catal.* , 249, **2007,** 15-23
23. F. van Laar, D. De Vos, D. Vanoppen, B. Sels, P.A. Jacobs, A. Del Guerzo, F. Pierard, A. Kirsch-De Mesmaeker, *Chem. Commun.*, **1998,** 267-268
24. B.F. Sels, D.E. De Vos, P.J. Grobet, F. Pierard, F. Kirsch-De Mesmaeker, P.A. Jacobs, *J. Phys. Chem. B*, 103, **1999,** 11114-11123
25. B.F. Sels, D.E. De Vos, P.J. Grobet, P.A. Jacobs, *Chem.--Eur. J.*, 7, **2001,** 2547-2556
26. F. van Laar, D.E. De Vos, F. Pierard, A.K. De Mesmaeker, L. Fiermans, P.A. Jacobs, *J. Catal.* , 197, **2001,** 139-150
27. J.M. Aubry, B. Cazin, *Inorg. Chem.*, 27, **1988,** 2013-2014

28. J. Wahlen, D.E. De Vos, B.F. Sels, V. Nardello, J.M. Aubry, P.L. Alsters, P.A. Jacobs, *Appl. Catal., A*, 293, **2005,** 120-128

29. V. Nardello, D. Brault, P. Chavalle, J.M. Aubry, *J. Photochem. Photobiol., B*, 39, **1997,** 146-155

30. S. Meyer, D. Tietze, S. Rau, B. Schaefer, G. Kreisel, *J. Photochem. Photobiol., A* 186, **2007,** 248-253

31. F. Wilkinson, W.P. Helman, A.B. Ross, *J. Phys. Chem. Ref. Data*, 24, **1995,** 663-1021

32. D.E. De Vos, J. Wahlen, B.F. Sels, P.A. Jacobs, *Synlett*, **2002,** 367-380

33. P. Kraft, J.A. Bajgrowicz, C. Denis, G. Frater, *Angew. Chem., Int. Ed.*, 39, **2000,** 2981-3010

34. V.R.L. Constantino, T.J. Pinnavaia, *Inorg. Chem.*, 34, **1995,** 883-892

35. H.H. Wasserman, J.L. Ives, *Tetrahedron*, 37, **1981,** 1825-1852

36. M.B.S.a.J. March, *March's advanced organic chemistry. Reactions, mechanisms and structure*, 5 ed., John Wiley & Sons, Inc., 2001.

37. C.S. Foote, R.W. Denny, *J. Am. Chem. Soc.*, 93, **1971,** 5162-&

38. M. Orfanopoulos, M. Stratakis, Y. Elemes, *J. Am. Chem. Soc.*, 112, **1990,** 6417-6419

39. L.M. Stephenson, M.J. Grdina, M. Orfanopoulos, *Acc. Chem. Res.*, 13, **1980,** 419-425

40. E.W.H. Asveld, R.M. Kellogg, *J. Org. Chem.* , 47, **1982,** 1250-1257

41. J.C. Mitchell, *Chem. Soc. Rev.*, 14, **1985,** 399-419

42. M. Orfanopoulos, I. Smonou, C.S. Foote, *J. Am. Chem. Soc.*, 112, **1990,** 3607-3614

43. A.V. Besserguenev, A.M. Fogg, R.J. Francis, S.J. Price, D. Ohare, V.P. Isupov, B.P. Tolochko, *Chem. Mater.*, 9, **1997,** 241-247

44. A.L. Maciuca, E. Dumitriu, F. Fajula, V. Hulea, *Applied Catalysis a-General*, 338, **2008,** 1-8

45. J.A. Connor, E.A.V. Ebsworth, *Adv. Inorg. Chem.* , 6, **1964,** 279-381

Chapter 5: Synthesis and Characterisation of MoO_3 and WO_3 Inorganic/Organic Hybrid Materials

5.1 Introduction

Metal oxide based materials have many interesting applications[1], such as in superconductivity[2-3], optics[4] and catalysis[5-6]. Traditional syntheses employed the 'ceramic method'[7], which essentially comprises of the successive heating and grinding of two or more non-volatile solids in a furnace at very high temperatures (typically between 1000-2000°C). One well known example is the well known reaction to form zircon, $ZrSiO_4$ which is synthesised by the direct reaction between zirconia (ZrO_2), and silica (SiO_2) at 1300°C. High temperature syntheses such as these usually lead to the formation of thermodynamically stable products, whereas hydrothermal routes can allow the formation of metastable phases[8]. Zeolites are typically synthesised hydrothermally[9] using a quaternary ammonium salt or an amine as a templating agent to allow pores of fixed size to form. *Ab initio* Hartree-Fock calculations, performed by Catlow et al[10-11] extended computational work previously carried out on zeolites[12] to predict that the use of diazobicyclooctane (DABCO) as a templating agent in syntheses of porous MO_3 (M=W and Mo) materials[10].

5.1.1 Isopolymetallates

Tungsten and molybdenum have the ability to form polymeric anions whose stoichiometries are highly dependant upon pH. At very low pH, molybdic and tungstic acids ($MoO_3.2H_2O$ and $WO_3.2H_2O$) are formed, whereas at high pH, the solutions contain tetrahedral MO_4^{2-} ions (i.e. molybdate and tungstate). However, between these two extremes, polymerisation occurs. For example, acidification below pH 6 of an aqueous molybdate solution forms the paramolybdate anion, $[Mo_7O_{24}]^{6-}$, according to Figure 5.1[13].

$$7[MoO_4]^{2-} + 8H^+ \rightleftharpoons [Mo_7O_{24}]^{6-} + 4H_2O$$

Figure 5.1 Formation of the paramolybdate anion in acidic solution

It is possible to crystallise this from solution using counter ions, such as protonated diethylenetriamine[14], forming $(H_3dien)_2[Mo_7O_{24}].4H_2O$. Two polymorphs can be obtained which differ only in the way that the $[Mo_7O_{24}]^{6-}$ units are arranged in the crystals.

The $[Mo_7O_{24}]^{6-}$ anion, see Figures 5.2 (c), and 5.3, which forms clusters of edge sharing MoO_6 octahedra (Figure 5.2) appears to be an important intermediate in the formation of more complex polyanions[15]. NMR studies involving ^{17}O and ^{95}Mo have elucidated a possible mechanism[16] for the conversion of $[Mo_7O_{24}]^{6-}$ to β-$[Mo_8O_{26}]^{4-}$, see Figure 5.2 (e) (again with clusters of edge sharing MoO_6 octahedra, this time arranged slightly differently) giving a route to even larger polyanions. β-$[Mo_8O_{26}]^{4-}$ can also exist in several isomeric forms[17]. Interestingly, it is also possible to crystallise isomeric forms of $[Mo_8O_{26}]^{4-}$, where the isomer β-$[Mo_8O_{26}]^{4-}$ is by far the major species in solution[18]. It is also found that the counter-cation is crucial to the formation of the polymeric molybdate species. A study[18] was conducted where a series of amines, ($[NH_4^+]$, $[(NH_2)_3C]^+$, $[(CH_3)_4N]^+$ and $[(C_4H_9)_4N]^+$ showed cation dependant isomerisation between α-$[Mo_8O_{26}]^{4-}$ and β-$[Mo_8O_{26}]^{4-}$ because, while both species exist at pH 3-4, α-$[Mo_8O_{26}]^{4-}$ becomes dominant at pH 2.7 and β-$[Mo_8O_{26}]^{4-}$ at 2.0. In the same study, it was found that larger cations, with lower charge densities favour the formation of α-$[Mo_8O_{26}]^{4-}$ and β-$[Mo_8O_{26}]^{4-}$ whereas smaller cations with higher charge densities favour the formation of $[Mo_3O_{10}]_n^{2n-}$ chains and $[Mo_7O_{24}]^{6-}$ cations. Another study also found that amine charge density affects the three dimensional packing of Mo coordination polymers. In a study by Nelson *et al*[15], 5 straight chain aliphatic amines (Figure 5.4) were used to probe the effects of charge density on polyanionic molybdate species. It was found that $[Mo_3O_{10}]_n^{2n-}$ chains were most easily formed using the 1,3-diaminopropane (1,3-DAP) and 1,4-diaminobutane (1,4-DAB) cations and when 1,7-DAHep was the only amine capable of producing β-$[Mo_8O_{26}]^{4-}$ anions. Furthermore, concentration effects proved crucial in this study, with the Mo:amine ratio proving crucial, with $[Mo_3O_{10}]_n^{2n-}$ being favoured under conditions of high template excess and $[Mo_5O_{16}]_n^{2n-}$ layers, $[Mo_8O_{26}]_n^{4n-}$ chains and $[Mo_8O_{26}]^{4-}$ (see Figure 5.2 (d) and (e)) molecular anions being favoured at low template concentrations, as fewer template molecules are required per Mo. The formation of two isomeric $[Mo_3O_{10}]_n^{2n-}$ is also possible, with Type 1 chains see Figure 5.4) only exhibiting edge sharing, Type 2 share either two edges and one corner; one edge and one face; or one face, one edge and one corner see Figure 5.6.

The formation of other anions is also sensitive to acidity, concentration, temperature and rate of crystallisation. For example, it is possible to form the dimolybdate[19], $[Mo_2O_7]^{2-}$, the hexamolybdate[20], $[Mo_6O_{19}]^{2-}$ (which offer promise in the development of conducting molecular materials).

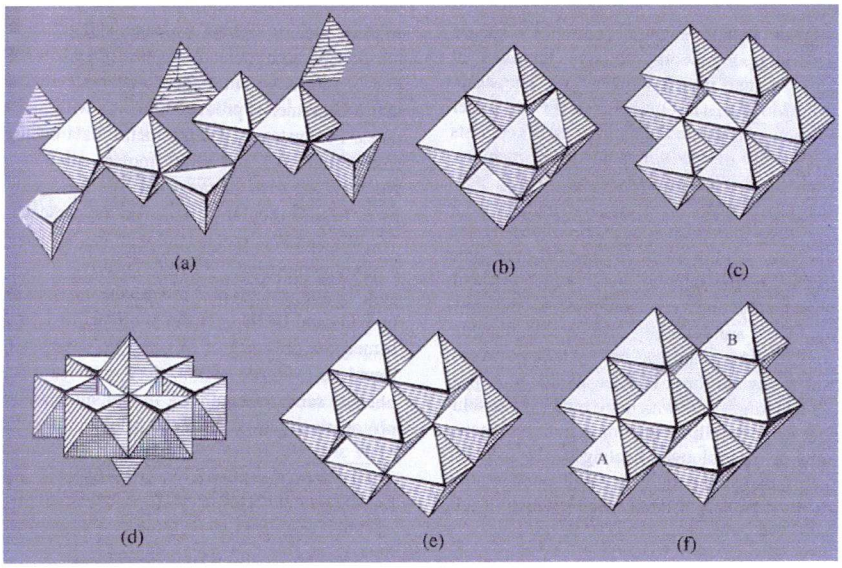

Figure 5.2 Structure of POM ions: (a) $[Mo_2O_7]^{2-}{}_n$ chains; (b) $[Mo_6O_{19}]^{2-}$ (with the sixth octahedron obscured); (c) The paramolybdate anion, $[Mo_7O_{24}]^{6-}$ which can be viewed as $Mo_{10}O_{28}$, with a line of three octahedra removed; (d) α-$[Mo_8O_{26}]^{4-}$, i.e. a ring of six octahedral capped by two tetrahedral; (e) β-$[Mo_8O_{26}]^{4-}$ (with one octahedron obscured); (f) γ-$[Mo_8O_{26}]^{4-}$. One of the three terminal positions for coordination in both octahedral labelled A and B is unoccupied. Filling the positions with suitable ligands confers stability upon this otherwise labile anion.

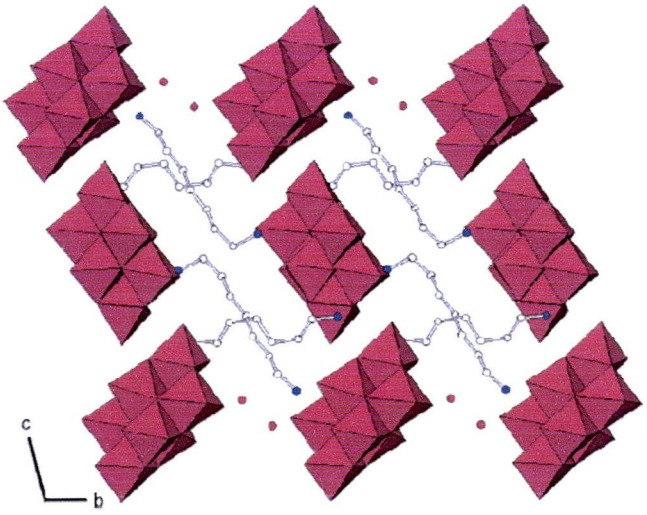

Figure 5.3 β-$[Mo_8O_{26}]^{4-}$ ions formed from the reaction between 1,7-DAHep and MoO_3 in acidic media[15]

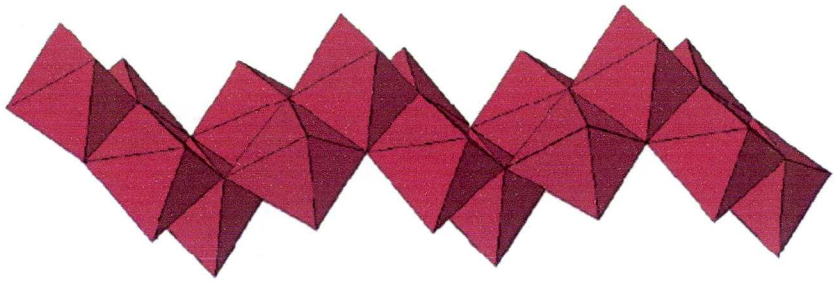

Figure 5.4 Type 1 $[Mo_3O_{10}]_n^{2n-}$ with only edge sharing observed in the MoO_6 octahedra

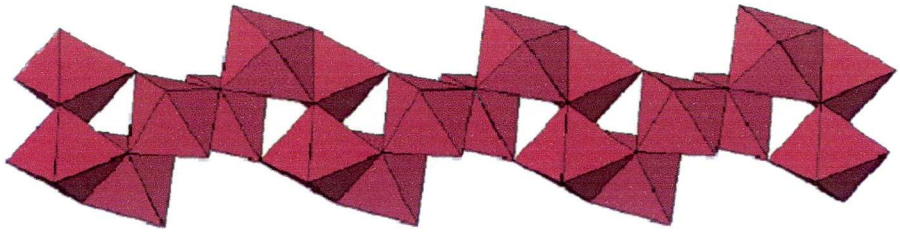

Figure 5.5 Type 2 $[Mo_3O_{10}]_n^{2n-}$ with the MoO_6 octahedra sharing either two edges and one corner; one edge and one face; or one face, one edge and one corner

Traditional determination of the solid state structures of the polyanions was by X-ray and infra-red analysis[21]. Modern techniques, such as NMR however are beginning to unravel the structures and formations of the ions in solution[22-23]. Isopolytungstates and isopolymolybdates have several structural features in common, for example:

- No metal-metal bonding occurs in the structures, in each case the cage is formed by oxygen bridges
- In both cases the cage is constructed from MO_6 octahedra, connected via shared oxygen atoms

There is however one main difference between polymeric tungstates and molybdates, namely:

- In most isopolymolybdates, the basic unit is MoO_6 octahedra with a pair of *cis*-terminal oxygens, whereas in isopolytungstates, the units are WO_6 octahedra with only one terminal oxygen

Structures for both $[Mo_7O_{24}]^{6-}$ [14] and $[W_6O_{19}]^{2-}$ [24] are shown in Figure 5.6.

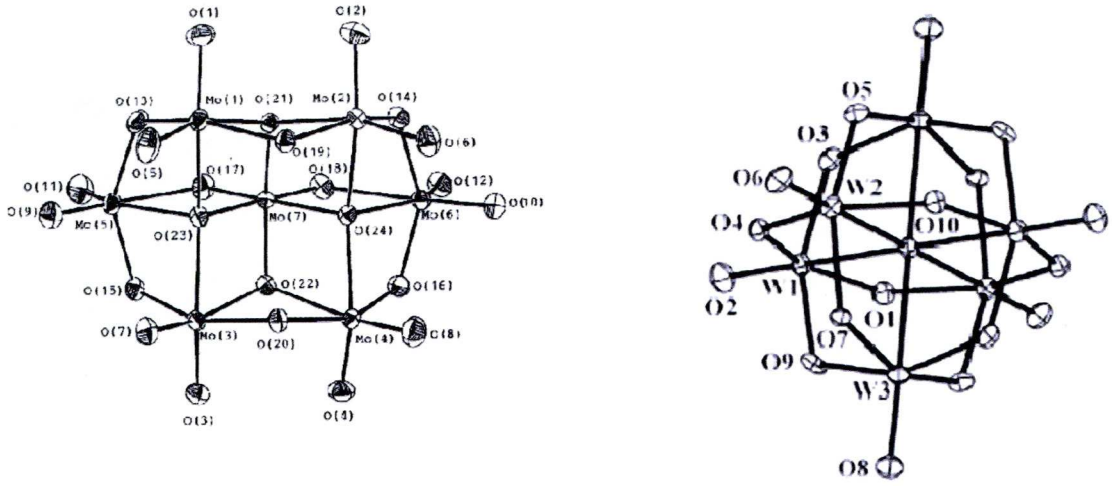

Figure 5.6 Structure of both $[Mo_7O_{24}]^{6-}$ [14] and $[W_6O_{19}]^{2-}$ [24]. Showing similarities and differences between isopolymetallates.

Polytungstates are less well understood than polymolybdates, due to a complex series of equilibria[25]. An important species occurring upon acidification of solutions of the simple tungstate anion, WO_4^{2-} is the paratungstate anion, $[W_7O_{24}]^{6-}$. Further acidification (Figure 5.7) produces other species which can take days or even months to crystallise from solution. Initial results suggested that the paratungstate was a hexamer, however, more detailed studies, including ^{183}W and ^{17}O NMR[26] showed the species to be indeed the heptamer, $[W_7O_{24}]^{6-}$. The paratungstate ion, $[W_7O_{24}]^{6-}$ is isostructural with its Mo containing analogue.

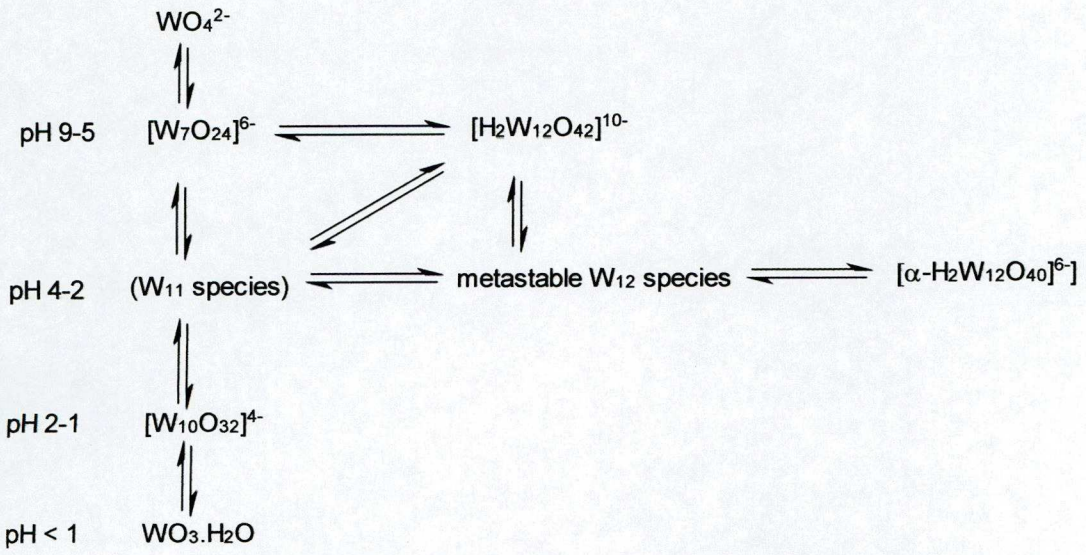

Figure 5.7 Tungsten species which exist in solution at different pH values[25]

It may be possible to rationalise the structures of polymetallates. It is unusual (apart from in the solid state) to find MO_6 octahedral units with more than two terminal oxygens . If there were more than two, this would lengthen and weaken the π-bonds holding the metal to the anion. Electrostatic effects can also be considered where repulsion between neighbouring anions will also contribute to the distorting effect of M-O π-bonding which would make the metal in the interconnected MO_6 octahedra move off-centre. This effect would then increase as the octahedra go from corner to edge-sharing. High charge favours edge sharing as there are less O^{2-} ions. Off centre distortions become harder to accommodate as polyanion size increases making edge sharing no longer feasible. This point is reached with W^{VI} before Mo^{VI} due to its larger size. In polytungstates and polymolybdates, corner sharing is much more prevalent in larger polytungstates than polymolybdates. It is, however, less clear why there are few isostructural polyanions of W and Mo.

5.1.2 Heteropolymetallates

Another interesting feature of the chemistry of tungsten and molybdenum is their ability to form heteropolymetallates. In 1826, Berzelius showed that upon acidification of solutions containing both molybdate and phosphate, a yellow precipitate was obtained. Over 100 years later, in 1934, the structure of this first example, $[PMo_{12}O_{40}]^{3-}$, was solved via X-ray diffraction by Keggin[27].

Heteropolyanions are important as both homogeneous catalysts[28], which are water soluble either as acids, i.e. with H^+ , or salts of other small cations such as K^+; and also as insoluble heterogeneous 'green' catalysts[29-30], where the counter cation is large (e.g. Cs^+, Ba^{2+}, Pb^{2+}). Two groups of the heteropolyanions are important:

- α-Keggin anions: $[XM_{12}O_{40}]^{n-}$ (where M=Mo or W. X=P or As for n=3. X=Si for n=4. X=B for n=5), shown in Figure 5.8
- α-Dawson anions: $[X_2M_{18}O_{62}]^{n-}$ (where M=Mo or W. X=P or As and n=6), shown in Figure 5.9

The α-Keggin structure of $[PW_{12}O_{40}]^{3-}$ consists of WO_6 octahedra, each of these are linked to each other via corner sharing. This traps the heteroatom tetrahedrally inside the cage. The α-Dawson anions can be visualised by removing the three basal octahedral from two α-Keggin ions, which are then fused together[25].

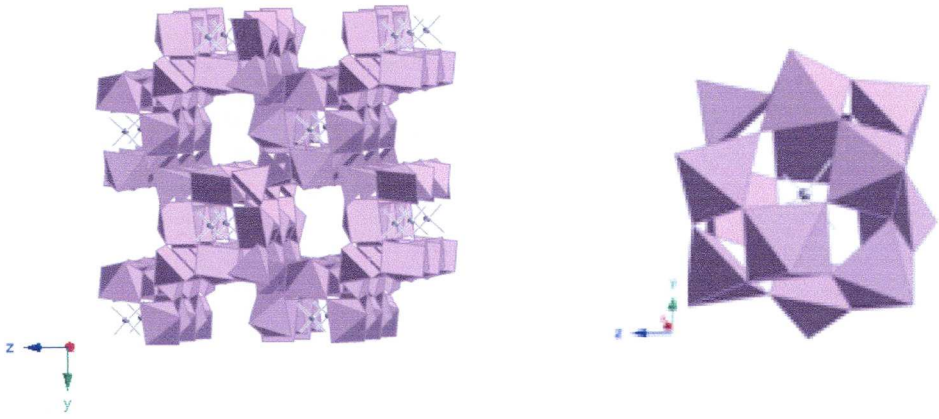

Figure 5.8 Structural representations of α-Keggin ion

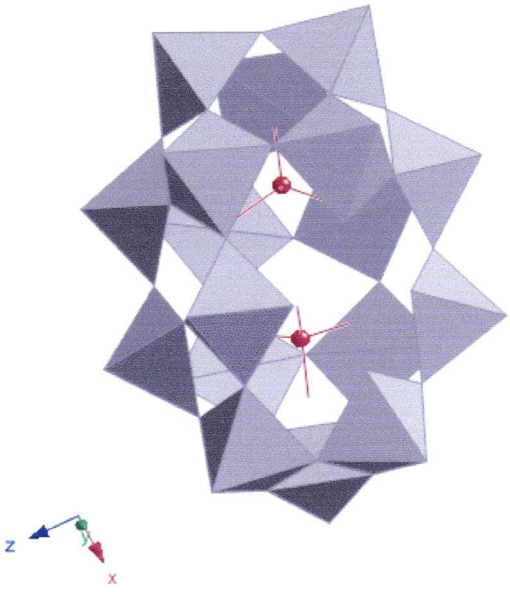

Figure 5.9 Structural representations of α-Dawson ion

It is also possible for the formation of so called 'lacunary' ions, where the POM have vacancies, created by loss of one or more of the MO_6 octahedra, making the hetero atom in the species sit in a 'basket' rather than the cage of standard POMs[31]. An example of the formation of a lacunary ion would be the formation of the anion $[PW_9O_{39}]^{9-}$ in aqueous solution at pH 2:

$$[PW_{12}O_{40}]^{3-} \rightleftharpoons [PW_9O_{39}]^{9-} + W(VI)$$

The species $[PW_9O_{39}]^{9-}$ is stable until pH 8 when it degrades further to give a further lacunary species having 3 vacant sites, $[PW_9O_{34}]^{9-}$ [31]. Lacunary complexes are therefore excellent at coordination of metal ions, with many examples being known such as K^+ [32] and even trivalent cations, such as the lanthanides, in monosubstituted complexes[33].

It is also possible to substitute tungsten for other metals in the polyoxometalate structure. A recent paper by Mizuno *et al*[34] described a vanadium(V) substituted POM which was used in bio-mimetic regioselective hydroxylations of alkanes using H_2O_2 as the sole oxidant. The bulky POM (Figure 5.10) gives rise to a selective oxidation of stronger secondary C-H bonds, over the weaker tertiary C-H bonds, notwithstanding electronic effects (Figure 5.11).

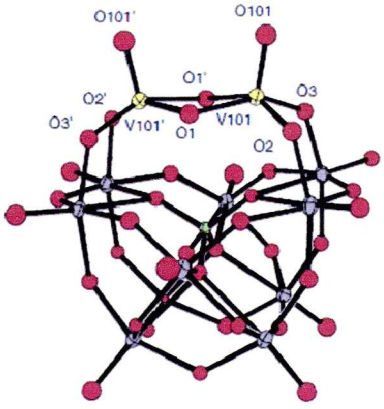

Figure 5.10 $V^{(V)}$ containing POM[34]. The structure shows that the POM has a bulky framework structure, giving rise to unusual selectivities in the hydroxylation of organic molecules

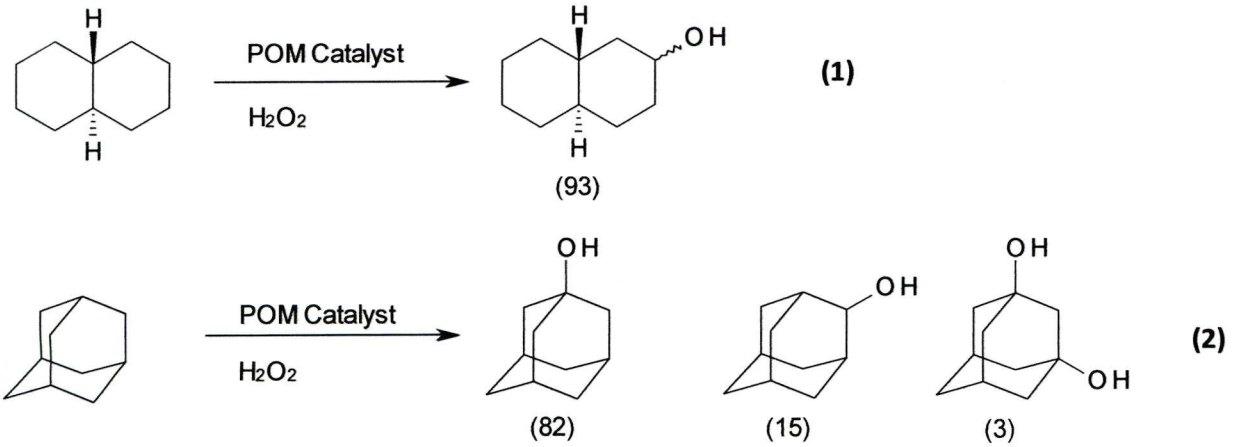

Figure 5.11 The bulky $V^{(V)}$ POM, preferentially oxidising secondary C-H bonds over tertiary C-H bonds (1). However, when molecules such as adamantane are used, the hydroxylation occurs at electron rich tertiary C-H bonds (2). Selectivities are shown underneath each product.

5.1.3 Molybdenum Containing Polyoxometallates

Polyoxometallates containing molybdenum exhibit a high degree of structural diversity[35-36]. Huge clusters can also be formed from smaller fragments, including the wheel like compounds described by Müller *et al*[37], where mixed valent (Mo^{V}/Mo^{VI}) compounds with molecular weights >240000 $gmol^{-1}$ and formula $(NH_4)_{25\pm5}[Mo_{154}(NO)_{14})O_{420}(OH)_{28}(H_2O)_{70}].\approx350H_2O$ were synthesised (Figure 5.12).

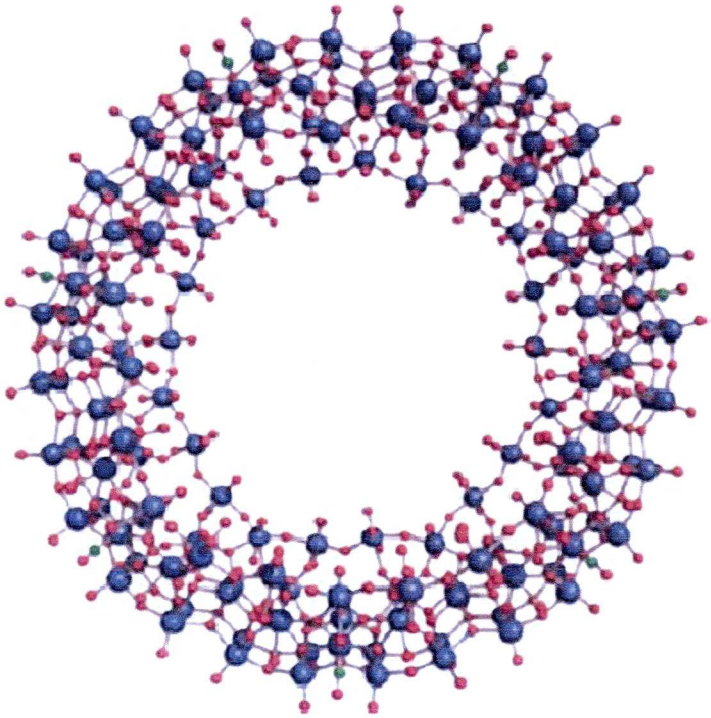

Figure 5.13 Giant mixed valency Mo^{V}/Mo^{VI} wheels, as synthesised by Müller *et al*[37].

(Mo atoms, blue; O atoms, red; N atoms, blue)

5.1.4 Zero Dimensional POMs

An example of a zero dimensional POM is a reduced Mo^{V} phosphate with the formula $(H_2dien)_4[CaMo_{12}O_{24}(OH)_6(HPO_4)_8].nH_2O$, where dien=diethylenetriamine[38]. The compound was prepared via a hydrothermal route. The structure (shown in Figure 5.13) shows $[Mo_6P_4]$ units linked by octahedral Ca^{II} cations into $[Ca(Mo_6P_4)_2]$ clusters (Figure 5.14).

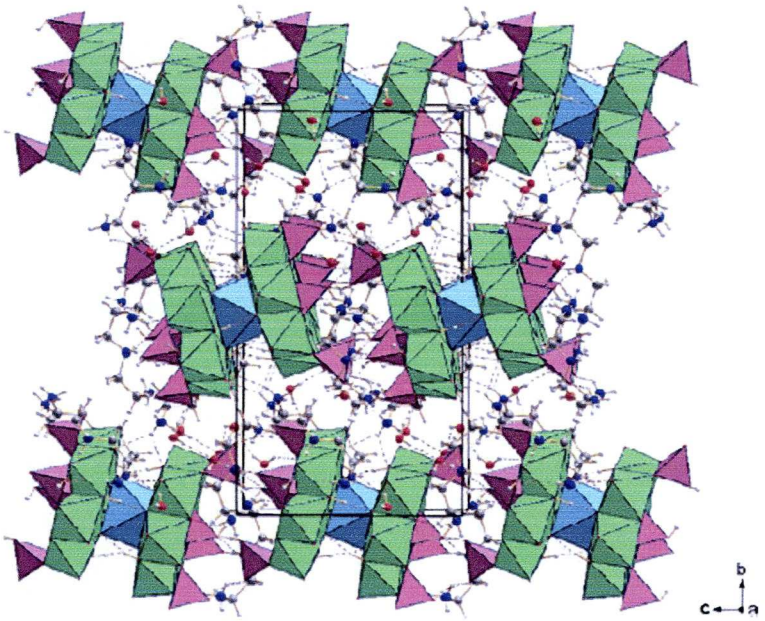

Figure 5.13 $(H_2dien)_4[CaMo_{12}O_{24}(OH)_6(HPO_4)_8].nH_2O$, an example of a zero-dimensional POM[38]. Mo_6 octahedra are shown in green, P_4 tetrahedra are purple, Ca octahedral are blue, with the (H_2dien) molecules being shown as ball and stick.

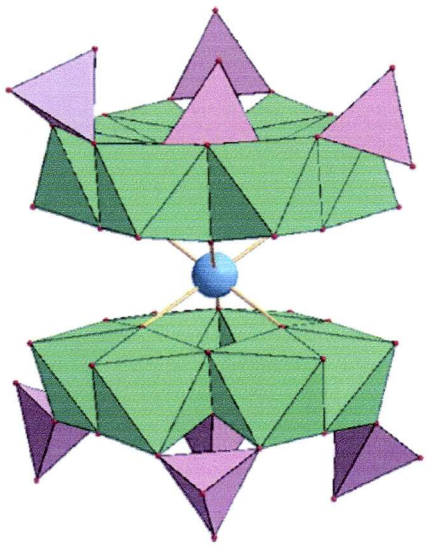

Figure 5.14 The building unit of $(H_2dien)_4[CaMo_{12}O_{24}(OH)_6(HPO_4)_8].nH_2O$, a $[Ca(Mo_6P_4)_2]$ cluster[38]. Mo_6 octahedra are shown in green, P_4 tetrahedra are purple and the Ca ion is shown as blue

5.1.5 One-Dimensional POMs

One-dimensional POMs tend to be templated by organoammonium cations such as protonated ethylenediamine[39] and organoammonium cations such as tetramethylammonium hydroxide[40]. Nitrogen containing molecules coordinated to the MoO_3 structure can also be used, such as 2, 2'-bipyridyl[41]. All consist of chains of distorted MoO_6 octahedra, which can face, edge and corner share. The way the chains arrange is dependant on the templating cation used, for example, if the cation is ammonium[42], the MoO_6 octahedra face and edge share (Figure 5.15).

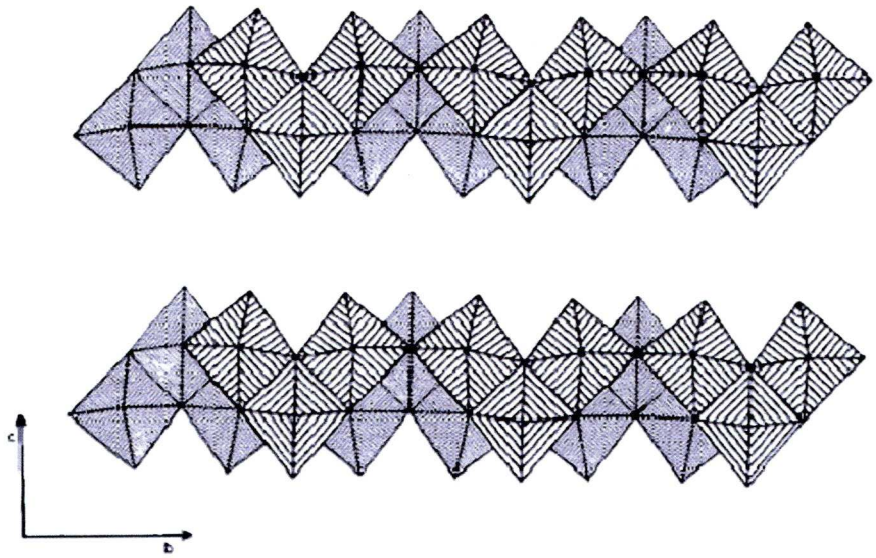

Figure 5.15 Face and edge sharing octahedral in MoO_6 chains when an ammonium cation is used[42]. The ammonium cation resides between the chains

When potassium is used as a cation, forming $K_2Mo_3O_{10}$, the MoO_6 octahedra are accompanied by MoO_5 square pyramids, which edge share forming chains. The chains are held together via 10 coordinate K^+ cations[43] (Figure 5.16). Whereas if ethylenediamine is used[39], the structure consists of a more complicated arrangement of a double chain of MoO_6 octahedra in an array of corner, face and edge sharing, (Figure 5.17)

The N-containing ligand does not have to be protonated under the synthetic conditions, for example, if 2,2'-bipyridine is used[41], the resulting molybdenum chains consist of corner sharing MoO_4N_2 octahedra and MoO_4 tetrahedra (Figure 5.18).

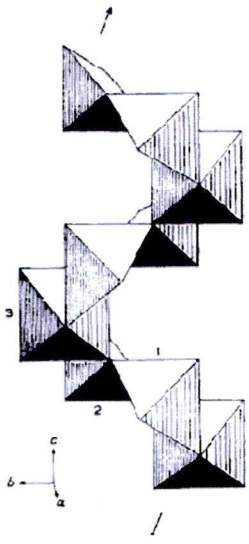

Figure 5.16 Arrangement of edge sharing MoO_6 octahedra and MoO_5 square pyramids in $K_2Mo_3O_{10}$[43]

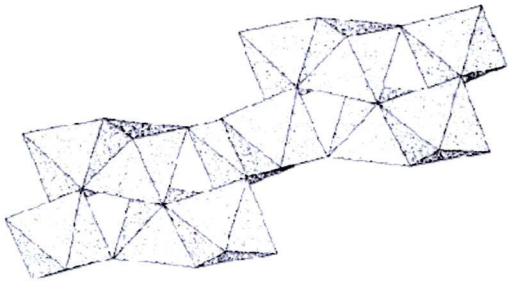

Figure 5.17 Complex arrangement of corner, face and edge sharing octahedral in $(H_3NCH_2CH_2NH_3)Mo_3O_{10}$[39]

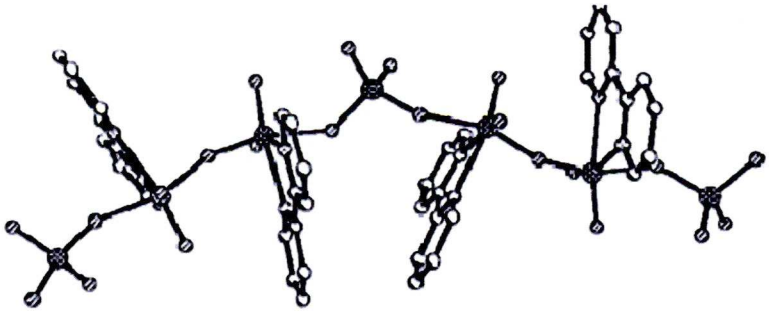

Figure 5.18 Arrangement of MoO_4N_2 octahedra and MoO_4 tetrahedra in MoO_3-2, 2'-BIPY[41]

5.1.6 Two Dimensional POMs

Two dimensional POMs have been synthesised by the intercalation of an alkali metal cation into the layers of MoO_3, and then exchanging the alkali metal cations with a weak base, such as 4,4'-azodianiline[44] (Figure 5.19). This can be monitored by isolating each intercalate and looking at the interlayer separation using X-ray diffraction.

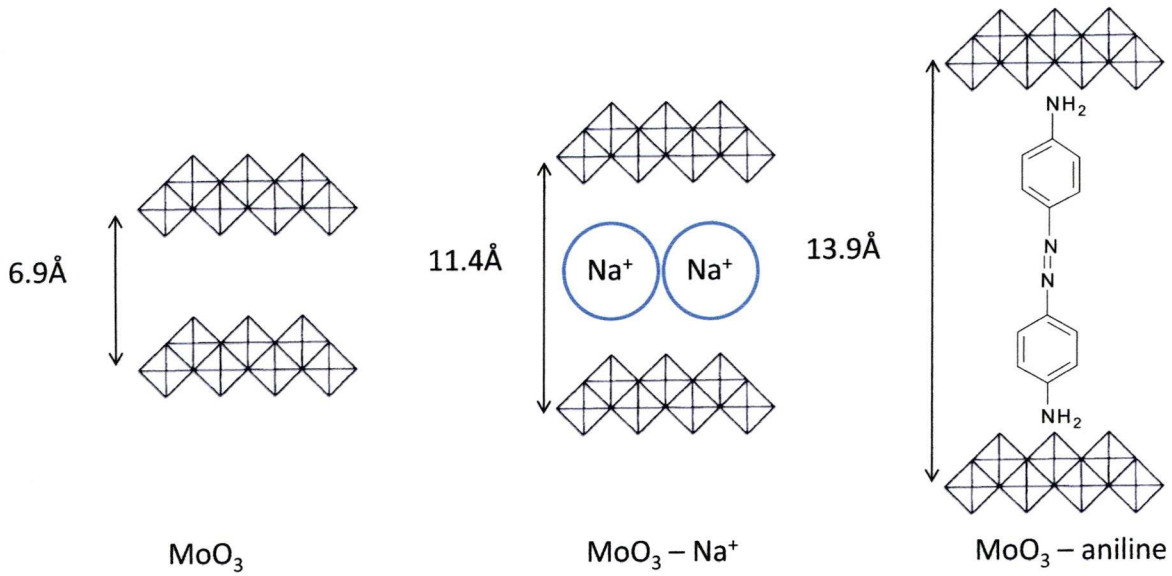

Figure 5.19 Stepwise intercalation of Na^+ ions and then 4, 4'-azodianiline into MoO_3 forming a layered material

5.1.7 Three Dimensional POMs

Three dimensional frameworks offer exciting possibilities in fields such as catalysis, magnetism and optics[45]. A paper by Lu *et al*[46] in 2005 showed that it was possible to approach the synthesis of three dimensional POMs from similar syntheses of MOFs, where, instead of using organic linkers, POM clusters were used as pillars. This has the advantage of the ability of the O atoms on the surface of the POMs to coordinate to other metals, for example in metal based coordination polymer sheets. As the pillars are metal based, they could also offer a larger degree of thermal stability than their organic based counterparts. The synthesised compound has the formula $[H_2bpy]_2[(Cu(bpy)_2)Mo_5P_2O_{23}].4H_2O$, where bpy=4, 4'-bipyridine. The compound consists of a three dimensional framework with one dimensional channels built up from $[Cu(bpy)_2]_n^{2n+}$ sheets pillared by $[Mo_5P_2O_{23}]^{6-}$ clusters (Figure 5.20).

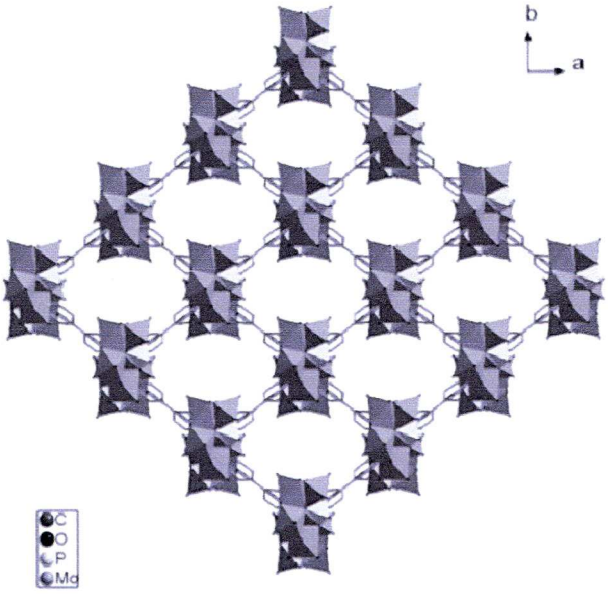

Figure 5.20 $[H_2bpy]_2[(Cu(bpy)_2)Mo_5P_2O_{23}].4H_2O$[46]. In this diagram, the $Cu(bpy)_2]_n^{2n+}$ guest ions found in the channels have been omitted for clarity

5.2 Tungsten Containing Hybrid Material Hydrothermal Syntheses

Following on from the *Ab initio* Hartree-Fock calculations by Catlow *et al*[10-11], the first hydrothermal syntheses attempted were between WO_3 and DABCO at varying molar ratios and varying temperatures, in an attempt to synthesise a microporous tungsten oxide. After these initial screening reactions, it was found that a hydrothermal synthesis using a molar ratio of 5:1 WO_3:DABCO (0.3800g WO_3: 0.1845g DABCO) in water (10ml) for 48 hours at 200°C under autogeneous pressure gave a blue solution containing crystals which were subsequently filtered and analysed. PXRD results, compared to WO_3 and DABCO starting materials indicated that a new phase had been formed (Figure 5.21). Samples of the crystals were then submitted for single crystal X-ray analysis, however, absorption was found to be a big problem, due to the presence of tungsten and the fact that the compound contains a large unit cell. It was however possible to obtain a partial structure, which suggested that each unit cell contained two asymmetric $W_{12}O_{40}$ clusters in a Keggin type structure, and not the microporous tungsten oxide as predicted. As can be seen from Figure 5.5, the $W_{12}O_{40}$ species only forms at pH 4-2. Clearly, DABCO is an organic base, however, DABCO decomposes above 160°C and it is probable that this affects the reaction (carried out at 200°C). A possible explanation is that a pH of 5-9 is generated by the dissolution of DABCO, forming the $[H_2W_{12}O_{42}]^{10-}$ anion, then as the temperature increases and the DABCO decomposes, species exist in the solution which act to lower the pH, forming the metatungsate $[\alpha\text{-}H_2W_{12}O_{40}]^{6-}$ anion.

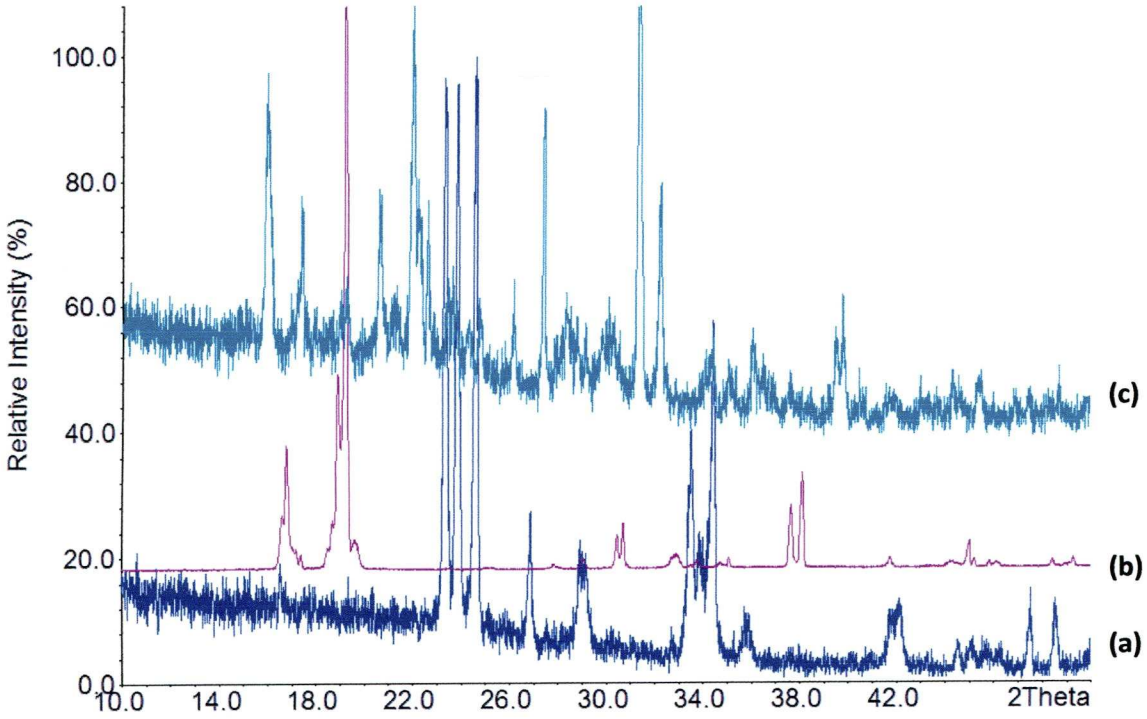

Figure 5.21 Comparison between PXRD patterns for (a) WO_3, (b) DABCO and (c) new phase

5.3 Molybdenum Containing Hybrid Material Syntheses

5.3.1 MoO_3-DABCO

Following the partial success of the W containing hybrid materials, similar work was carried out upon MoO_3. Again, screening was carried out at various temperatures, times and MoO_3:DABCO ratios. This time it was found that a 10:1 ratio of MoO_3:DABCO (2.0650g MoO_3:0.1610g DABCO) in water (10ml) for 12 hours at 200°C under autogeneous pressure was necessary to generate product (other reactions simply yielded MoO_3 starting material). Here small, clear needles were formed on top of an excess of MoO_3. The needles were physically separated and analysed. Initial PXRD analysis indicated a different phase (see Figure 5.22). The crystals were then analysed by single crystal X-ray analysis, which found layers of edge sharing MoO_6 octahedra held together by ethylenediamine bridges (see Figure 5.22). This indicates that the DABCO structure is indeed undergoing decomposition at these elevated temperatures. The structure (see Figure 5.23) is also the same as one previously reported by Zubieta *et al*[39] where ethylenediamine was used in a slight variation of this synthesis.

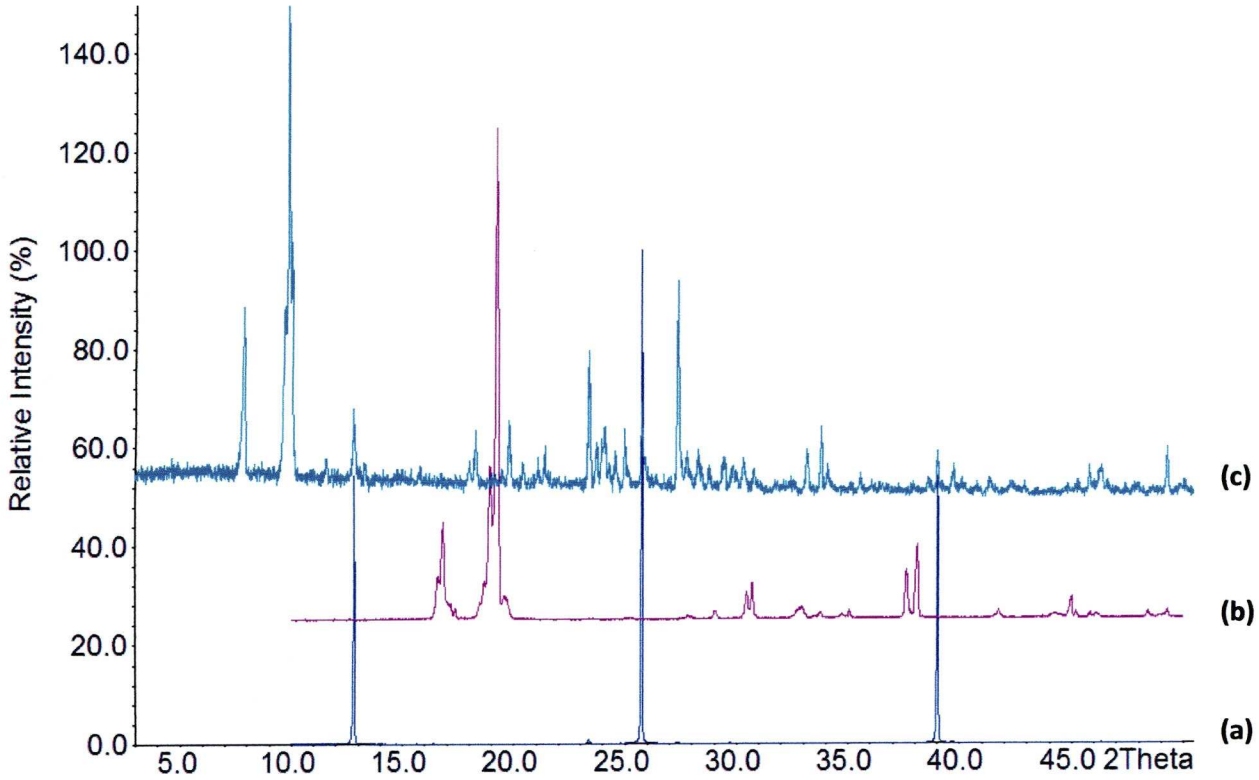

Figure 5.22 PXRD patterns for (a) MoO_3, (b) DABCO and (c) new phase

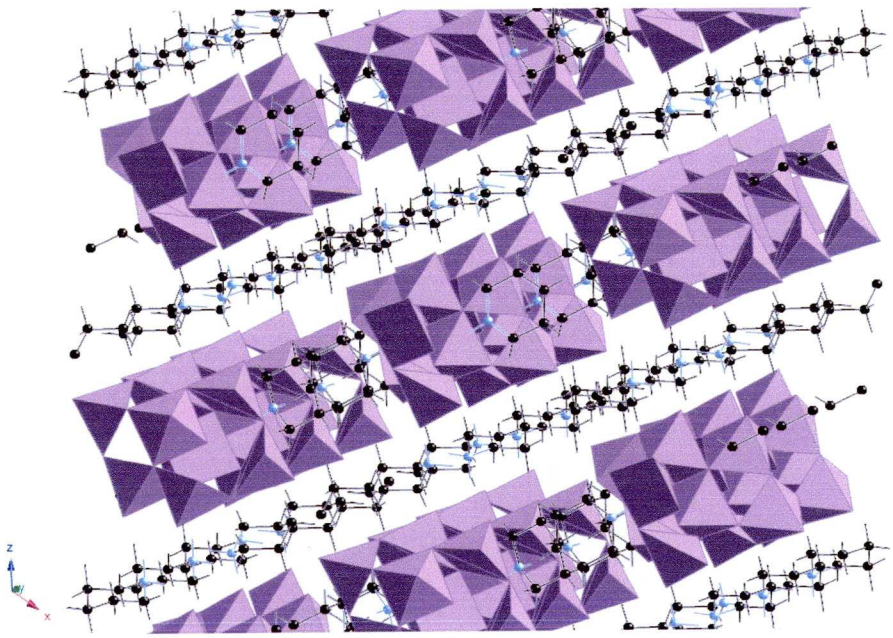

Figure 5.23 Crystal structure of MoO_3-ethylenediamine

Following the success of this synthesis, various other amines and amides were tried, most did not work, possibly due to decomposition of the amine, however, the screening produced five MoO_3-amine coordination polymers, which will be discussed in the following sections.

From the screening, it became clear that a molar ratio of 5:1 MoO_3:amine along with hydrothermal reaction conditions of 48 hours at 180°C in 10ml H_2O under autogenous pressure were good conditions for obtaining crystals.

5.3.2 MoO_3-BIPY

A molar ratio of 5:1 MoO_3:4, 4'-bipyridine (1.0325g MoO_3:0.2241g BIPY) in 10ml H_2O was heated in an autoclave for 48 hours at 180°C. After cooling, brown crystals were found and subsequently analysed. PXRD for the crystals showed a reaction had indeed taken place (Figure 5.24). Single crystal analysis was subsequently performed, showing the structure consisted of layers of corner sharing MoO_5N octahedra pillared by 4, 4'-bipyridine ligands in a three dimensional hybrid material (Figure 5.25), which agrees well with previously published structures[47]. Elemental analysis was also in broad agreement with predicted values based on this structure, as seen in Table 5.1, giving a formula of $(C_5H_{12}N^+)_4(Mo_8O_{26}^{4-}).4H_2O$. TGA analysis was also carried out on the material as shown in Figure 5.26. This highlights the thermal stability of the compound, with no mass loss occurring until 400°C. One main mass loss of 42.5% was observed (calculated, 43.3%), corresponding to the loss of the pillaring 4,4'-bipyridine molecules with the subsequent reformation of MoO_3. This agrees with previously reported values[48].

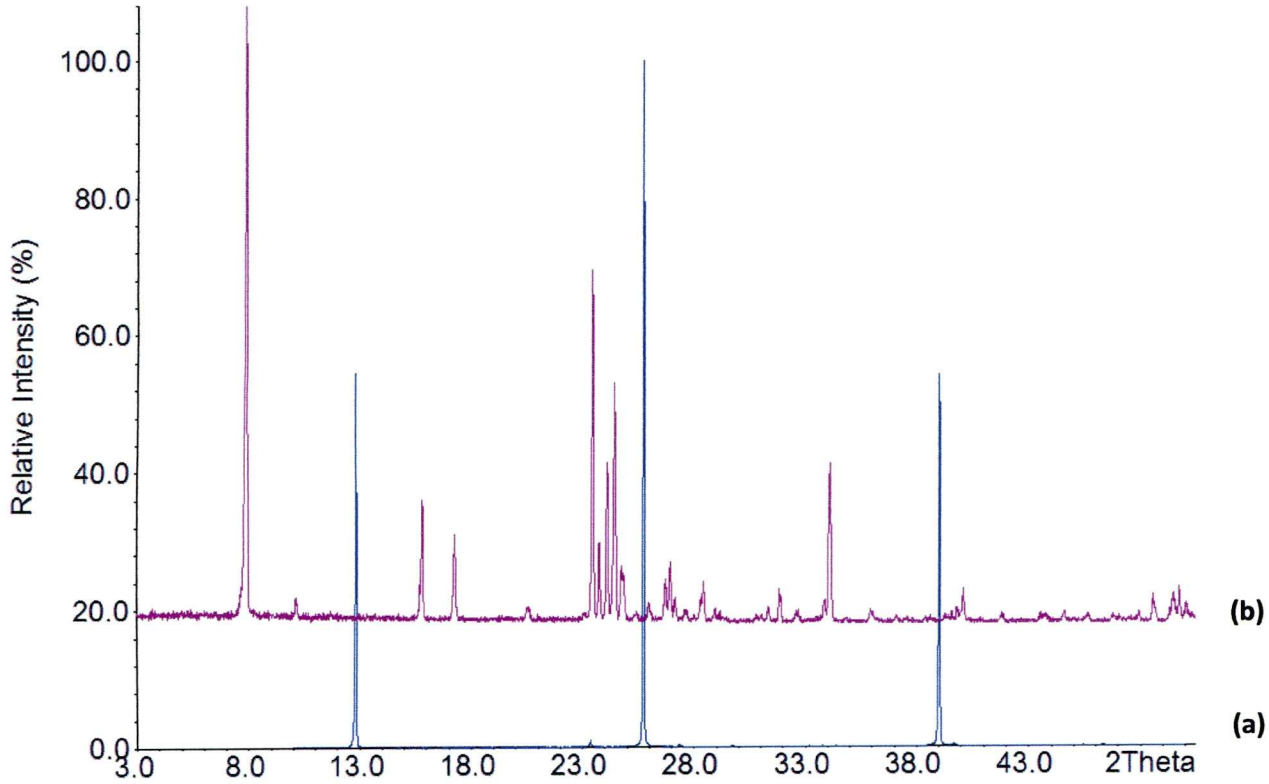

Figure 5.24 PXRD pattern for (a) MoO_3 and (b) MoO_3-4, 4'bipyridine

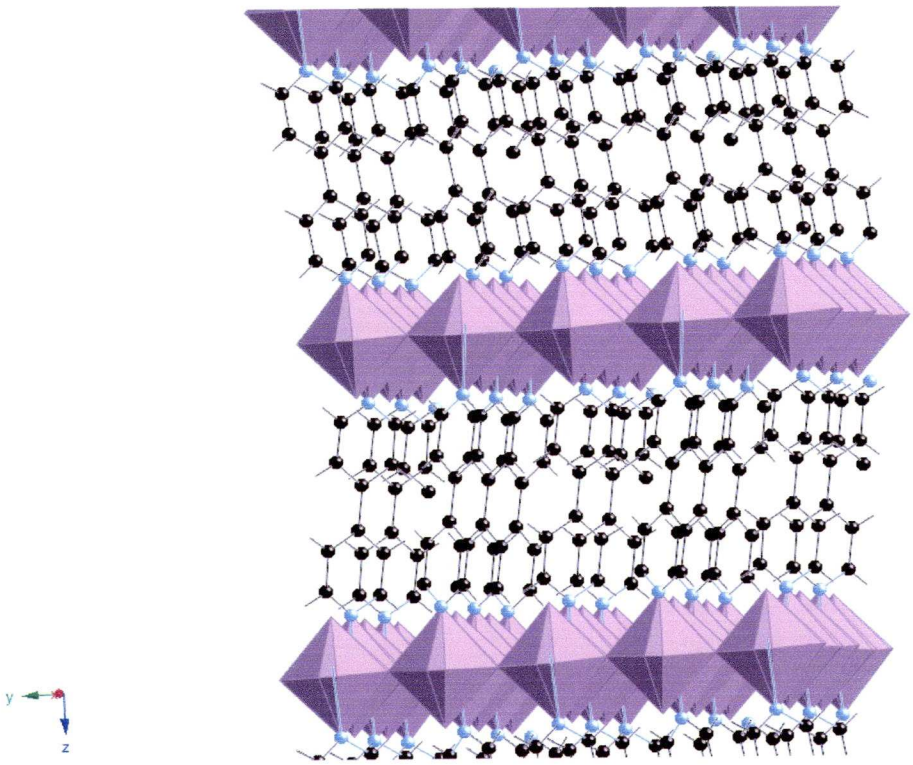

Figure 5.25 Crystal structure of MoO_3-4, 4'-bipyridine

$(C_5H_{12}N^+)_4(Mo_8O_{26}^{4-}).4H_2O$	Calculated	Found
C	23.6	24.72
H	1.60	1.63
N	5.50	4.10
Mo	37.78	40.02

Table 5.1 Comparison of calculated and observed values for elemental analyses for MoO_3-BIPY

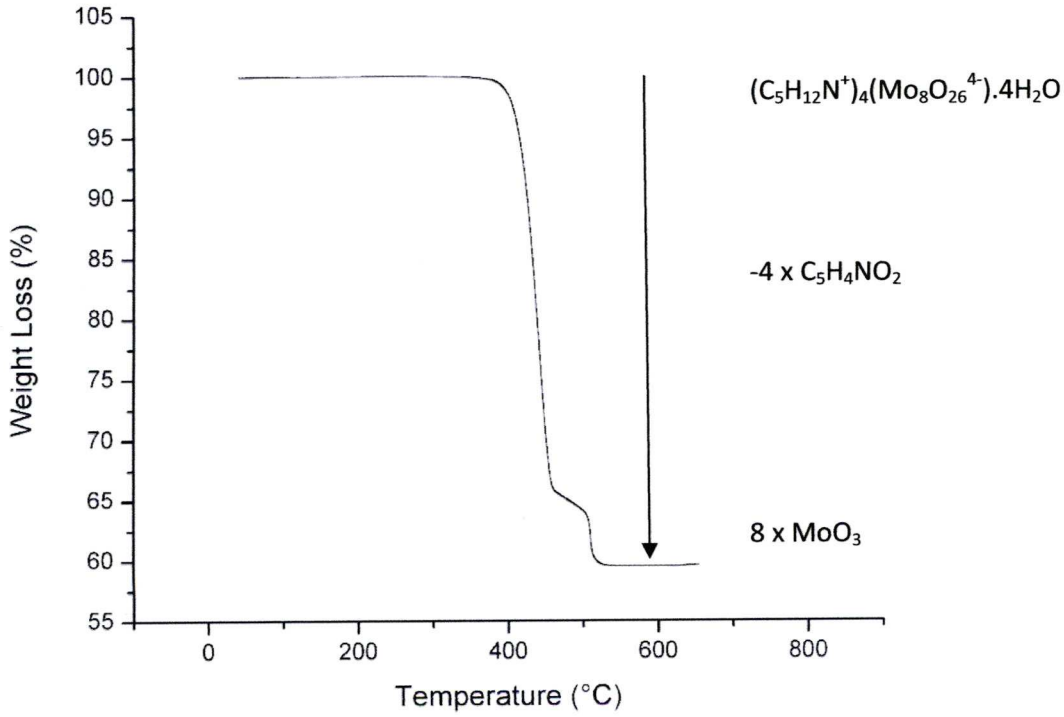

Figure 5.26 TGA curve for MoO_3-4, 4'-bipyridine. The compound exhibits high thermal stability with only one main mass loss occurring at 400°C corresponding to the loss of pillaring 4, 4'-bipyridine and the reforming of MoO_3

5.3.3 MoO_3-1, 3-diaminopropane

Similar to the previous synthesis, MoO_3 and 1, 3-diaminopropane (1.0325g:120µl, a 5:1 molar ratio) were heated in 10ml H_2O in an autoclave for 48 hours at 180°C at autogenous pressure. The resulting product consisted of fluffy, needle like crystals, which were removed and analysed. PXRD analysis again showed a new phase (Figure 5.27). Single crystal analysis showed the structure to be similar to the MoO_3-ethylenediamine structure, i.e. layers of edge sharing MoO_6 octahedra joined this time by protonated 1,3-diaminopropane bridges. This agrees well with a previously reported

synthesis[49] (Figure 5.28). Elemental analysis was also in broad agreement with predicted values based on this structure, as seen in Table 5.2, giving a formula of $(Mo_3O_{10})(C_3H_{16}N_2).2H_2O$. TGA analysis , shown in Figure 5.29 showed two major mass losses; the first of 9.1% being a loss of 2 molecules of co-crystallised water (calculated 3.2%). The second major mass loss of 25.3% (calculated 29.1%) corresponds to the reforming of MoO_3 with the loss of the 1, 3-diaminopropane bridges and molecules of oxygen, probably in a mechanism whereby the organic molecules are oxidised by the oxygen before leaving the structure. The large discrepancy for the water loss is probably due to the sample being wet. The compound exhibited a high degree of water uptake from atmospheric water, as can be seen from the initial parts of the TGA trace.

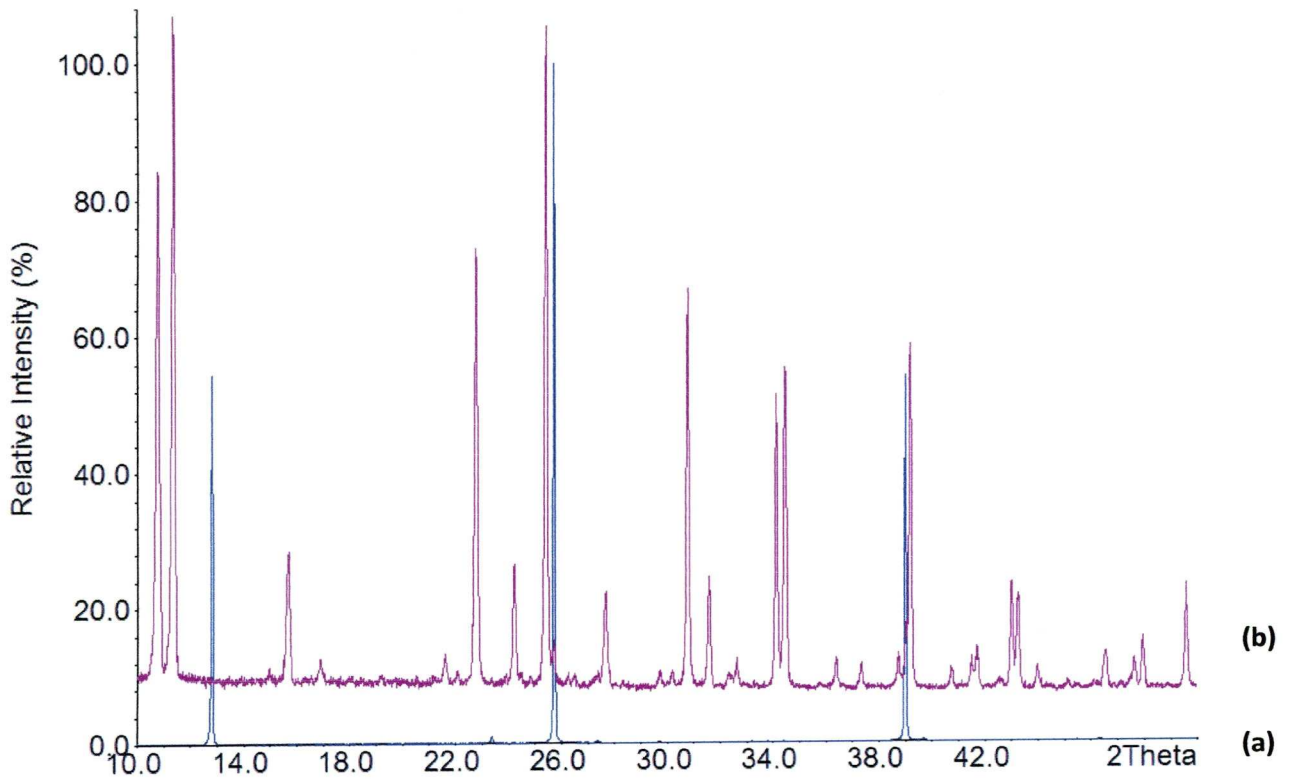

Figure 5.27 PXRD pattern for (a) MoO_3 and (b) MoO_3-1, 3-diaminopropane

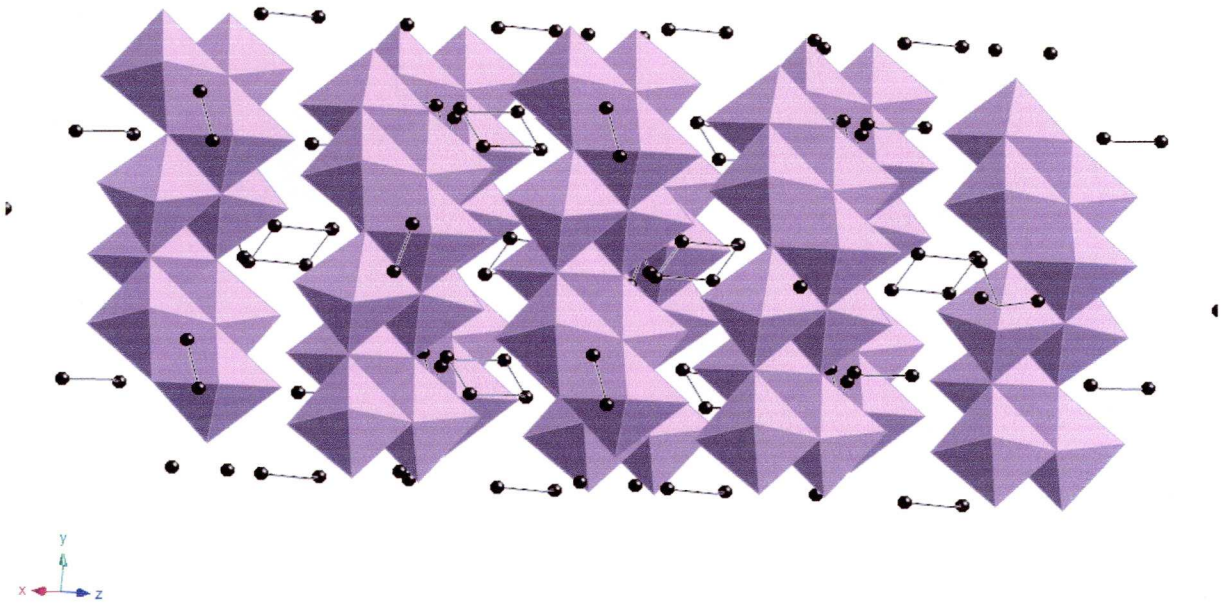

Figure 5.28 Crystal structure of MoO_3-1, 3-diaminopropane from work done by Ding *et al* [49] showing chains of MoO_6 octahedra separated by protonated 1, 3-diaminopropane cations. The structure is linked in a three dimensional network via hydrogen bonds.

$(Mo_3O_{10})(C_3H_{16}N_2).2H_2O$	**Calculated**	**Found**
C	6.43	6.12
H	2.88	2.58
N	5.00	4.03
Mo	51.41	43.79

Table 5.2 Table comparing calculated and observed values for elemental analyses for MoO_3-1, 3-diaminopropane

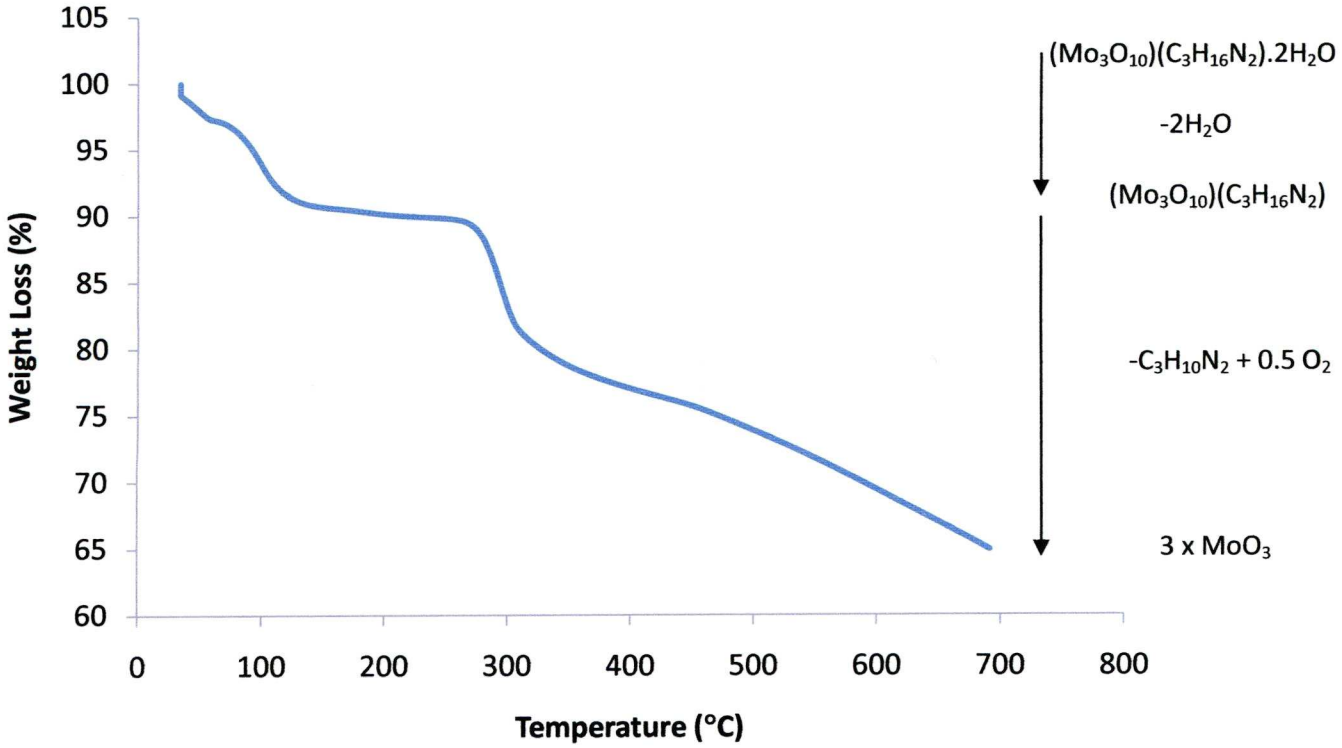

Figure 5.29 TGA trace for for MoO_3-1, 3-diaminopropane. Two major mass losses are shown. The first being a loss of co-crystallised water and the second being the organic 1, 3-diaminopropane.

5.3.4 MoO_3-Piperidine

Similar to the previous synthesis, MoO_3 and piperidine (1.0325g:142µl, a 5:1 molar ratio) were heated in 10ml H_2O in an autoclave for 48 hours at 180°C at autogenous pressure. The resulting product consisted of plate like crystals, which were removed and analysed. PXRD analysis showed a new phase had formed as shown in Figure 5.30, with a small amount of residual MoO_3 remaining . The structure of MoO_3-piperidine was determined via X-ray analysis of the single crystals as shown in Figure 5.31, data shown in Table 5.3. The structure consists of clusters of corner sharing MoO_6 octahedra separated by protonated piperidine ions. The $Mo_8O_{26}^{4-}$ ions are well characterised in the literature, with the NMR studies using ^{17}O being conducted and Day and Klemperer in 1977[50] using *n*-C_4H_9N as a counter ion. More recently, the ion has been found[51] in organic-inorganic compounds with organic counter-ions such as thiosemicarbazone. Elemental analyses also agreed well with calculated values (Table 5.4), giving a formula of $(Mo_8O_{26})(C_5H_{12}N)_4.2H_2O$. Analysis of the TGA data (Figure 5.32) showed relative thermal stability after the initial loss of co-crystallised water occurring at 120°C (observed 4.0%, calculated 2.3%), forming the material with composition $(Mo_8O_{26})(C_5H_{12}N)_4$.The material then began to decompose at around 280°C resulting in the loss of the piperidine organic material and the reforming of MoO_3 (observed 24.1%, calculated 24.6%). The

structure can be compared to the work described in Section 5.1.1 by Nelson *et al*[15] where $[Mo_8O_{26}]^{4-}$ ions formed from the reaction between 1,7-DAHep and MoO_3 in acidic media.

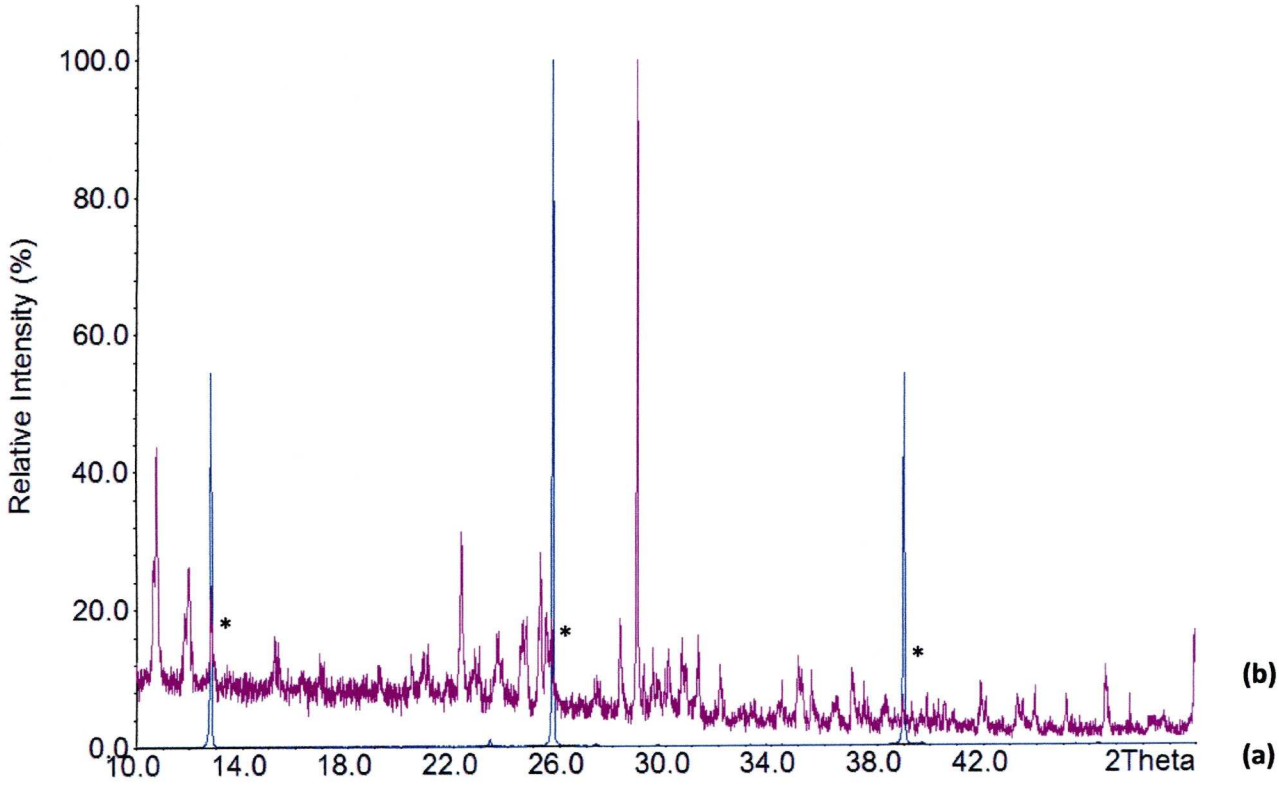

Figure 5.30 PXRD pattern for (a) MoO_3 and (b) MoO_3-piperidine

Note: * Denotes a small amount of unreacted MoO_3

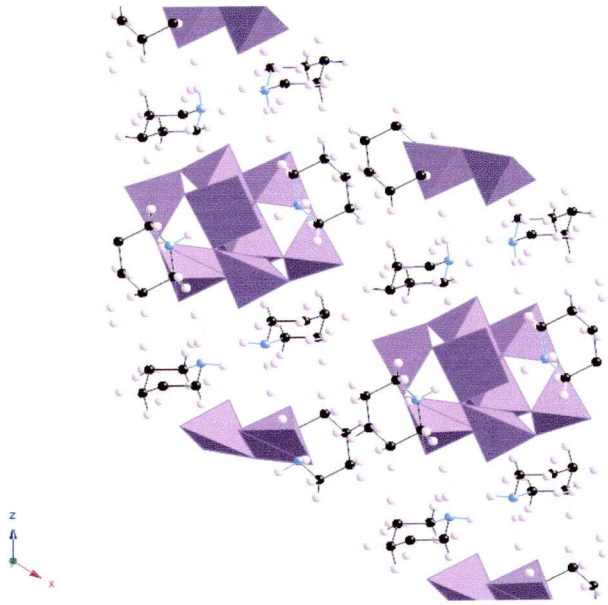

Figure 5.31 Crystal structure for MoO_3-piperidine, $(Mo_8O_{26})(C_5H_{12}N)_4.2H_2O$

Composition	$(C_5H_{12}N^+)_4(Mo_8O_{26}^{4-}).2H_2O$
Space Group	$P2_1/c$
Point Group	Monoclinic
a(Å)	12.837(2)
b(Å)	9.1560(16)
c(Å)	22.478(3)
β(°)	122.168(7)
V(Å^3)	2236.46
Z	2
Density$_{(calculated)}$ (g/cm^3)	2.376
T (K)	100
μ (mm^{-1})	2.264
Number of Collected Reflections	15587
R	0.0235
R_w	0.0567
Crystal Dimensions (mm)	0.48 x 0.37 x 0.31
M (gmol^{-1})	1600.21
Appearance	Colourless prisms
Radiation	Mo $K\alpha$

Table 5.3 Summarising crystallographic data for MoO_3-Piperidine

$(C_5H_{12}N^+)_4(Mo_8O_{26}^{4-}).2(H_2O)$	**Calculated %**	**Found %**
C	15.00	13.94
H	3.50	3.28
N	3.50	3.20
Mo	47.98	44.23

Table 5.4 Table comparing calculated and observed values for elemental analyses for MoO_3-piperidine, $(C_5H_{12}N^+)_4(Mo_8O_{26}^{4-}).2H_2O$

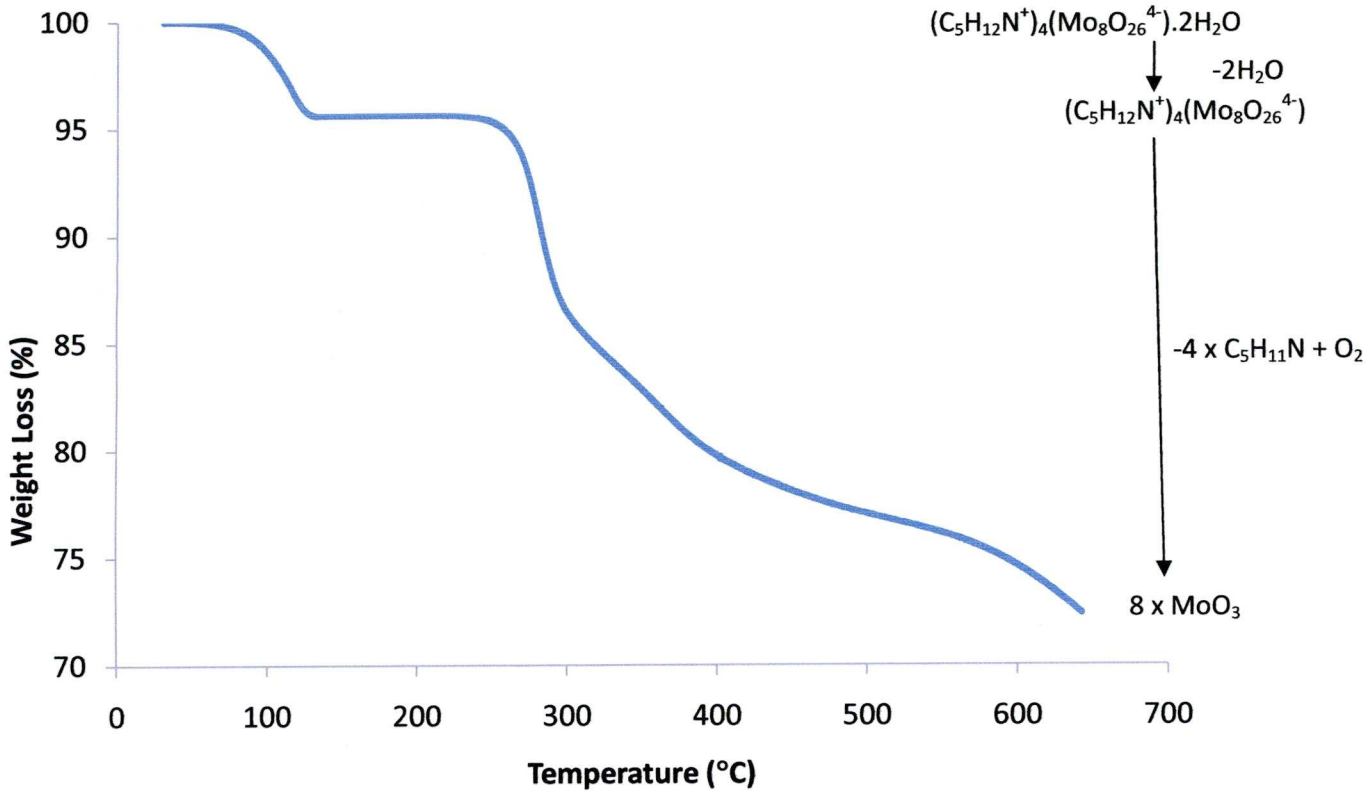

Figure 5.32 TGA Curve for MoO_3-Piperidine. The compound shows relatively high thermal stability after the initial loss of co-crystallised water, remaining stable until the loss of organic material at around 280°C, reforming the MoO_3 starting material

5.3.5 MoO_3-Urea

Similar to the previous synthesis, MoO_3 and urea (1.0325g:0.0862g, a 5:1 molar ratio) were heated in 10ml H_2O in an autoclave for 48 hours at 180°C at autogenous pressure. The resulting product consisted of needle like crystals, which were removed and analysed. PXRD analysis showed a new phase had formed as shown in Figure 5.33, however, after comparing the material to other compounds on the ICDD database, it was found to simply be a different, known, hexagonal three dimensional framework phase of MoO_3 compared to the orthorhombic starting material. No further structural work was therefore carried out on this material.

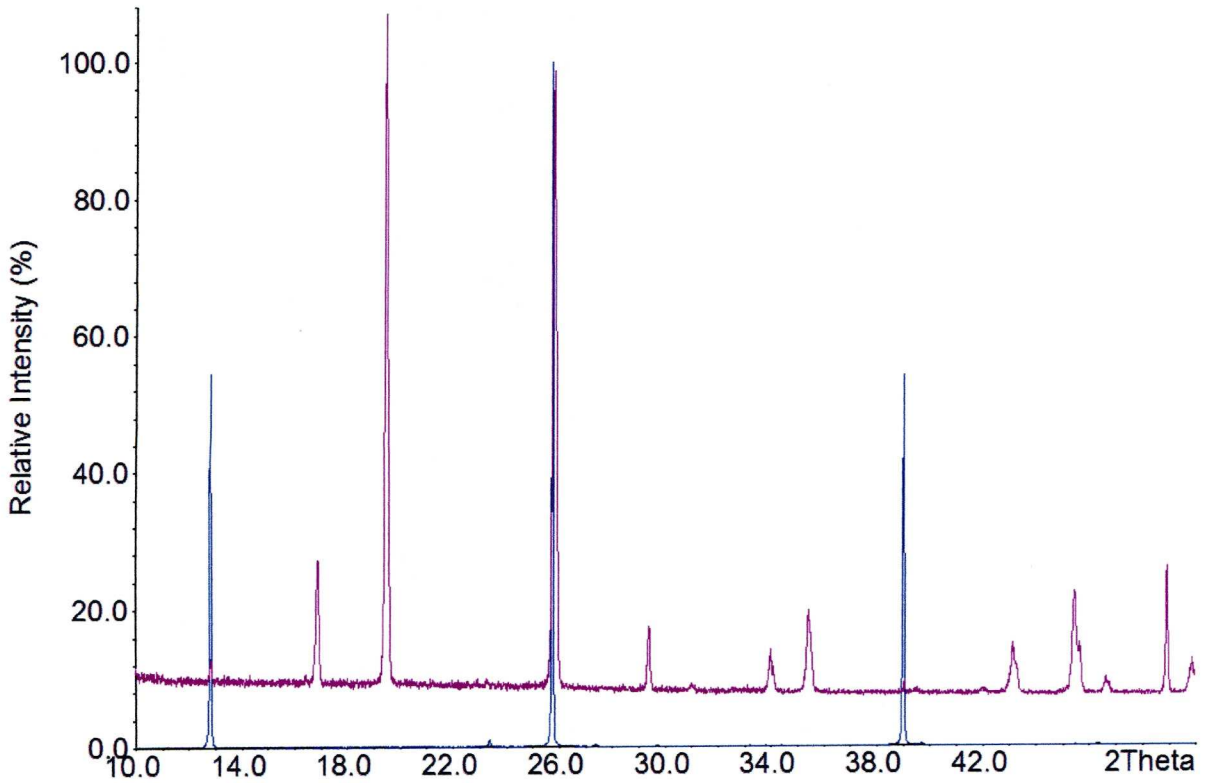

Figure 5.33 PXRD patterns comparing MoO_3 and MoO_3 in a different phase

5.4 Conclusions

Inorganic-organic hybrid materials have been synthesised successfully via the hydrothermal route, with the use of MoO_3 rather than WO_3 proving more fruitful with several compounds being synthesised including $(C_5H_{12}N^+)_4(Mo_8O_{26}^{4-}).2H_2O$, a previously unknown compound

5.5 References

1. A.K. Cheetham, *Science*, 264, **1994,** 794-795

2. K.A. Muller, J.G. Bednorz, *Science*, 237, **1987,** 1133-1139

3. J.T. Vaughey, J.P. Thiel, E.F. Hasty, D.A. Groenke, C.L. Stern, K.R. Poeppelmeier, B. Dabrowski, D.G. Hinks, A.W. Mitchell, *Chem. Mater.*, 3, **1991,** 935-940

4. B.S. Lu, J. Wang, H.F. Pan, M.H. Jiang, E.Q. Liu, X.Y. Hou, *J. Appl. Phys.*, 66, **1989,** 6052-6054

5. PY Chen, NS Chang,TK Chuang,SJ Chu,LY Chen, *Zeolites as catalysts, sorbants and detergent builders*, Elsevier Science Publishers B.V., Amsterdam, 1989.

6. C.T. Kresge, M.E. Leonowicz, W.J. Roth, J.C. Vartuli, J.S. Beck, *Nature*, 359, **1992,** 710-712

7. L.E. Smart, E.A. Moore, *Solid state chemistry: An introduction*, 3 ed., CRC Press, 2005.

8. J. Gopalakrishnan, *Chem. Mater.*, 7, **1995,** 1265-1275

9. R.F. Lobo, M.J. Annen, M.E. Davis, *J. Chem. Soc., Faraday Trans.*, 88, **1992,** 2791-2795

10. F. Cora, D.W. Lewis, C.R.A. Catlow, *Chem. Commun.*, **1998,** 1943-1944

11. F. Corà, C.R.A. Catlow, D.W. Lewis, *J. Mol. Catal. A: Chem.*, 166, **2001,** 123-134

12. D.W. Lewis, D.J. Willock, C.R.A. Catlow, J.M. Thomas, G.J. Hutchings, *Nature*, 382, **1996,** 604-606

13. N.N. Greenwood, A. Eranshaw, *Chemistry of the elements*, 2 ed., Butterworth-Heinemann, 2002.

14. P. Roman, A. Luque, A. Aranzabe, J.M. Gutierrez-Zorrilla, *Polyhedron*, 11, **1992,** 2027-2038

15. J.H. Nelson, A.R. Johnston, A.N. Sarjeant, A.J. Norquist, *Solid State Sci.*, 9, **2007,** 472-484

16. O.W. Howarth, P. Kelly, L. Pettersson, *J. Chem. Soc., Dalton Trans.*, **1990,** 81-84

17. W.G. Klemperer, W. Shum, *J. Am. Chem. Soc.*, 98, **1976,** 8291-8293

18. S. Himeno, H. Niiya, T. Ueda, *Bull. Chem. Soc. Jpn.*, 70, **1997,** 631-637

19. H.-J. Koo, C. Lee, G.B. Wilson-Short, D. Dai, M.-H. Whangbo, *Inorg. Chem.*, 46, **2007,** 2498-2502

20. S. Gatard, S. Blanchard, B. Schollhorn, P. Gouzerh, A. Proust, K. Boubekeur, *Chem.--Eur. J.*, 16, **2010,** 8390-8399

21. S. Triki, L. Ouahab, J. Padiou, D. Grandjean, *J. Chem. Soc., Chem. Commun.*, **1989,** 1068-1070

22. E.F. Wilson, H. Abbas, B.J. Duncombe, C. Streb, D.-L. Long, L. Cronin, *J. Am. Chem. Soc.*, 130, **2008,** 13876-13884

23. R. Khoshnavazi, R. Sadeghi, L. Bahrami, *Polyhedron*, 27, **2008,** 1855-1859

24. M. Sarma, T. Chatterjee, S. Das, *Inorg. Chem. Commun.*, 13, **2010,** 1114-1117

25. N.N. Greenwood, A. Earnshaw, *Chemistry of the elements*, 2 ed., Butterworth Heinemann, 2002.

26. J.J. Hastings, O.W. Howarth, *J. Chem. Soc., Dalton Trans.*, **1992,** 209-215

27. J.F. Keggin, *Proc. R. Soc. A*, 144, **1934,** 75-100

28. W.P. Griffith, *Transition Met. Chem.*, 16, **1991,** 548-552

29. I.V. Kozhevnikov, *J. Mol. Catal. A: Chem.*, 262, **2007,** 86-92

30. Y. Leng, J. Wang, D. Zhu, Y. Wu, P. Zhao, *J. Mol. Catal. A: Chem.*, 313, **2009,** 1-6

31. I.V. Kozhevnikov, *Catalysts for fine chemical synthesis: Catalysis by polyoxometallates*, John Wiley and Sons Ltd, 2002.

32. A. Muller, F. Peters, M.T. Pope, D. Gatteschi, *Chem. Rev.*, 98, **1998,** 239-271

33. R. Copping, A.J. Gaunt, I. May, M.J. Sarsfield, D. Collison, M. Helliwell, I.S. Denniss, D.C. Apperley, *Dalton Trans.*, **2005,** 1256-1262

34. K. Kamata, K. Yonehara, Y. Nakagawa, K. Uehara, N. Mizuno, *Nat Chem*, 2, **2010,** 478-483

35. P.J. Hagrman, D. Hagrman, J. Zubieta, *Angew. Chem., Int. Ed.*, 38, **1999,** 2639-2684

36. C.C. Jiang, G. Liu, Y.G. Wei, W. Wang, S.W. Zhang, *Inorg. Chem. Commun.*, 2, **1999,** 258-260

37. A. Muller, E. Krickemeyer, J. Meyer, H. Bogge, F. Peters, W. Plass, E. Diemann, S. Dillinger, F. Nonnenbruch, M. Randerath, C. Menke, *Angew. Chem., Int. Ed.*, 34, **1995,** 2122-2124

38. B.Z. Lin, X.Z. Liu, B.H. Xu, Q.Q. Wang, Z.J. Xiao, *Solid State Sci.*, 10, **2008,** 1517-1524

39. M.I. Khan, Q. Chen, J. Zubieta, *Inorg. Chim. Acta*, 213, **1993,** 325-327

40. Y. Xu, L.H. An, L.L. Koh, *Chem. Mater.*, 8, **1996,** 814-818

41. P.J. Zapf, R.C. Haushalter, J. Zubieta, *Chem. Mater.*, 9, **1997,** 2019-2024

42. K.-J. Range, A. Fassler, *Acta Crystallogr., Sect. C: Cryst. Struct. Commun.*, 46, **1990,** 488-489

43. B.M. Gatehouse, P. Leverett, *J. Chem. Soc. A*, **1968,** 1398-1405

44. H. Tagaya, K. Ara, J. Kadokawa, M. Karasu, K. Chiba, *J. Mater. Chem.*, 4, **1994,** 551-555

45. D.E. Katsoulis, *Chem. Rev.*, 98, **1998,** 359-387

46. Y. Lu, Y.G. Li, E.B. Wang, J. Lu, L. Xu, R. Clerac, *Eur. J. Inorg. Chem.*, **2005,** 1239-1244

47. P.J. Hagrman, R.L. LaDuca, H.J. Koo, R. Rarig, R.C. Haushalter, M.H. Whangbo, J. Zubieta, *Inorg. Chem.*, 39, **2000,** 4311-4317

48. X.M. Wei, H.C. Zeng, *Chem. Mater.*, 15, **2002,** 433-442

49. C. Ding, B.Z. Lin, G.H. Han, L. Bai, *Acta Crystallogr., Sect. C: Cryst. Struct. Commun.*, 63, **2007,** M256-M258

50. V. Day, M. Fredrich, W. Klemperer, W. Shum, *J. Am. Chem. Soc.*, 99, **1977,** 952-953

51. R. Gil-Garcia, R. Zichner, V. Diez-Gomez, B. Donnadieu, G. Madariaga, M. Insausti, *Eur. J. Inorg. Chem.*, 2010, **2010,** 4513-4525

Chapter 6: Experimental Details

6.1 Analytical Techniques

6.1.1 Elemental Analysis

Elemental analyses were performed by the microanalytical service at the University of Liverpool. C, H and N contents were calculated by quantitative combustion of the samples using a Flash EA1112 instrument. Metals analyses were calculated using inductively coupled plasma (ICP) atomic emission spectroscopy on a Ciros CCD spectrometer, following complete digestion of the samples in hot concentrated HCl.

6.1.2 Powder X-ray Diffraction

PXRD patters were recorded using Cu $K\alpha_1$ radiation on a Stoe Stadi-P diffractometer in either Bragg-Brentano or Debye-Scherrer geometry. For the Bragg-Brentano, the samples were mounted on a zero background holder. No reflections are observed for the plate at the range of interest for the samples being analysed. For the transmission, samples were either mounted on a sample spinner between two thin acetate sheets, with the sample being held with a small amount of grease, with no interference in the PXRD patterns, or for samples exhibiting air sensitivity, sealed in 0.5mm glass capillaries in a glove box under an argon atmosphere.

6.1.3 Solution NMR Spectroscopy

^{1}H NMR spectra were recorded using a Brucker AMX 400 spectrometer (operating at a ^{1}H frequency of 400MHz), fitted with an automatic sample changer. NMR data were collected at ambient temperature. ^{1}H chemical shifts are quoted relative to tetramethylsilane (TMS).

6.1.4 Thermogravimetric Analysis

Thermogravimetric analysis was carried out on a Perkin-Elmer STA 6000 simultaneous thermal analyser. A sample (approx 30-50mg) was accurately weighed in an alumina crucible and mounted in a furnace and heated at a rate of 10°C/minute, up to 1000°C under a flow of N_2.

6.2 Experimental Details for Chapter 2

6.2.1 Synthesis of Layered Double Hydroxides

Gibbsite was supplied by the laboratory of Prof. Dermot O Hare at the University of Oxford, and was activated by adding a small amount of de-ionised water make to a paste like consistency before grinding in a mill using zirconia beads for several days. The resulting paste was then filtered and dried in air before being used. All metal salts used in the LDH synthesis were obtained from Aldrich (>98% purity) and used without any further purification.

Hydrothermal reactions were carried out in poly(tetrafluoroethylene) (PTFE) lined 23 ml stainless steel autoclaves, supplied by the Parr Instrument Company (shown in Figure 6.1). Typically, reagents are weighed into the Teflon liners, before being placed in the autoclaves. The autoclave lid is then firmly screwed to ensure a good seal. The sealed autoclaves were then placed into a Eurotherm controlled oven, and followed the temperature program specific to that particular reaction, which included specific heating rates, a temperature hold and then a specific cooling rate. Once the autoclaves had cooled, then solid products were removed via vacuum filtration, and washed extensively to remove soluble inpurities. The recovered solids were then dried with a small amount of acetone to facilitate drying, and left to dry under vacuum. All products were then characterised using X-ray diffraction, along with additional techniques if appropriate.

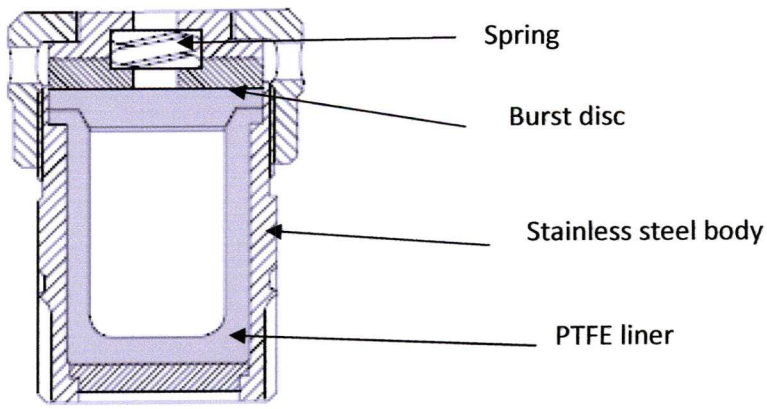

Figure 6.1 Schematic of a PTFE lined autoclave used for hydothermal synthesis

6.2.1.1 $[LiAl_2(OH)_6]X.yH_2O$

The materials $[LiAl_2(OH)_6]X.yH_2O$ were synthesised using previously reported methods[1]. In a standard experiment, $Al(OH)_3$ (0.5g) was combined with a 5 molar aqueous solution of LiX ($X = NO_3^-$, Cl^-, OH^-) and stirred for 24h at 90°C in a sealed ampoule. The solid product was recovered by filtration through a sinter funnel and washed several times with de-ionised water before a final wash with acetone (to aid drying) before being allowed to dry fully in air.

6.2.1.2 $[MAl_4(OH)_{12}](NO_3)_2.yH_2O$

The materials $[MAl_4(OH)_{12}](NO_3)_2.yH_2O$ were synthesised as follows. Activated gibbsite (1g) was placed in a 23 ml PTFE-lined stainless steel autoclave with 10ml of a 10M solution of $M(NO_3)_2$. The mixture was then treated hydrothermally (as described in section 6.2.1) at 150°C for 48h to yield the novel $[MAl_4(OH)_{12}](NO_3)_2.yH_2O$ (M = Zn, Cu, Ni or Co) materials. After cooling to room temperature, the solid products were recovered by filtration through a sinter funnel and washed several times with de-ionised water before a final wash with acetone (to aid drying) before being allowed to dry fully in air.

6.2.2 Solid State NMR Spectroscopy

Solid state magic angle spinning (MAS) NMR experiments were conducted at 9.4T on a Brucker Avance DSX-400 spectrometer equipped with a 4mm $^1H/X/Y$ CP/MAS probehead using zirconia rotors of 4mm external diameter. ^{27}Al MAS NMR spectra were acquired at 104.2 MHz using a $\pi/18$ pulse length of 0.40µs at a MAS rate of 10.0kHz. The recycle delay was set to 1.0s with the position of the ^{27}Al resonances quoted in ppm being relative to a $[Al(H_2O)_6]^{3+}$ standard (0.1M aqueous $Al(NO_3)$). ^7Li MAS NMR were acquired at 155.52 MHz using a $\pi/9$ pulse rate of 0.60µs and a MAS rate of 10.0kHz. The recycle delay was set at 2.0s, with the position of the ^7Li resonances quoted in ppm from a 1M aqueous LiCl standard. This work was carried out by Dr. James Jones, a former PhD student of Dr. Yaroslav Khimyak, with Dr. Khimyak contributing to the interpretation of the spectra.

6.2.3 BET Measurements

Catalyst surface areas were obtained by BET from nitrogen physisorption measured at -196°C on a Micromeritics ASAP 2000 instrument. Before analysis, samples were degassed at 250°C. This work was carried out by Dr. Robert Hetterley, a former PhD student of Prof. Ivan Kozhevnikov.

6.2.4 Palladium Dispersion

Palladium dispersion on the catalysts was determined by hydrogen chemisorption measured via a pulse technique using a Micromeritics TPD/TPR 2900 instrument, according to previously reported methods[2]. Typically, a catalyst sample (0.5g) which has been exposed to air for several days at room

temperature was placed in a glass sample tube connected to the instrument and stabilised at 30±1°C under a flow of N_2 at 70ml/minute. Pulses of pure H_2 (50µl) were injected into the flow at 3 minute intervals until the catalyst had been saturated with hydrogen. Dispersion is defined as the fraction of Pt at the surface, $D=Pt_s/P_{total}$. This assumes the following stoichiometry of hydrogen adsorption[3]:

$$PtO + 1.5H_2 \rightarrow PtH + 1.5\ H_2O$$

This work was carried out by Dr. Robert Hetterley, a former PhD student of Prof. Ivan Kozhevnikov.

6.2.5 Catalytic Testing

The one-step conversion of acetone to MIBK was analysed via online gas-chromatography, using a Varian Star 3400CX instrument equipped with a flame ionisation detector (FID) and a 30m x 0.25mm HP-INNOWAX capillary column. This was performed by Dr. Robert Hetterley, a former PhD student of Prof. Ivan Kozhevnikov. A schematic of the experimental apparatus is shown in Figure 6.2

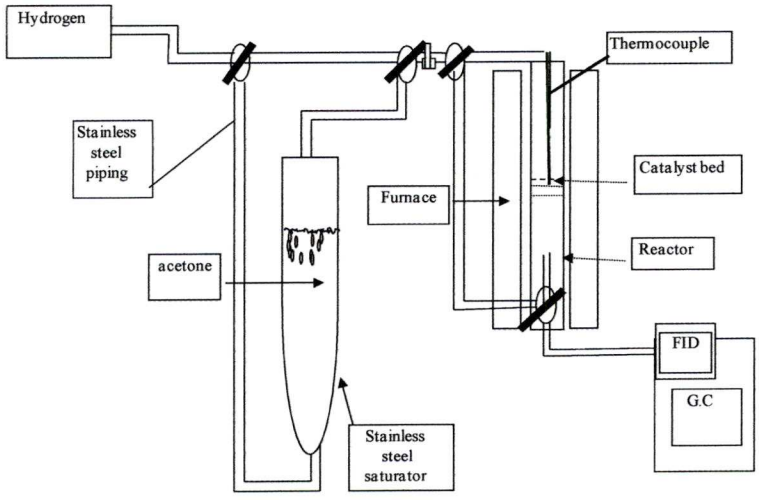

Figure 6.2 Schematic of experimental apparatus for one pot synthesis of MIBK

6.3 Experimental Details for Chapter 3

6.3.1 Synthesis of Catalysts

$[LiAl_2(OH)_6](NO_3).H_2O]$ was synthesised as detailed in Section 6.2.1.2. The nitrate anion in this host material was then exchanged for tungstate. The Li/Al-LDH host (0.1500g, 0.617mmol) was suspended in a 10ml aqueous solution containing a 2 fold excess of $Na_2WO_4.2H_2O$ (0.4059g, 1.23mmol) and stirred at 50°C overnight in a glass ampoule sealed with a Young's tap. The solid product was recovered via vacuum filtration and washed with deionised water to remove soluble impurities before a final wash with acetone to ease drying. The solid was then left to dry in the air before being characterised using PXRD.

6.3.2 Oxidative Bromination of Phenol Red

In a typical reaction[4-6], Li/Al-WO_4-LDH (0.0607g, 0.2mmol) as synthesised in the previous section was placed in a round bottomed flask with phenol red (0.0177g, 0.05mmol) along with ammonium bromide (0.1959g, 2.00mmol). To this a mixture of H_2O, methanol and tetrahydrofuran (THF) in the ratio 4:3:2 (20ml) was added before allowing the mixture to stir for 30 minutes. After this time, a UV-Visible spectrum was taken as detailed in Section 6.3.3. Once the spectrum had been recorded, H_2O_2 (30%, 2.5mmol) was added and the reaction was allowed to proceed, with a sample being taken every 5 minutes for spectrophotometric analysis. After the reaction had gone to completion, the reaction mixture was worked up, allowing the bromophenol blue product to be extracted for further analysis. The mixture was first filtered in order to remove the heterogeneous Li/Al-WO_4-LDH catalyst before extracting the bromophenol blue in dichloromethane using tetra-*n*-hexylammonium chloride and evaporating to dryness. A ^1H NMR spectrum was then taken to confirm that bromination had indeed taken place.

6.3.3 UV-Visible Spectrophotometry

The conversion of phenol red to bromophenol blue was monitored using a Perkin-Elmer lambda 650S UV-Visible spectrometer. In each experiment, a sample (35µl) was taken using a Fisherbrand Finnpipette II (range 10-100µl) and diluted with the reaction solvent; H_2O, methanol and THF in the ratio 4:3:2 (3.00ml), using an Eppendorf Research pipette (range 1-10ml). The sample was diluted in a quartz cuvette before being placed in the instrument and analysed in the range 200-800nm at a scan rate of 266.75nm/minute.

6.4 Experimental Details for Chapter 4

6.4.1 Synthesis of Catalysts

$[LiAl_2(OH)_6](NO_3).H_2O]$ was synthesised as detailed in Section 7.2.1. The nitrate anion in this host material was then exchanged for molybdate. The Li/Al-LDH host (0.1500g, 0.617mmol) was suspended in a 10ml aqueous solution containing a 2 fold excess of $Na_2MoO_4.2H_2O$ (0.2988g, 1.23mmol) and stirred at 50°C overnight in a glass ampoule sealed with a Young's tap. The solid product was recovered via vacuum filtration and washed with deionised water to remove soluble impurities before a final wash with acetone to ease drying. The solid was then left to dry in the air before being characterised using PXRD.

6.4.2 Oxidation of Citronellol

In a typical reaction[7], the Li/Al-MoO_4-LDH was suspended in 10ml of methanol containing (-)-S-β-citronellol (911µl, 5mmol) and stirred for 30 minutes ensuring complete dispersion of the catalyst before taking an initial gas chromatograph, as detailed in Section 6.4.3. H_2O_2 (30%) was then added in 200µl portions. A sample was taken once the reaction solution had gone from red to yellow, as the gradual addition of the H_2O_2 solution has been shown to favour the formation of the yellow triperoxomolybdate species, the more efficient species for the production of $^1O_2$ as compared to the red tetraperoxo species[8].

6.4.3 Gas Chromatography

Gas chromatography was used to monitor the oxidation of S-Citronellol. Before performing a gas-chromatograph of the reaction mixture, the solution was treated with sodium sulphite, which quantitatively reduces the hydroperoxide species formed by the reaction into the corresponding alcohol. It is not possible to detect a hydroperoxide species using GC due to inherently unstable nature of that functional group. GC was performed on Shimaduzi gas chromatograph GC14B, using a 30m x 0.32mm EC Wax column with a film thickness of 0. 25µm and employing a 50:1 split injection, using He carrier gas and a flame ionisation detector. The temperature programme used was as follows: hold at 120°C for 2 minutes, ramp at 10°C/minute, hold at 200°C for 5 minutes. A drop of the reaction mixture, after being reduced with sodium sulphite was diluted with dichloromethane (3ml). 5µl of this solution was then injected into the gas chromatograph.

6.4.4 Gas Chromatography-Mass Spectrometry

To identify all products present in the final mixture, GC-MS was performed on the sample, using a Trio-1000 mass spectrometer in electron ionisation (EI) mode. The software associated with the machine was then able to search/match the corresponding product peaks and suggest molecules which fit the pattern. The search/match findings were in good agreement with expected products.

6.5 Experimental Details for Chapter 5

6.5.1 Synthesis of WO_3/MoO_3 Materials

All WO_3/MoO_3 organic materials were synthesised via the hydrothermal method. In a typical experiment, WO_3 or MoO_3 was suspended in 10ml H_2O along with the organic component at a ratio of WO_3/MoO_3:organic of 5:1. The suspension was then treated hydrothermally for 48 hours (at 200°C for WO_3 materials and 180°C for MoO_3 materials) before being allowed to cool to room temperature. The materials were then washed with de-ionised water before being allowed to air dry. Acetone was not used to facilitate drying for these materials due to their solubility in this solvent.

6.5.2 Single Crystal X-ray Diffraction

Single crystals were analysed either by Dr. John Bacsa at the University of Liverpool, or by the National Crystallography Service, based at the University of Southampton. In a typical measurement run by Dr. John Bacsa, the crystal was mounted on a glass fibre and placed in a cold stream at 100K. Single crystal X-ray data were collected on a Bruker D8 diffractometer with an APEX CCD detector, and 1.5 kW graphite monochromated Mo radiation. The detector to crystal distance was 50 mm. Exposure times of 10 s per frame and scan widths of 0.3° were used throughout the data collection. The data collection was performed using three ω scans yielding data in the θ range 3.3 to 27.5° with an average completeness of 99%. The frames were integrated with the SAINT v6.45a (Bruker, 2005)[9]. A multi-scan absorption correction was carried out using the program SADABS V2008-1 (Bruker, 2008)[10]. The structure was solved and refined with X-SEED[11], a graphical interface to SHELX (Sheldrick, 2008)[12]. Samples run at the University of Liverpool included WO_3-DABCO, MoO_3-BIPY, MoO_3-Piperidine.

Samples run by the National Crystallography Service were run on a Bruker-Nonius KappaCCD diffractometer, located on opposite windows of a Bruker-Nonius FR591 rotating anode X-ray generator with a conventional graphite monochromated beam, and a Kappa CCD detector. Samples run here were MoO_3-1,3-diaminopropane and MoO_3-urea.

6.6 References

1. A.V. Besserguenev, A.M. Fogg, R.J. Francis, S.J. Price, D. Ohare, V.P. Isupov, B.P. Tolochko, *Chemistry of Materials*, 9, **1997,** 241-247

2. M. Musawir, E.F. Kozhevnikova, I.V. Kozhevnikov, *J. Mol. Catal. A: Chem.*, 262, **2007,** 93-97

3. J.E. Benson, M. Boudart, *J. Catal.* , 4, **1965,** 704-&

4. B. Sels, D. De Vos, M. Buntinx, F. Pierard, A. Kirsch-De Mesmaeker, P. Jacobs, *Nature*, 400, **1999,** 855-857

5. B.F. Sels, D.E. De Vos, M. Buntinx, P.A. Jacobs, *J. Catal.* , 216, **2003,** 288-297

6. B.F. Sels, D.E. De Vos, P.A. Jacobs, *J. Am. Chem. Soc.*, 123, **2001,** 8350-8359

7. J. Wahlen, D.E. De Vos, B.F. Sels, V. Nardello, J.M. Aubry, P.L. Alsters, P.A. Jacobs, *Appl. Catal., A*, 293, **2005,** 120-128

8. D.E. De Vos, J. Wahlen, B.F. Sels, P.A. Jacobs, *Synlett*, **2002,** 367-380

9. *Bruker (2005), saint v6.45a, bruker axs inc., madison, wi, USA.* , in.

10.

11. L.J. Barbour, *J. Supramol. Chem.*, 1, 189-191

12. G. Sheldrick, *Acta Crystallogr., Sect. A: Found. Crystallogr.*, 64, **2008,** 112-122

Chapter 7: Conclusions

Layered double hydroxides (LDHs) are a class of inorganic layered materials with general formula $[M^{z+}_{1-x}M^{3+}_{x}(OH)_2]^{q+}(X^{n-})_{q/n}.yH_2O$, where x is the ratio $M^{3+}/(M^{2+} + M^{3+})$. Z is usually 2, and can be Ca^{2+}, Mg^{2+}, Mn^{2+}, Fe^{2+}, Co^{2+}, Ni^{2+}, Cu^{2+} or Zn^{2+}. Al^{3+} and any trivalent transition metal cation can be used (apart from Ti^{3+}, due to the instability of Ti in this oxidation state). There are two families of LDH; the more studied is the family based on the naturally occurring mineral brucite, $[Mg(OH)_2]$, the structure of which consists of MgO_6 edge sharing octahedra forming infinite sheets. LDHs form where the divalent Mg^{2+} cations are substituted for trivalent cations. This results in a charge imbalance in the layers. To compensate for this, anions occupy the interlayer space along with water molecules. The second family is derived from the mineral gibbsite, $[\gamma\text{-}Al(OH)_3]$. The structure of gibbsite is layered and best understood as double layers of hexagonally packed O atoms with Al atoms occupying the octahedral holes in the layers in an ordered manner. The octahedral holes in gibbsite can also occupy metal cations where z=2 for M^{2+}= Zn, Co, Cu and Ni. There are also examples of z=1, where $M=Li^+$. LDHs have many applications in the catalysis of organic materials, both where the metals contained in the LDH are the catalyst, such as the use of $[Mg_6Al_2(OH)_{16}](CO_3).6H_2O$ (Mg/Al-CO_3-LDH with an Mg/Al ratio of 2.5) for aldol condensations[1] and the Knoevanagel reaction[2] or the use of Mg/Al-CO_3-LDH with a Mg/Al ratio of 5 in the formation of cyclic molecules from CO_2 and epoxides[3]. Interlayer anions are also used, for example the intercalation of Mg/Al-CO_3-LDH with a Mg/Al ratio of 1.8 with POM ions such as $Mo_7O_{24}^{6-}$ or $W_{12}O_{41}^{10-}$ in alkene epoxidation reactions[4]. There are several reviews[5-6] on brucite based LDHs showing a large body of research on the subject, there is, however little research on the gibbsite family of LDHs.

This thesis presents research into the properties of gibbsite $[\gamma\text{-}Al(OH)_3]$ based LDHs, previously unexplored in the field of catalysis. In Chapter 2, the use of $[LiAl_2(OH)_6]X.H_2O$, where $X = OH^-$, NO_3^-, and $[MAl_4(OH)_{12}]NO_3.H_2O$, where $M = Zn^{2+}$, Co^{2+}, Cu^{2+} and Ni^{2+}, is combined with a small amount of palladium, producing a bi-functional catalyst. The synthesis of methyl isobutyl ketone (MIBK) from acetone was used as a test reaction for these new catalysts, with a MIBK selectivity of 70% at a 20% conversion rate of acetone being found using Pd doped $[LiAl_2(OH)_6]NO_3.H_2O$ at 120°C. Higher acetone conversion rates of 77% were noted at the optimum reaction temperature of 250°C coupled with 91% MIBK and DIBK (diisobutyl ketone) selectivity using a Pd doped $[NiAl_4(OH)_{12}]NO_3.H_2O$ catalyst. The development of such reactions, where a re-useable, heterogeneous catalyst, with a high atom economy could be used in place of a homogeneous catalyst which is used once and generates significant amount of salt waste (such as the use of sodium hydroxide in this case), is

crucial to the ongoing sustainability and efficiency of key industrial processes[7]. This work[8] compares favourably to catalysts described in the literature based on polyoxometallates[9], mixed oxides[10] and zeolites[11].

The main advantage of the LDH system over the other systems is the ease of synthesis. The Pd impregnated LDHs used in this study were synthesised in three steps, simply by synthesising the pristine LDH by literature methods[12-13] before suspending in palladium acetate and reducing under H_2. In contrast, the heteropolyacid $Cs_{2.5}H_{0.5}PW_{12}O_{40}$ has to be supported on silica, as it forms colloidal solutions which cannot be separated by filtration alone. The process for supporting the heteropolyacid on silica is lengthy, laborious and energy intensive, requiring ageing and grinding steps to achieve the desired catalyst. The zeolite synthesis is also more lengthy and energy intensive than that of the LDH, requiring a calcination step to achieve the desired catalyst. This reaction could be further developed by scaling it up, allowing comparisons to be made to existing industrial processes employing Pd-doped acid resins and Pd doped zirconium phosphates[14], which are carried out in the liquid phase using high pressure (20-50 bar) H_2. Using such high pressures is obviously a disadvantage. The use of the system developed here would overcome those problems.

In Chapter 3, the use of a gibbsite based LDH, $[LiAl_2(OH)_6](WO_4)_{0.5}.H_2O$ in catalysis was explored. This LDH cannot be made directly, having to be synthesised by suspending $[LiAl_2(OH)_6](NO_3).H_2O$ in a solution of Na_2WO_4 for 24 hours, thereby allowing the NO_3^- anions to be replaced by WO_4^{2-}. The tungstate containing LDH was then used as a catalyst for the mild oxidative bromination of phenol red to bromophenol blue. Typical bromination reactions involve the use of toxic elemental bromine, or N-bromosuccinimide which generates stoichiometric amounts of waste. The system and bromination reaction was based upon that developed in work by de Vos *et al*[15-17], however, gibbsite based LDHs had again been unexplored in this area. The gibbsite based catalyst had a comparable performance with the brucite based catalysts found in the literature, giving a superior bromination rate, however, lower a turn over frequency and lower specific activity were found, which relate to the moles of catalytically active metal (i.e. the WO_4^{2-}) and the weight of catalyst respectively. Problems were also encountered in the characterisation of the $[LiAl_2(OH)_6](WO_4)_{0.5}.H_2O$ catalyst as it was poorly crystalline, making analysis by PXRD extremely challenging. The use of elemental analysis proved that tungstate had been incorporated, however, it was hard to say exactly where in the structure it resides due to the difficulty in analysing the sample by X-ray diffraction. In this thesis, the location of the anions was deduced by comparing reactions using the $[LiAl_2(OH)_6](WO_4)_{0.5}.H_2O$ catalyst, which was assumed to contain interlayer WO_4^{2-} anions, and a catalyst using gibbsite which had been stirred in a solution of Na_2WO_4 in an attempt to absorb tungstate anions on the surface of

the gibbsite. Comparisons of turnover frequencies, bromination rates and specific activities concluded that the $[LiAl_2(OH)_6](WO_4)_{0.5}.H_2O$ LDH was a superior catalyst and that the tungstate ions on the surface of the LDH contributed little to the oxidative bromination reaction, indicating that it was the anions in the interlayer space that were responsible for the catalytic activity. This method of chemical probing is unique to this thesis in that it has never been used to deduce the activity of anion exchanged LDH based catalysts before. Further work should focus on using the reaction to halogenate other more useful molecules such as those used in intermediates for the Suzuki cross coupling reaction. Pd doped brucite based LDHs have already been used in this reaction[18]. Further work could focus upon doping with Pd a LDH with tungstate in the interlayer space. It may then be possible to have a one-pot bromination and cross coupling reaction, with the brominated species being generated in-situ.

In Chapter 4, as in Chapter 3, a catalyst based on $[LiAl_2(OH)_6](MoO_4)_{0.5}.H_2O$ was synthesised. On this occasion, the interlayer nitrate anions were replaced with molybdate, MoO_4^{2-} anions, again by suspending the $[LiAl_2(OH)_6](NO_3).H_2O$ LDH this time in a solution of Na_2MoO_4 for 24 hours. The molybdate containing catalyst was then used in a test oxidation reaction, the oxidation of 3,7-dimethyloct-6-en-1-ol (citronellol) into a mixture of 3,7-dimethyl-5-octen-1,7-diol and 3,7-dimethyl-7-octen-1,6-diol; where singlet oxygen was generated in-situ by stirring the molybdate catalyst in a solution of hydrogen peroxide, citronellol and methanol. The reaction is based on a similar reaction found in the literature using brucite based LDHs[19-21]. Comparisons with the literature show that the gibbsite based catalyst studied in this thesis allows the reaction to proceed at a faster rate. Problems were again noted in the characterisation of the catalyst, with poor crystallinity hindering any attempts of using PXRD in characterisation. Elemental analysis indicated that the molybdate anions had indeed exchanged with the interlayer nitrate anions. As in the case of the tungstate system studied in Chapter 3, it is hard to say exactly where in the structure they resided due to the difficulty in analysing the sample by X-ray diffraction. Chemical methods were used to infer the location of the molybdate anions, with the method of absorption on gibbsite being employed. Again, following comparisons of the molybdate absorbed on gibbsite and the $[LiAl_2(OH)_6](MoO_4)_{0.5}.H_2O$ catalyst, the conclusion that the surface anions have little or no effect was reached. As in Chapter 3, this method of chemical probing of the LDH catalyst has never been explored in previous citronellol oxidation reactions found in the literature. Further work could focus upon the oxidation of other molecules such as allyl alcohols used in the synthesis of sulfonylimidates[22] which could have medicinal uses[23]. As citronellol itself is a valuable chemical, it would also be desirable to scale up this reaction, as currently the industrial process uses a 'light' oxidation, where a photo-initiator such as Rose Bengal is used. Problems using the 'light' method include fouling of the reaction vessel, letting less light

through and rendering the reaction less efficient. The LDH system developed here would overcome such problems.

In Chapter 5, compounds based upon WO_3 and MoO_3 were explored. In previous computational work by Catlow *et al*[24-26], it had been postulated that DABCO (1,4-diazabicyclo[2.2.2]octane) could be used as a templating agent in the synthesis of WO_3 and MoO_3 frameworks. Test reactions showed that instead of acting as a templating reagent, it was actually incorporated into a new compound containing large tungsten ionic clusters. Further work used MoO_3 and other organic compounds to successfully synthesise more materials of varied dimensionalities, however, upon single crystal analysis, it was found that all but one of the synthesised compounds was known. The new compound contained clusters of corner sharing MoO_6 octahedra separated by protonated piperidine cations with the composition $Mo_4O_{13}(C_5H_{12}N)_2$. The new compound was analysed by elemental analysis and TGA, and the data was found to be in good agreement with the formula obtained from single crystal analysis. Further work with this compound could include exploring any catalytic uses that it might have. As it contains molybdenum, a starting point could be exploring the reaction discussed in Chapter 4 - the oxidation of citronellol.

References

1. K.K. Rao, M. Gravelle, J.S. Valente, F. Figueras, *J. Catal.*, 173, **1998,** 115-121

2. M. Lakshmi Kantam, B. M. Choudary, C. Venkat Reddy, K. Koteswara Rao, F. Figueras, *Chem. Commun.*, **1998,** 1033-1034

3. K. Yamaguchi, K. Ebitani, T. Yoshida, H. Yoshida, K. Kaneda, *J. Am. Chem. Soc.*, 121, **1999,** 4526-4527

4. T. Tatsumi, K. Yamamoto, H. Tajima, H.-o. Tominaga, *Chem. Lett.*, 21, **1992,** 815-818

5. B.F. Sels, D.E. De Vos, P.A. Jacobs, *Catal. Rev. - Sci. Eng.* , 43, **2001,** 443-488

6. D. Tichit, B. Coq, *Cattech*, 7, **2003,** 206-217

7. J.-C. Wasilke, S.J. Obrey, R.T. Baker, G.C. Bazan, *Chem. Rev.*, 105, **2005,** 1001-1020

8. R.D. Hetterley, R. Mackey, J.T.A. Jones, Y.Z. Khimyak, A.M. Fogg, I.V. Kozhevnikov, *J. Catal.* , 258, **2008,** 250-255

9. R.D. Hetterley, E.F. Kozhevnikova, I.V. Kozhevnikov, *Chem. Commun.*, **2006,** 782-784

10. E.F. Kozhevnikova, I.V. Kozhevnikov, *J. Catal.* , 238, **2006,** 286-292

11. S.M. Yang, Y.M. Wu, *Appl. Catal., A*, 192, **2000,** 211-220

12. A.V. Besserguenev, A.M. Fogg, R.J. Francis, S.J. Price, D. Ohare, V.P. Isupov, B.P. Tolochko, *Chem. Mater.*, 9, **1997,** 241-247

13. A.M. Fogg, G.R. Williams, R. Chester, D. O'Hare, *J. Mater. Chem.*, 14, **2004,** 2369-2371

14. K. Weissermel, *Industrial organic chemistry*, 3 ed., Wiley, Weinheim, 1997.

15. B. Sels, D. De Vos, M. Buntinx, F. Pierard, A. Kirsch-De Mesmaeker, P. Jacobs, *Nature*, 400, **1999,** 855-857

16. B.F. Sels, D.E. De Vos, M. Buntinx, P.A. Jacobs, *J. Catal.* , 216, **2003,** 288-297

17. B.F. Sels, D.E. De Vos, P.A. Jacobs, *J. Am. Chem. Soc.*, 123, **2001,** 8350-8359

18. M. Mora, C. Jiménez-Sanchidrián, J.R. Ruiz, *J. Colloid Interface Sci.*, 302, **2006,** 568-575

19. B.F. Sels, D.E. De Vos, P.J. Grobet, P.A. Jacobs, *Chem.--Eur. J.*, 7, **2001,** 2547-2556

20. B.F. Sels, D.E. De Vos, P.J. Grobet, F. Pierard, F. Kirsch-De Mesmaeker, P.A. Jacobs, *J. Phys. Chem. B*, 103, **1999,** 11114-11123

21. B.F. Sels, D.E. De Vos, P.A. Jacobs, *J. Am. Chem. Soc.*, 129, **2007,** 6916-6926

22. R. Matsubara, K. Masuda, J. Nakano, S. Kobayashi, *Chem. Commun.*, 46, **2010,** 8662-8664

23. J.D. Larsen, H. Bundgaard, *Int. J. Pharm.*, 51, **1989,** 27-38

24. D.W. Lewis, D.J. Willock, C.R.A. Catlow, J.M. Thomas, G.J. Hutchings, *Nature*, 382, **1996,** 604-606

25. F. Cora, D.W. Lewis, C.R.A. Catlow, *Chem. Commun.*, **1998,** 1943-1944

26. F. Corà, C.R.A. Catlow, D.W. Lewis, *J. Mol. Catal. A: Chem.*, 166, **2001,** 123-134